The Advanced Centre for Biochemical Engineering

Department of Biochemical Engineering

University College London

Development of a Microbioreactor for Synthetic Biology Applications

Thesis submitted towards Doctor of Philosophy by

2018

Nelson Barrientos Lobos

Supervisor: Prof. Nicolas Szita

Advisor: Prof. Gary Lye

I, Nelson Barrientos Lobos, confirm that the work presented in this thesis is my own. Where information has been derived from other sources, I confirm than this has been indicated in the thesis.

ABSTRACT

This thesis details the development of a microbioreactor with application in synthetic biology. The aim was the development and engineering characterization of an instrumented microbioreactor system that could aid scientists in the phenotypic analysis of genetically engineered strains.

An existing prototype of a microbioreactor was modified to improve mixing. The microbioreactor was then critically evaluated by: assessing two mixing methods, assessing the prototype against a second reactor design option, characterizing oxygen transfer and mixing, comparing performance with a commercially available minibioreactor, and successfully culturing the genetically modified, gram-positive bacterium, *Staphylococcus carnosus* using the chemostat mode of operation. Engineering characterization of the device was used to inform the selection of process conditions for chemostat studies.

K_La values of ~ 113 h^{-1} and mixing times of ~ 1.2 s were achieved. Residence time distribution analysis demonstrated operation under nearly ideally mixed conditions with ~ 1% of stagnant volumes. Continuous fermentations using different dilution rates and glucose feed concentrations demonstrated the ability of the system to control the growth rate and create a controlled change in OD concentration, respectively. The oxygen uptake rate (OUR) was determined at two dilution rates, which are to the knowledge of the author, the first OUR values reported for *Staphylococcus carnosus* in a microchemostat. Overall, the results provided a more complete engineering understanding of the device, which will facilitate further improvement of the microbioreactor set up to create a high-throughput experimental platform capable of rapidly screening for growth conditions.

IMPACT STATEMENT

The underpinning research of this project focused on the design and fabrication of a microfluidic cassette device for fermentations in continuous mode. The device, however, lacked detailed characterization data about oxygen transfer and mixing phenomena, and biological data on chemostat operation at steady-state conditions.

The present thesis responded to this by rigorously characterizing oxygen transfer and mixing in the device, comparing performance with a commercially available minibioreactor, and culturing *Staphylococcus carnosus* in chemostat mode under different operational conditions. An automated methodology for the measurement of mixing time was developed, which represented a substantial improvement in accuracy, reproducibility and comparability of the results compared to visual inspection. Additionally, a methodology for the measurement of residence time distribution was developed, which provided an accurate description of the mixing in the reactor. Residence time distribution analysis confirmed true chemostat operation at well-mixed conditions. Finally, fermentation results growing the gram-positive *Staphylococcus carnosus* at steady-state conditions were demonstrated. Results are new for its kind since most of the research in microbioreactors has been done using *Escherichia coli* or *Saccharomyces cerevisiae*. This provided useful characterization data of a novel production chassis with unknown capabilities that could be further improved *via* synthetic biology.

The research presented here advanced understanding of how a microfluidic experimental platform can be used in the development of processes to produce a variety of products with applications in healthcare, food, materials and biofuels.

The experimental methodology presented here benefits academia within the specific area of microbioreactors for early bioprocess development.

Benefits outside academia will come from potential commercial activity of the finalized version of the microbioreactor platform. In this sense, a few patents related to the information provided here have already been published by the supervisor.

Main success of the thesis is the demonstration of chemostat operation and the analysis of the effect of two key operational variables. Impact of the investigation is international and within the whole field of biotechnology. This has been demonstrated over a range of conferences (national and international) in which the author has disseminated the main results of the thesis. The results also plan to be published in a scholarly journal.

This research has also a potential ethical impact in the UK and world-wide. If the microbioreactor system presented here can be further developed and used in synthetic biology, one of the most important applications is the manufacturing of novel antibiotic molecules effective against many prominent pathogens. This will ultimately benefit health and quality of life in the world.

This doctoral project brought together a multi-disciplinary team of staff, including not only the supervisor and the advisor but also post-doctoral research assistants who contributed to this research with their advice. This was materialized in regular group meetings where most of the input to this research was delivered.

ACKNOWLEDGEMENT

TABLE OF CONTENTS

LIST OF FIGURES

LIST OF TABLES

NOMENCLATURE

a Specific mass-transfer area

CAD   Computer aided designing

CAM   Computer aided machining

CNC   Computer numerical control

C^* Oxygen saturation concentration

C_L Concentration of oxygen in the liquid

CSTR   Continuous flow stirred-tank reactor

D Dilution rate

D_{crit} Critical dilution rate

DO   Dissolved oxygen

D_{H20} Diffusivity of oxygen in water

D_{PDMS} Diffusivity of oxygen in PDMS

δ PDMS membrane thickness

F Feeding stream

H Henry's constant

h Enthalpy

$K_{L,overall}$ Overall oxygen mass transfer coefficient

$K_L a$ Volumetric oxygen transfer coefficient

K_L Liquid resistance coefficient

K_G Gas resistance coefficient

K_S Monod saturation constant

LFR   Laminar flow reactor

LED   Light-emitting diode

M Mass flow

MAPE   Mean absolute percentage error

MEMS	Microelectromechanical systems
μ	Specific growth rate
μ_{max}	Maximum specific growth rate
μTAS	Micro Total Analysis Systems
N	Stirring speed
N_P	Power number
OD	Optical density
OTR	Oxygen Transfer Rate
OUR	Oxygen Uptake Rate
ω	Angular velocity
PC	Polycarbonate
PDMS	Poly-dimethyl siloxane
PMMA	Poly (methyl methacrylate)
P_{out}	Output mechanical power
Q	Energy rate as heat
Re	Reynolds number
ρ	Density
RTD	Residence Time Distribution
RO	Reverse Osmosis
S	Limiting substrate concentration
S_0	Substrate concentration in the feeding stream
T	Torque
τ	Hydraulic residence time
τ_s	Sensor response time
V	Reactor volume

1 INTRODUCTION

The efficiency of cell culture production processes depends on selecting the best performing strain and the optimal process conditions. This implies that many experiments need to be conducted and high-throughput experimental platforms be developed.

Microbioreactor technology is making important advances towards its application in bioprocess development, particularly in cell cultivation (Krull *et al* 2016:99; Hegab *et al* 2013; Gernaey *et al* 2012; Pasirayi *et al* 2011; Schäpper *et al* 2009). The technology promises flexible and controllable devices capable to perform parallelized experimentation at low cost and with high-throughput screening volumes. Microbioreactors here will be considered as submillimeter structures (< 1 ml) with monitoring capabilities of cell culture parameters (*e.g.* cell density and dissolved oxygen).

Microbioreactors offer several advantages, for example, they can be fabricated using cheap and disposable materials and with optical sensor technology provide *in situ*, real time and non-invasive monitoring of cell culture parameters. Furthermore, the laminar flow regime encountered in these devices allow more predictive fluid dynamics modelling. This understanding of the flow can improve the control over the soluble, physical and mechanical environment of the cells.

One emerging area of biology and engineering that could make very good use of the advantages offered by microbioreactors is synthetic biology. One of the aims of synthetic biology is the artificial synthesis of novel strains capable to produce

a variety of products with applications in healthcare, food, materials and biofuels. These strains need to be rigorously characterized regarding optimum growth and product expression conditions to subsequently develop bioprocesses. Characterization of strains involves two key challenges: screening and process development.

Screening requires testing multiple strain candidates at numerous experimental conditions to identify the best strain/clone relative to the productivity or the yield of the desired product. Here a multiplexed microbioreactor system capable of parallelized experimentation would be very useful. But not only screening is required. The process development stage demands detailed characterization of the cellular environment and the growth and product expression conditions. This is currently achieved using bench-scale (0.5 – 10 L) bioreactors which consume important quantities of expensive biological and chemical reagents. These systems are labour intensive (*e.g.* autoclaving of the reactors, sampling for long periods, cleaning after operation) and a long time to obtain results is involved. Microbioreactors combine tiny volumes with state of the art monitoring and control capabilities that could benefit process development. Different microbioreactor designs have been demonstrated operating in batch, fed-batch and continuous modes (Krull and Peterat 2016; Kirk *et al* 2016; Lee *et al* 2011; Funke *et al* 2010a; Zhang *et al* 2006a; Zanzotto *et al* 2004). Among these modes of operation, the chemostat mode that maintain cells in steady-state conditions could provide a link between genetic engineering of the strains and quantifying product expression. This will be further explored in this chapter.

1.1   Application of Microfluidics in Synthetic Biology

1.1.1 Synthetic Biology

Synthetic Biology, the interdisciplinary field of biology (mainly genetics) and engineering, attempts to deal with the immense complexity of biological systems. This is not a simple task since even the most simple microorganism (*e.g.* the haploid red alga *Cyanidioschyzon merolae* which contains only a single chloroplast and single mitochondrion in its cellular architecture) has more than 5,000 genes in its DNA, which make it complex to study from a genetic point of view (Matsuzaki *et al* 2004).

The following definitions of synthetic biology can be found in the literature:

"Synthetic biology is a rigorous engineering discipline that aims to create, control and programme cellular behaviour" (Cameron *et al* 2014)

"An emerging discipline that uses engineering principles to design and assemble biological components" (Wellhausen and Oye 2007)

"Synthetic biology aims to use modular, well-characterized biological parts to predictably construct novel genetic devices and complex cell-based systems following engineering principles". (Endy 2005).

An example of the application of synthetic biology is the production of antibiotics. A major problem with the current antimicrobial drugs is that its mechanism of action is fixed and has no way to deal with the development of resistance (Davies J and Davies D 2010). Antimicrobial drug resistance has been classified by the World Health Organization as a "serious threat [that] is no longer a prediction for the future, it is happening right now in every region of the world and has the potential to affect anyone, of any age, in any country" (WHO 2014).

Acquired resistance to antibiotics is the result of mutations in the microbial chromosome or the acquisition of extra-chromosomal DNA (Nikaido 2009). Resistance development is extremely difficult to predict, making the production of antibiotics to combat pathogenic microbes a daunting task.

Synthetic biology's approach to solve the problem of resistance is to use the tools provided by molecular biology to design and synthetize new peptides (and new potential classes of antibiotics). The peptides are combined by a production chassis (genetically engineered microorganism) to produce more complex proteins and finally potentially effective antibiotics (the way peptides are combined determines antibiotic effectivity). Thus, a production chassis of a well-characterized genome (*e.g. Staphylococcus carnosus* or *Escherichia coli*) is needed. *Staphylococcus carnosus* is a microorganism of interest for this thesis and will be briefly revised here.

1.1.1.1 *Staphylococcus carnosus*

Staphylococcus carnosus is a gram-positive, facultative anaerobic bacterium (BacMap Genome Atlas 2017). *Staphylococcus carnosus* is of round shape (*cocci*) and form-in grape-like clusters (Fig. 1.1). The microorganism is non-motile and non-sporulating, it grows optimally between 30 and 40 ºC and its diameter ranges from 0.5 to 1.5 µm (Schliefer and Fischer 1982).

Staphylococcus carnosus lacks its outer membrane and does not produce endotoxins. This bacterium secretes proteins into the culture medium which can make it a good production chassis after genetic modification (Götz 1990). *Staphylococcus carnosus* has the highest GC content (36.4%) of the currently sequenced *staphylococcal* species (Rosenstein *et al* 2009).

The subspecies of *Staphylococcus carnosus* used in this thesis was *Staphylococcus carnosus subsp. carnosus* TM300. The genome of TM300 does not contain mobile elements such as plasmids, insertion sequences or transposons, and has only 1 prophage (BacMap Genome Atlas 2017). The genome stability of TM300 is high since the number of repeated sequences is low. *Staphylococcus carnosus* lacks the toxins typical of *Staphylococcus aureus* as well as genes related to biofilm formation.
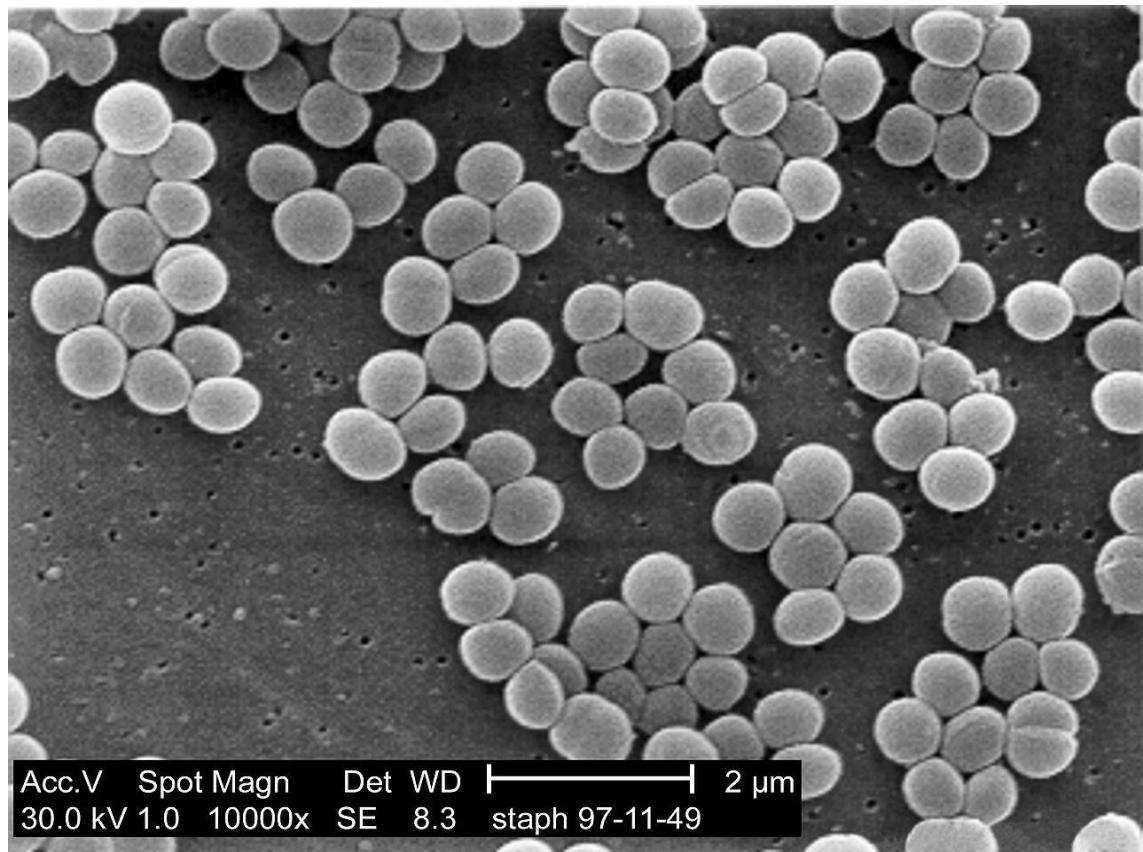
Figure 1.1 Micrograph of Staphylococcus colonies. Source: Centre for Disease Control and Prevention's Public Health Image Library (PHIL). Credits to CDC/ Matthew J. Arduino, DRPH; Janice Haney Carr.

Staphylococcus carnosus is a non-pathogenic microorganism and as such it has been used in the fermentation of dry sausages (Schliefer and Fischer 1982). *Staphylococcus carnosus* exerts several desired functions during fermentation such as giving the desired flavour and red colour to the sausage. Commercial starters of *Staphylococcus carnosus* are manufactured in many countries and the microorganism is of common use.

Given the widely spread commercial use of *Staphylococcus carnosus*, a good amount of information exists regarding characterizing its genome and modifying its DNA (Rosenstein and Götz 2010; Rosenstein *et al* 2009; Wagner *et al* 1998; Brückner 1997). Thus, since the genome of *Staphylococcus carnosus* is currently

well-characterized, it was thought it was worth-while to characterize the growth of this microorganism in the microbioreactor.

1.1.2 Microfluidics

Microfluidics can be defined as the "science and technology of systems that process or manipulate tiny (10^{-9} to 10^{-18} litres) amounts of fluids, using channels (or structures) with physical dimensions of tens of hundreds of micrometres" (Whitesides 2006). In addition, other definitions for microfluidics can be found in the literature:

"*The science and engineering of systems in which fluid behaviour differs from conventional flow theory primary due to the small length scale of the system*" (Nguyen and Wereley 2006:1).

"*Theoretical microfluidics is a field that deals with the theory of flows of fluids and of suspensions in submillimeter-sized systems influenced by external forces*" (Bruus 2007:1).

Among its most important advantages microfluidics enables low consumption of reagents. Dealing with samples of the order of microliters implies tiny structures that use less space and can be more easily parallelized. This allows for a dramatic increase in throughput (Dittrich and Manz 2006), cheaper experimentation, less use of chemicals and less waste generation.

In addition, there are other more "physical" advantages of microfluidics. For example, due to the small distances, the mass and heat transport processes occur more quickly than at larger scales (Hardt and Schonfeld 2007). This allows

precise control over the microenvironment (*i.e.* mechanical and/or chemical/biochemical control), shorter analysis time and higher sensitivities.

1.1.3 Advantages of the Application of Microfluidic Devices in Different Areas of Synthetic Biology.

The previous section stated the advantages offered by microfluidics, mainly the reduction of sample and reagents volumes and the enhancement of analytical performance due to the shorter times and the higher sensitivities. This section will discuss how synthetic biology can capitalize on the properties of microfluidics to solve complex experimental problems in synthetic biology. Categorization of items was based on Szita and Polizzi *et al* (2010).

1.1.3.1 Microfluidic Techniques for the Global Analysis of Cells

DNA sequencing

Microfluidic devices allow researchers to address DNA sequencing using a much lower amount of nucleic acids. The reduction in volume is such that is possible to achieve single cell resolution.

Important steps in DNA sequencing have been successfully addressed using microfluidic chips. A good example is the electrophoresis-based sequencing chip developed by Fredlake *et al* (2008) which demonstrated very rapid time of analysis for short DNA sequences. The time reduction reported was over an order of magnitude compared to traditional capillary array electrophoresis instruments.

But not only short DNA sequences have been addressed. Large regions of interest in the genome have also been targeted and amplified for sequencing. For example, Tewhey *et al* (2009) used a microfluidics-based droplet method to perform a great number of PCR reactions (up to 1.5 million of reactions in parallel). Once amplified, the sequenced DNA data was of quality comparable to what is obtained with traditional approaches.

Abate *et al* (2013) used droplet-based microfluidics to read the sequences of DNA molecules with a fluorescence resonance energy transfer (FRET)-based assay. The approach was analogous to a microarray in which each position tested a specific base sequence. Nevertheless, rather than performing the reactions in a physical array, the authors performed them in sequential sets of flowing microdroplets.

One problem in DNA sequencing is the ability to accurately read long DNA sequences. Lan *et al* (2016) demonstrated a method that used droplet microfluidics to isolate and barcode (index) single DNA molecules in aqueous droplets. The methodology consisted of breaking large template molecules into short fragments. The short fragments were then labelled with known barcode sequences (DNA barcoding primer), read and sequenced. Readings from the short fragments and the labels were used to reconstruct long reads and subsequently sequence full-length DNA molecules.

In a later study, the same author (Lan *et al* 2017) used droplet microfluidics to isolate, fragment, and barcode the genomes of single cells, allowing the sequencing of the genome of each individual cell. The authors demonstrated sequencing of more than 50,000 cells (ultra-high-throughput) in a synthetic community of gram-negative and gram-positive bacteria and fungi.

<u>Transcriptome analysis</u>

Transcriptome here will be understood as the sum of all the messenger RNA molecules expressed by the microorganism. Similar to DNA sequencing, microfluidic techniques for transcriptome analysis use a much lower amount of nucleic acids. The difference, however, relies on the focus in the integration of preparatory unit operations. Thus, a few examples report integration of cell lysis, protein digestion, RNase inactivation and DNA digestion on chip (Irimia *et al* 2009; Zhong *et al* 2008).

The first true example of an integrated microfluidic system for complete gene expression analysis was reported by Toriello *et al* (2008). Implemented in a PDMS/glass microfluidic chip, their chip design encompasses unit operations for sample preparation, amplification of DNA fragments and the downstream treatment of the amplicons. This study clearly demonstrated how a microfluidic chip can be used for single cell gene expression studies.

Research on RNA sequencing of single cells enables more precise measurements of biological variations since RNA levels are a useful marker of phenotypic heterogeneity. The low quantity of RNA in a single cell, however, represents a limitation since it hinders the efficiency of the reverse transcription and amplification of cDNA. Microfluidic platforms can facilitate single-cell manipulation and provide improved detection sensitivity and measurement precision. For example, Streets *et al* (2014) captured and lysed cells in a microfluidic device where mRNAs with poly(A) tails were released from the lysed cells, reverse-transcribed into cDNA and collected and sequenced using a sequencing platform. The implementation of the microfluidic device not only

facilitated single-cell manipulation and minimized contamination but also increased the mRNA detection sensitivity and precision compared to tube-based methods.

Rotem *et al* (2015) used drop-based microfluidics to encapsulate single cells in drops that were later fused with drops containing copies of a DNA barcode that labelled the transcriptome of the cells by hybridizing to its RNA transcripts. The content of the labeled drops was then amplified and sequenced. This allowed recovering information from the transcriptome of each individual cell from the labels. More recently, Zilionis *et al* (2017) developed a method called inDrops, with capability to index more than 15,000 cells in an hour. Authors used microfluidics to encapsulate cells into nanolitre droplets with hydrogel beads. The article describes in detail the protocols for: establishing of microfluidics platform, encapsulation of cells and DNA primers into droplets, lysis of cells and indexing of mRNA by reverse transcription reaction, and RNA-sequencing library preparation.

Proteome and metabolome analysis

Decoding the proteome and metabolome of microorganisms is currently very challenging since the amount of proteins and metabolites available is scarce and the amplification methods for nucleic acids are not applicable. In addition, protein and metabolites are incredibly varied, and their purification requires high-resolution separation methods and very sensitive detection techniques. Nevertheless, microfluidic devices are currently addressing these issues with interesting results.

Several unit operations are involved in the analysis of the proteome, including pre-concentration of proteins, protein digestion, on-chip high resolution separation and coupling with mass-spectrometry. Luk and Wheeler (2009), for example, integrated several protein processing steps on chip, including reduction, alkylation and enzymatic digestion. The system allowed efficient sample preparation and separation although it relied on off-chip detection.

Yang *et al* (2016) aimed at the protein identification using a microfluidic platform and isobaric tags for relative and absolute quantitation (iTRAQ)-labels and mass spectrometry (MALDI-TOF). Simultaneous protein digestion and labelling were performed on chip, including the matrix preparation for final MALDI-TOF analysis (off-chip).

An example of detection of a single protein on a microfluidic device is the work of Mok *et al* (2014) who developed a proteomic platform for protein biomarker detection. The authors used a two-chamber architecture that integrated capture/reaction of proteins and detection *via* electrical impedance sensing. Protein abundance and activity (using Abelson tyrosine kinase) of the human cytokine interleukin 6 were measured.

Similarly, microfluidic techniques for metabolome analysis have been mainly applied for sample preparation and separation. The key challenge is the integration of off-chip instruments for detection of metabolites. Both integration with Nuclear magnetic resonance (NMR) spectroscopy and Mass Spectroscopy (MS) is possible, although MS is considered the most powerful tool due to the great amount of structural information obtained from a MS spectrogram.

Fidalgo *et al* (2009), used microfluidics to encapsulate peptides in single droplets for subsequent online MS analysis. This approach could be extended to other

metabolites. Van den Brink *et al* (2015) generated short-lived drug metabolites in an electrochemical microfluidic chip. The authors integrated an electrospray emitter between the microfluidic chip and the online MS. This enabled a short transit time ($\sim$4.5 s) between the chip and the MS, allowing the detection of short-lived radical molecules that are too unstable to be detected with traditional test assays. Key to the microchip-MS combination was the interface between the microfluidic flow and the MS ionization region, as mentioned in other reports (Lin L and Lin JM 2015).

The same author further modified the microfluidic chip to allow electrochemical protein cleavage of peptide bonds (Van den Brink *et al* 2016). Efficient cleavage of the proteins bovine insulin and chicken egg white was reported before analysis using liquid chromatography–tandem mass spectrometry (LC–MS/MS) for protein identification. The authors suggested this instrumental approach could eventually lead to more detailed proteomic studies in conjunction with MS.

Phenotypic analysis

Microfluidic bioreactors for phenotypic studies offer approaches that alleviate issues encountered at larger scales (mainly the large volume of reagents used, the low experimental throughput and the lack of control over environmental parameters).

In a pioneering study, Bocazzi *et al* (2006) combined real time monitoring of optical density, pH and dissolved oxygen with global gene expression analysis of *Saccharomyces cerevisiae* cultures. The authors measured the expression of the core genes of the GAL operon: GAL2, GAL1, GAL7, and GAL10, growing cells in media with galactose and glucose. In galactose-grown cells, GAL genes were upregulated 100-fold relative to glucose-grown cells.

Although in Bocazzi's experiment the volume of the reactor was sacrificed during exponential growth to take samples for RNA isolation, the authors mentioned that the microbioreactor could be integrated with microscale methods for mRNA isolation similar than the ones described in the transcriptome analysis section.

Bocazzi *et al* (2006) only performed batch cultures, although continuous cultures (particularly chemostat) are of tremendous interest. Chemostat allows accurate control over the dilution rate, maintaining cells in a well-defined steady state in terms of metabolic activity (and by extension gene expression). The chemostat mode of operation could provide a link between genetic engineering of the strains and quantifying product expression. Chemostat microbioreactors have then the potential to bridge synthetic biology results to process development.

Although a few studies on microchemostat have been reported (Krull and Peterat 2016; Kim *et al* 2015; Long Z *et al* 2014; Dénervaud 2013), most of them serve simply as screening platforms and are not applied to synthetic biology for bioprocess improvement. Additionally, research growing new strains (genetically modified or with new properties) in microbioreactors is needed since most studies use *Saccharomyces cerevisiae* or *Escherichia coli*. This will be discussed in detail in the next section (state of the art in the field of microbioreactors).

Finally, microfluidic flow control can be used to generate precisely characterized perturbations to the culture (*e.g.* in steady state conditions). These perturbations can be employed to elucidate intracellular signalling pathways and genetic regulation in different microorganisms (Han *et al* 2014; Bennett *et al* 2009).

Table 1.1 presents a summary of the main advantages of microfluidic devices as discussed in this section.

Table 1.1. A summary of the main advantages of microfluidic devices in different areas of synthetic biology applied to the global analysis of cells.

Area of Synthetic Biology	Application
Genome and transcriptome analysis	Use of droplet microfluidics and DNA barcoding allows the sequencing of the genome and the transcriptome of single cells.
Proteome and metabolome analysis	Microfluidic chips facilitate several unit operations, from sample preparation to separation. Chips are integrated with off-chip instruments for detection.
Phenotypic analysis	Microfluidic bioreactors can generate rapid and precisely characterized perturbations in the cell microenvironment, allowing the study of gene regulation pathways.

1.2 Tools for Cell Culture Process Development

Phenotypic analysis of strains is related to cell culture process development. Shake flasks, microtiter plates and bioreactors have traditionally been used for this in both industry and academia. This section will review some of the advantages and disadvantages of these systems, with a focus on growing microbial strains in continuous mode.

1.2.1 Shake Flasks

Shake flasks have been widely used in many applications since they are inexpensive, easy to operate and hermetic to mechanical complications. They generally have volumes between 10 and 500 ml and can be used in parallel. Parallelization and throughput are the main advantages, while on the downside, shake flasks are generally not instrumented, and data is obtained as discrete data points (samples).

A series of efforts have been made to instrument shake flasks. One example is the work of Anderlei *et al* (2004) who connected gas sensors to the headspace of a shaking flask of 250 ml. The authors measured the oxygen and carbon dioxide partial pressures and a computer calculated the oxygen and carbon dioxide transfer rate (under the assumption of linear changes in measuring), and finally the respiratory quotient.

With the aid of optical sensor technology, monitoring of cell culture parameters in shake flaks is possible. One example is the PreSens shake flask reader system (PreSens 2010) which uses optical sensing technology to monitor dissolved oxygen and pH. Several shake flasks can be operated simultaneously and the flasks (containing the sensors) are delivered to the customer calibrated and gamma irradiated. Similar systems (Hitec Zang 2001) contain in addition gas sensors (in headspace) for monitoring of the respiration activity.

Mixing in flasks is usually achieved by orbital shaking. Tan *et al* (2011) measured mixing time in shake flasks by introducing a rotating camera for observation of

the flow. They reported mixing time values between 10 and 1 seconds, depending on the shaking frequency and the filling volume. Additionally, novel techniques for mixing (*e.g.* resonant acoustic mixing) have been developed (Reynoso-Cereceda *et al* 2016).

Characterization of oxygen transfer in shake flasks has been traditionally performed using the sulphite system, demonstrating oxygen transfer rates proportional to shaking frequency, shaking diameter, filling volume and flask diameter. Correlations between OTR and these factors have been developed for a wide range of operating conditions, different media compositions and different microorganisms (Meier *et al* 2016).

Although shake flasks seem to be emerging as very complete tool for process development, they are usually designed to operate in batch mode, which represents a limitation for the purposes of this thesis.

1.2.2 Microtiter Plates

A microtiter plate consists of an arrange of several wells in a plate. The number of wells is typically 6, 12, 24, 96 and 384, with up to 1536 and 3456.

Microtiter plates perform many parallel reactions at a very small scale. Their stronger features are parallelization and throughput and they are frequently used in the screening stage of a bioprocess, typically allowing the study of batch and fed-batch reactions.

Mixing in microtiter plates is generally achieved by means of orbital shaking of the entire plate, although pipette aspiration or magnetically-agitated stirrer bars have also been implemented (Betts and Baganz 2006). Wells can be of circular or rectangular shape, with square/rectangular shapes aiding mixing by mimicking the action of baffles. Mixing in microtiter plates have very different properties compared to bench scale, stirrer-tank reactors. For example, characterization of the power input (Dürauer *et al* 2016) for the 6 and 96-well plates provided values between 40 to 90 W/m^3 and 40 to 140 W/m^3, respectively, which was significantly lower than a 5 L stirrer-tank reactor (450 to 2100 W/m^3).

Oxygenation of microtiter plates occurs *via* surface aeration due to orbital shaking. In general, oxygen transfer is proportional to shaking amplitude and frequency and inversely proportional to the filling volume. $k_L a$ and OTR values have been determined for different plates configurations. The OTR in round-shaped wells, for example, was determined by Hermann *et al* (2003) with a clear influence of the interfacial tension.

Islam *et al* (2008) determined $k_L a$ values between 20 and 250 h^{-1} for microwell plates (96) between 100 µL and 2 ml. Running and Bansal (2016) determined the oxygen transfer rates of the 96, 48, and 24-well square deepwell microtiter plates using the sulfite oxidation method. Under their experimental conditions, 24-well MTPs obtained the highest OTR values of the study. 24-well MTPs had OTRs comparable to corner-baffled, 250-mL flasks (~100 mM/h).

Finally, microtiter plates are being combined with instrumented shake flasks (RAMOS) to provide dense quantitative process information, reducing the number of experiments in laboratory-scale tank reactors for basic bioprocess development (Wewetzer *et al* 2015).

Similar to shake flasks, microtiter plates are usually designed to operate in batch or fed-batch mode. Microfluidic tools can, however, be used to provide continuous flow, although this usually makes the fluidic set-up mechanically complicated. Thus, microtiter plates are not considered in this thesis.

1.2.3 Miniature Stirred Bioreactor Systems

Only miniature bioreactors (< 500 ml) will be discussed here out of relevance although bench-scale, stirrer tank bioreactors up to 10 litres are widely used in both academia and industry.

Miniature bioreactors typically model larger, bench scale traditional bioreactors. They can be actively aerated and agitated and are easy to instrument with optical probes to measure dissolved oxygen tension (DOT) and pH online (Peng and Biqiang 2016; Betts and Baganz 2006; Betts et al 2006).

One of the first reports in minibioreactors (Betts et al 2005) showed how a prototype, 18 ml stainless steel minibioreactor was characterized in terms of mixing and oxygen transfer. The system was capable of mimicking larger, conventional STRs in many cell cultivations of different rheology, shear-sensitivity and oxygen demand. The device provided high k_La values (480 h^{-1} at 7000 rpm using the dynamic gassing-out method) and short mixing times (4.8 s at 7000 rpm). It was mentioned that although the miniature bioreactor was a prototype, it was possible to multiplex it to provide higher experimental throughput.

Efforts in the development of parallel fermentation systems have materialized in a group of commercially available, benchtop multiple small bioreactors equipped with configurable control systems, analysers, data mining tools, and occasionally a Design of Experiment (DoE) tool (Long Q *et al* 2014). Among the most popular of these systems are the Dasgip parallel bioreactor system (Eppendorf 2017), the MiniBio systems (Applikon Biotechnology 2017), the Multifors 2/2 cell (Infors 2017) and the Advanced Microscale Bioreactors ambr™ (Sartorius Stedim Biotech 2017).

When testing the Dasgip, MiniBio and Multifors systems, Long Q *et al* (2014) described problems with maintaining an efficient temperature control (for the culture of *Pichia pastoris* and *Saccharomyces cerevisiae* during exponential growth phase). Additionally, DO and pH probes were used intensively and time-consuming maintenance of the probes was needed to ensure reliable operation.

TAP Biosystems introduced in the market the ambr250™, which uses optical sensor technology for the monitoring of pH and DO. This system is capable of the parallel control of 12 or 24 single-use bioreactors (100-250ml working volume) equipped with gas, liquid and sensor connections. The workstation is a class II laminar hood that allows the automated handling of liquids and the transfer between bioreactors, sample beds, or media bottles.

A few reports on the use of minibioreactors in continuous fermentations are available (Schmideder *et al* 2015; Klein *et al* 2013; Walther *et al*; 1994). Schmideder *et al* (2015), for example, presents the estimation of kinetic growth parameters during the chemostat culture of *Escherichia coli* in a 10 ml minibioreactor with DO and pH optical sensors. The fluidic configuration of the system was complicated with long sections of tubing added to the set-up (inlets

and outlets). Microbioreactors, by contrast, offer the capability of continuous flow at lower pipeline volumes and will be described in the next section (state of the art in the field of microbioreactors).

Table 1.2 lists the properties of the tools for cell culture process development discussed in this section. A miniature bubble column bioreactor is also included for comparison.

Table 1.2 Properties of various tools for cell culture process development reported in peer reviewed publications.

Reference	Based on	Volume	Agitation; Aeration	pH/DO and OD instrumentation	k_La (h^{-1})	Parallelization
Tsai *et al* 2012	Shake Flask Reader (PreSens)	Different sizes available. 250 ml standard.	Orbital Shaker	pH and DO optical sensors	2 to 16[*]	Up to 63
Ramirez-Vargas *et al* 2014	Microwell plates (24)	3.4 ml (0.38-0.57 ml working volume)	Orbital Shaker (up to 800 rpm); gas sparging	DO optical sensor	8 to 90	24
Xu *et al* 2017	Ambr250™ Miniature stirred bioreactor	100-250 ml	Marine helix, Rushton turbines and Paddle impellers available. Two 3-blade pitched impellers used; gas sparging	pH and DO optical sensors; OD offline	Up to 14	12 to 24
Puskeiler *et al* 2005	Stirred-tank reactor (bioreactor block)	8-12 ml	Gas-inducing single impeller (up to 4000 rpm)	DO optically; pH and OD *via* plate reader	700-1600	48
Betts *et al* 2006	Stirred-tank reactor	18 ml	Triple turbine impeller (up to 700 rpm); gas sparging	pH and DO optical sensors; OD offline	Up to 480	Not reported
Kheradmandnia *et al* 2015	Miniature bubble column bioreactor	20 ml	Gas-sparging	pH electrode and DO optical sensor; OD offline	100–800	3

* Plastic flasks were used. A maximum k_La of 40 h^{-1} was obtained using water in glass flasks and sparging air directly into the headspace (Ries *et al* 2010).

1.3 Microbioreactor Technology

So far various tools for cell culture process development have been considered and their potential for continuous culture discussed. Microbioreactors (< 1 ml) with monitoring capabilities of cell culture parameters offer unique opportunities for the continuous cultivation of microbial strains.

First, the general properties of microbioreactors will be discussed. Second, the state of the art in the field of microbioreactors for cell culture process development will be highlighted.

1.3.1 Materials and Fabrication Techniques

Microbioreactors can be fabricated from a variety of materials, including glass, metals and thermoplastic polymers. Among the polymers, poly(dimethylsiloxane) (PDMS), an elastomeric, thermosetting polymer is the most used. PDMS is optically transparent (for wavelengths greater than 230 nm), non-toxic and highly gas permeable. These properties enable the use of PDMS in microfabrication techniques, microscopic analysis, fluorescent analysis and gas delivery.

Other materials used in the fabrication of microbioreactors are polycarbonate and Poly (methyl methacrylate) (PMMA), which are transparent and non-toxic, but non-gas permeable.

Microfabrication techniques used for microbioreactors focus on introducing micro-level features into a piece of substrate and the bonding of substrates. For

example, laser ablation (Becker and Gartner 2008) uses a high intensity laser beam to remove substrate material. Laser ablation typically uses pulsed laser shots. The amount of removed material varies with laser intensity, material type and laser wavelength. A laser shot typically ablates about 1 µm of material.

Another popular technique is micromilling. Micromilling uses tiny cutters to physically cut the substrate and remove material. This technique is very accurate and can produce very exact boundaries. However, it is also time consuming since the rate of tool travel is limited by the heat generated (cooling of the tool is needed) and by the force applied to move the tool. Some of the smallest tools to work at the microfluidic level are of the order of 5 µm (PMT 2014).

Finally, one of the most common techniques for applying thin films to substrates is spin coating. With spin coating, a small amount of material (*e.g.* liquid PDMS) is applied in the center of a wafer. The wafer is then rotated at high speeds to spread the material evenly by centrifugal force. Spin coating can produce very uniform films with thicknesses ranging from a few nanometres to a few microns (Ossila 2016).

1.3.2 Heat and Mass Transfer in Microbioreactors

1.3.2.1 Heat Transfer

Heat transfer at the microfluidic scale occurs naturally *via* thermal diffusion. Given the small characteristic lengths and the high surface area to volume ratios the

efficiency of heat transfer, characterized by the time it takes to heat up/cool down a volume of fluid, is very good (Hardt and Schönfeld 2007).

The downside is that high surface areas to volume ratios imply quicker evaporation. The problem is further accentuated if PDMS structures (*e.g.* aeration membranes) are used since water vapour can easily diffuse through PDMS (Berthier *et al* 2008).

In microbioreactors, evaporation can have undesired consequences, affecting both concentrations of cells and substrates and optical measurements. Solutions involve either preventing evaporation or replenishing the volume that is lost.

Preventing evaporation can be done by placing the microbioreactor in a humidified chamber, although this makes access to the reactor complicated. Replenishing the evaporated volume can also be done by connecting an elevated water reservoir to the reactor generating a slight extra-pressure. This, however, also increases the probability of contamination, and it is difficult to implement in the case of continuous or fed-batch fermentations since the water reservoir represents an extra input with undefined characteristics (Schäpper *et al* 2009). This thesis will explore a third solution which is compensating for the volume that is lost by pumping water at the evaporation rate.

1.3.2.2 Mass Transfer and Mixing

In the context of microfluidics, mixing is the process through which uniformity of concentration is achieved (Karnik 2015). Mixing is very important in bioreactors since it affects cellular growth by changing the distribution of substrates and

microorganisms. Additionally, mixing can also affect heat transfer by influencing the temperature distribution.

Mixing can be achieved using both active and passive methods. Mixing at the microscale is dominated by diffusion (passive) but can be further enhanced by using active methods (Lo 2013). Active methods use moving parts to actively disturb the liquid bulk whereas passive methods have no moving parts and rely only on molecular diffusion and/or chaotic advection.

Active mixers can be classified considering the type of external force that is applied, for instance: pressure, temperature, electrodynamics, dielectrophoresis, electro-kinetics, magneto-hydrodynamics and acoustics (Nguyen and Wu 2005).

In microbioreactors, mixing focuses on actively mixing the liquid inside the chamber (which generally has no headspace). For example, microbioreactors can include stirring bars (Zhang *et al* 2006b), peristaltic mixers using inflatable air cushions (Lee *et al* 2006) or electromagnetically actuated beads (Tan *et al* 2015). It must be noticed that mixing at the microscale is different than at the macroscale since it is practically impossible to achieve the turbulent conditions and high Reynolds numbers associated with good mixing.

Passive mixers, on the other hand, rely on diffusion and chaotic advection. They usually expose two liquid phases to contact for a prolonged period. Based on the arrangement of the mixed phases, passive mixing can be classified as: lamination, chaotic advection, injection and droplet (Nguyen and Wu 2005). A good example of passive mixing by chaotic advection is microchannels containing an internal, microfabricated structure imposing motion upon the fluid, stretching and folding it. This was reported by O'Sullivan *et al* 2012 who

fabricated a microfluidic T-junction microbioreactor with a staggered herringbone micromixer.

Oxygen Transfer

Oxygen transfer is one of the most challenging mass transfer processes in bioprocesses. This is due to the low solubility of oxygen in water/fermentation broths which implies a continuous supply to fulfil the microorganism demand. In microbioreactors, oxygen transfer is usually achieved using a gas permeable PDMS membrane.

A process parameter that is often used for the characterization of oxygen transfer in bioreactors is the volumetric oxygen transfer coefficient or k_La (Acevedo *et al* 2002:223; Doran 1995:198). k_La allows the comparison of oxygen transport performance across different bioreactor scales.

In bench scale bioreactors, dissolved oxygen concentration is traditionally measured by amperometry using Clark type electrodes. These electrodes generally work well at the macroscale but have limitations at the microscale. For example, given the relatively low quantity of dissolved oxygen available, the consumption of oxygen by these electrodes may make them unsuitable for their use with microbioreactors (Kirk and Szita 2013). Thus, microbioreactors are generally instrumented with oxygen optical sensors (optodes) based on the quenching of fluorescence by oxygen (PreSens 2016).

1.3.3 State of the Art in the Field of Microbioreactors

Microbioreactors with volumes of microliters are highly controllable devices capable of performing experiments at low cost. The use of microbioreactors holds considerable promise for a range of fields, including drug discovery, tissue engineering, bioprocessing optimization and cell-based screening studies (Pasirayi *et al* 2011).

Although a few articles report how structures like microtiter plates or printed circuit boards (PCB) have been adapted into microbioreactors (Maharbiz *et al* 2004), the first publication in which microfluidic techniques such as spin coating and materials such as PDMS and glass were used in the fabrication of a bioreactor was presented by Zanzotto *et al* (2004). These researchers fabricated a 5-50 µL reactor out of glass and PDMS. PDMS was used in the aeration membrane, the reactor body and the bottom of the reactor. Glass was used as base support and for optical access. Each of the PDMS layers was fabricated *via* spin coating into silanized silicon wafers. The thickness of the reactor body was 300 µm (reactor depth). The PDMS reactor layer was cut to create both the reactor chamber and the two recesses in which commercially available optical sensor spots (DO and pH) were positioned. All three PDMS layers were attached to each other and to the glass using a special adhesive.

Mixing and oxygenation in Zanzotto's reactor relied on diffusion only. A k_La value of 60 h^{-1} was measured using the gassing-out method. Limitations in oxygen transfer were attributed to the resistance offered by the PDMS membrane and the bulging of the PDMS membrane (upwards) increasing the chamber height.

Zanzotto *et al* (2004) determined Optical Density (OD) by carrying out transmittance measurements using an Orange Light Emitting Diode (LED) with a wavelength of 600 nm. For DO and pH measurements, fluorescence lifetime-based sensors were excited with a square-wave modulated blue-green LED (505 nm wavelength) and blue LED (465 nm wavelength), respectively. Excited fluorescence sensors emitted a signal "out of phase" compared to the original emission signal (*i.e.* signals differed in their position over time). A lock-in amplifier measured the "phase-shit" in fluorescence which was related to DO and pH concentrations.

Zanzotto *et al* evaluated the performance of their microbioreactor in relation to a 500-ml bench scale bioreactor. They carried out *Escherichia coli* fermentations at both scales and compared growth kinetics, dissolved oxygen profiles, pH profiles, final number of cells, and cell morphology. Similar OD, DO and pH profiles were shown although no statistical analysis stating the degree of difference between concentration profiles was made. In batch fermentations of a duration of 10 h, Zanzotto's system supported ODs of ~5 with air, and ~6 with pure oxygen flushing of the head space. The device was used in two further *Escherichia coli* studies, with integrated bioluminescence and fluorescence monitoring (Zanzotto *et al* 2006), and endpoint gene expression analysis (Boccazzi *et al* 2005).

The measurement of fluorescence in microbioreactors can aid the characterization of strains for synthetic biology applications. Zanzotto *et al* (2006) demonstrated methods for the *in-situ* measurement of fluorescence and bioluminescence using a photomultiplier tube (PMT). A PMT is an extremely sensitive detector capable of multiplying the incident light millions of times. This

instrument is therefore suitable when the flux of light is very low (*e.g.* gene expression in bacteria). For fluorescence measurement, light coming from a blue LED (465 nm wavelength) was passed through a collimating lens and split into two halves using a bifurcated fiber. One half was used as a reference and the other half was passed through the reactor chamber. The emitted light was collected with a plano-convex lens and passed through a longpass filter before being collected by the PMT. Fluorescence results in the microbioreactor were compared to fluorescence measurements in a 500-ml bench scale bioreactor (Sixfors ®) using an off-line luminometer and taking samples manually. Total measurements of fluorescence increased with biomass (optical density) as expected. Measurements were similar at both scales, although results on the bench scale bioreactors showed the limitations of off-line sampling. On-line measurements in the microbioreactor therefore appeared more accurate since the effect of high cell density on light attenuation was minimized.

Active mixing in microbioreactors came next. Zhang *et al* (2006b) fabricated a 150 μL microbioreactor out of PMMA and PDMS. The reactor consisted of two PMMA layers with two PDMS layers sandwiched in between. In the bottom PMMA layer, computer-numerical-controlled (CNC) milling was used to create reactor structures such as a central post designed to position a stir bar to provide mixing. Optical instrumentation of the reactor was like the one reported by Zanzotto *et al* (2004).

Zhang *et al* (2006) characterized their microbioreactor in terms of oxygen transfer and mixing. They performed $k_L a$ measurements using the gassing-out method and determined values between 20 and 75 h^{-1}, depending on stirring speed. The authors measured mixing time using a coloured dye (phenol red) and determined

by visual inspection a value of 30 seconds at 180 rpm. Neither mixing times nor k_La values were correlated to the Reynolds number or other dimensionless groups.

A few batch fermentations were undertaken by Zhang *et al* (2006) with *Escherichia coli*, with final ODs of ~ 6 (after 16 h) and oxygen depletion times of ~2.5 h. The authors also compared their microbioreactor with conventional 500 ml minibioreactors (Sixfors ®). They found comparable growth kinetics in terms of time profiles and final OD, pH and DO values when k_La was kept constant across the scales. No statistical analysis stating the degree of difference between OD profiles was made.

Zhang's design was modified slightly by increasing chamber height to 2mm and integrating a grid above the membrane to prevent bulging. This new, modified version was used in two studies that followed next: differential end-point gene expression studies for *Saccharomyces cerevisiae* grown in galactose and glucose media (Boccazzi *et al* 2006) and the development of a multiplexed array of microbioreactors (Szita *et al* 2005).

Szita *et al* (2005) developed a multiplexed microbioreactor system consisting of four units (150 µL volume each). Microbioreactors were made of PMMA and PDMS and contained miniaturized magnetic stirring bars and DO and pH optical sensors. The four microbioreactors were mounted on a platform, and the instrumentation was multiplexed by optical fibers on a bracket connected to a mechanical slider, driven by a motor. The bracket sequentially read the information coming from reactor 1 to reactor 4. This configuration reduced the number of optical components required, but also the frequency with which parameters were measured (sampling period~10 min).

Szita's system was designed to be re-configured to work with two different reactor designs. None of the designs were characterized for $k_L a$. Szita *et al* (2005) compared their system to the commercially available Sixfors ®. The comparison was favourable in terms of OD, DO and pH profiles. Additionally, the authors sacrificed the reactor volume at the end of the fermentations and took samples to analyse gene expression and consumption of substrates by HPLC.

Soon after, continuous culture in microbioreactors was reported by the same research group (Zhang *et al* 2006a). In their publication, two developments facilitated chemostat operation:

First, the movement of microorganisms in response to substrate stimulus towards the media reservoir (*i.e.* chemotaxis) was prevented by a local heating element at the inlet of the reactor. The heating element reversed the driving force for chemotaxis. In addition, the flow rate was chosen to counteract the bacterial swimming upwards to the reservoir through the microchannels.

Second, cell wall-growth in the reactor chamber was prevented by using (ethylene glycol) (PEG) – grafted poly (acrylic acid) (PAA) copolymer films to modify the inner surfaces of PMMA and PDMS and create bio-inert surfaces resistant to cell-adhesion. This was an interesting development although it would be potentially costly and difficult to perform at a manufacturing scale.

Zhang *et al* (2006a) studied chemostat operation at different flow rates (0.5 µL/min, 1 µL/min and 1.5 µL/min) and demonstrated steady values for OD, DO and pH. The authors found lower DO steady values at higher flow rates which was an indication of faster growth and metabolism. On the other hand, OD levels for the different flow rates remained relatively constant which the authors claimed was consistent with bioprocess stoichiometry for glucose as the only source of

carbon. This was not confirmed by mass balances or stoichiometric analysis. Finally, neither stirring speed nor $k_L a$ were reported.

Balagaddé *et al* (2005) used soft lithography to create a series of 6 bioreactors (16 nL each) made from PDMS. Each bioreactor consisted of a growth chamber, supply channels, a peristaltic pump, and a waste channel. The reactors were monitored *in-situ* by optical microscopy to provide real-time, automated and non-invasive measurements of cell density and morphology.

The authors created a system that used micro-plumbing networks to prevent film formation during chemostat operation. The system operated in two modes: (*i*) continuous circulation and (*ii*) cleaning and dilution. During continuous circulation, the micropump in the growth chamber moved the culture around. During cleaning and dilution, a segment of the reactor was isolated (using micromechanical valves) and a lysis buffer was flushed to remove the cells (including any cells on the walls). The segment was then reunited with the rest of the chamber and the operation continued. This cleaning step, however, interrupted what otherwise would have been a truly continuous operation.

Balagaddé *et al* (2005) used the device to study the population dynamics of *Escherichia coli.* They performed over 40 experiments at different conditions and found steady state growth over a range of dilution rates from 0.072 to 0.37 h^{-1}. The authors plotted the number of cells per picoliter against the dilution rate and determined how the culture approached washout when the dilution rate increased. Balagaddé *et al* (2005) mentioned that reducing the reactor volume to the nano-level suppressed the total mutation rate and created a genetically homogenous population. No mutations or changes in cell morphology were reported. Unfortunately, no monitoring of dissolved oxygen concentration was reported which could have provided more information on cell growth.

Lee *et al* (2006) developed an integrated array of eight microbioreactors, with 100 µL working volume each, comprising a "peristaltic oxygenating mixer" and injectors. The reactor chambers were of an irregular oval shape ~15mm in maximum dimension and 500mm high. The aeration membranes on top of the chambers were 70 µm thick, PDMS membranes. A series of channels above the membranes could be pressurized with air or a gas mix, deflecting the membranes into the growth wells. Mixing times of ~5 s (estimated by visual inspection) and an impressive value of k_La of 360 h^{-1} were obtained when actuating at 40Hz frequency and 4psi in a propagating pattern.

Lee's system had the advantage of no moving parts inside the reactor chamber. Additionally, it was the first published system offering control over variables other than temperature (in this case pH and DO). Eight-hour *Escherichia coli* batch fermentations were performed reaching very high ODs (~40 or 13.8 g dcw/L). DO control was set to maintain a concentration of 50% air saturation but in practice DO% about 40-50% was maintained after 3 hours but with considerable variance.

Lee *et al* (2006) developed a device capable of achieving higher OTRs and faster mixing. Nevertheless, the reactor setup was complex and operation in continuous mode (or any attempted continuous fluid flow) was probably affected by the mixing technique.

Edlich *et al* (2010) developed a diffusion-based microbioreactor system, with a reaction volume of 8 µl, capable of operating in continuous mode. The reactor had a special geometry chosen to achieve homogeneous flow during continuous operation. The device consisted of a structured PDMS top covalently bonded to a glass bottom containing a cavity for a DO sensor spot. The authors used Computer Fluid Dynamics (CFD) simulations to decide the best geometry design and verified this *via* microparticle-image-velocimetry (µPIV). No concentration gradients occurred along the entire reaction volume due to rapid diffusive mixing.

The authors determined a relatively low k_La value of 0.004 s^{-1} (14.4 h^{-1}) for their device using a 300 µm membrane. Optimum growth conditions for chemostat experiments were determined at lab scale, with a specific maximum growth rate of 0.47 h^{-1}, without replicates to provide an idea of variability.

Edlich *et al* (2010) studied the fermentation of *Saccharomyces cerevisiae* in the microbioreactor at three dilution rates in the range of 0.01-0.47 h^{-1}. Biomass concentration values showed a descending trend for increasing dilution rates. Additionally, the lower the dilution rate the later the stationary state was achieved. The authors reported strong reactor wall growth of *Saccharomyces cerevisiae* resembling a biofilm. Wash-out conditions were not assessed completely.

Schäpper *et al* (2010) presented a cylindrical, PDMS reactor of 100 µl volume. Mixing was achieved with a free-rotating stirrer bar which provided the upward current necessary to lift cells of *Saccharomyces cerevisiae* in suspension. The

device offered control of pH and temperature and online measurement of DO and OD. The reactor design consisted of 4 layers which were bonded together to form one single block of material. The top layer was designed to improve aeration and contained a meandering aeration channel (0.75 mm deep and 0.5mm wide).

The authors reported a k_La value of ~63 ± 7h−1 and a mixing time of ~1.2 s measured by visual inspection using a bromothymol blue solution (addition of base induced a colour change from yellow to blue, addition of acid reversed the change). Schäpper *et al* (2010) performed a series of batch cultivations of *Saccharomyces cerevisiae*. Data showed a lag phase of approximately 2 hours followed by exponential growth until 13 hours. DO levels started to decrease after 5 hours of operation achieving close to zero values at 15 hours (at this point OD was approximately 11). Three independent batch fermentations averaged a maximum specific growth rate of 0.34 h^{-1} ± 0.02. Suitability of the device for continuous operation was claimed but no fermentation data on this was presented.

Lee *et al* (2011) fabricated a 1 ml working volume bioreactor out of PDMS and plastic. Lee's device consisted of three interconnected, horizontally split, 500 µl chambers, linked with channels and deformed pneumatically to induce peristaltic motion. Only two of the chambers operated simultaneously (working volume 1 ml) allowing compliance for mixing. The chambers acted as valves that were inflated and filled with liquid (or deflated to remove liquid). Actuation of the chambers was in a circular pattern creating mixing through a common interconnected channel. The device operated in three different modes: injection of substrates, mixing mode and evaporation refill mode. Surfaces of the reactor were modified as in Zhang *et al* (2006a).

Lee *et al* (2011) characterized their system in terms of oxygen transfer and mixing. k_La values between 57.6 and 90 h^{-1}, and mixing times of 2 s were reported. For mixing time, authors determined the change in colour of bromothymol coloured dye after addition of 0.1 M hydrochloric acid and sodium hydroxide. Determination was by visual inspection with a digital camera.

Lee *et al* (2011) carried out continuous culture experiments with *Escherichia coli* using glucose and other salts separated into different bottles that were independently addressed and connected to the reactor. This allowed the peristaltic pump at the entrance of the growth chamber to vary the concentration of glucose in the feed. The authors performed several experiments at both chemostat and turbidostat conditions.

The authors performed a continuous fermentation of a duration of 3 weeks with OD values typically between 1 and 2 (with a maximum of 4). Chemostat operation at different flow rates and glucose concentrations was reported with several dynamic states and steady states demonstrated. Turbidostat operation at different glucose concentration was also reported with a control variance within 1.2%.

Most of the literature so far refers to microfluidic devices fabricated with bonding techniques. Davies *et al* (2013) developed a microfluidic "cassette" design in which polycarbonate layers were clamped using 3 mm diameter screws. Assembly of reactor parts was straightforward. The design concept allowed versatility for batch and continuous operation while maintaining key aspects of single-use: for example, the reactor body was made disposable to reduce sterilization and cleaning loads.

Davies *et al* (2013) demonstrated batch and chemostat operation with *Staphylococcus carnosus* achieving ODs of ~11 and 1.3, respectively. A free-rotating bar was used for mixing (mixing time of 1.5 s at 220 rpm). This was the first demonstration of chemostat operation of a gram-positive bacterium in a microbioreactor. The authors did not report k_La values.

The same device reported by Lee *et al* (2011) was soon after used in a synthetic biology experiment (Han *et al* 2014). A *Saccharomyces cerevisiae* strain with a dual inducible fluorescent reporter system was tested at turbidostat conditions for precise induction control using glucose and galactose. A control algorithm was used to alter the concentration of the injected glucose/galactose so a target concentration in the reactor was achieved within 1 hour.

The genetic circuit in *Saccharomyces cerevisiae* allowed the induction of either a red fluorescent protein (RFP) or green fluorescent protein (GFP) depending on both the source of carbon and whether an inducer molecule was provided or not. Expression of GFP was achieved with either glucose or galactose (but only when the inducer was provided) whereas expression of RFP was only achieved using galactose (no inducer required) and was supressed by glucose.

A turbidostat culture (constant cell density) was used with alternating glucose (without inducer) and galactose sources. Samples were extracted at steady state conditions after reaching a first steady state with glucose (at ~8 h), after switching from glucose to galactose (at 24 h), and after switching back to glucose (at 48 h). Separately, a turbidostat experiment of induction of GFP expression with glucose and inducer molecule was performed. In addition, induction of the strain was carried out in a test tube with 24 hours as induction period (control).

Examination of the flow rate and the DO variation in the microbioreactor showed a clear lag phase when switching from glucose to galactose during turbidostat culture. Flow cytometry histograms showed that fold induction in the microbioreactor was much higher compared to test tubes. Additionally, protein expression throughout cell populations was more uniform and tightly distributed in the microbioreactor. Normalized standard deviation (standard deviation over the mean) of cell fluorescence intensity decreased from 0.98 to 0.47 after galactose induction and from 0.87 to 0.37 after the injection of glucose and inducer molecule.

Experiments performed by Han *et al* (2014) demonstrated control over an artificial gene circuit. Chemostat studies at varying dilution rates were not performed, which would have provided indication of possible variations in protein expression with the growth rate.

Tan *et al* (2015) developed a novel stirring method involving the movement of an electromagnetically actuated bead by sequenced activation of electromagnets located underneath the reactor chamber. Cylindrical, diamond and triangular shaped reactor chambers were used. Mixing time measurements were performed for each chamber design using different electromagnet on/off sequences resulting in values of 4.5 s, 2,9 s and 2.5 s for the cylindrical, diamond and triangular shaped chambers, respectively. Image analysis software was used in the determination of mixing time.

Tan *et al* (2015) used a thin PDMS membrane for oxygenation of the reactor but did not report $k_L a$ values. Noticeably, the use of a diamond-shaped chamber improved the priming and removal of bubbles from the reactor compared to a

cylindrical chamber. Additionally, a duplex microbioreactor set-up (parallelization attempt) was tested with two diamond-shaped chambers with separate electromagnet actuators placed side by side. Consistent mixing behaviour was observed for the two chambers. The authors did not perform fermentations.

Kirk *et al* (2016) developed a membrane-aerated microbioreactor in which mixing was achieved using an eccentrically oscillating jet. The jet was promoted by a syringe which infused and withdrew the culture medium to and from the reactor, respectively. The authors characterized mixing (through the analysis of images using a Python script) and oxygen transfer in the device, with mixing times of $\sim$7 s and $k_L a$ values of $\sim$170 h^{-1}. DO control was reported using a solenoid microvalve. Batch fermentations of *Saccharomyces cerevisiae* under oxygen-controlled conditions were performed. Cell densities of 6.7 g dcw $l^{-1}$and oxygen uptake rates of $\sim$34 mmol l^{-1} h^{-1} were achieved.

Krull and Peterat (2016) fabricated a 57 µL multiphase microreactor capable to operate as a micro-chemostat. The device was applied as a vertical microbubble column in which aeration was achieved by creating an additional gaseous phase in the form of the rising microbubbles. Risk of blockage due to the carbon dioxide produced by *Saccharomyces cerevisiae* was minimized since gas bubbles were released through buoyancy in the upper part of the reactor. The reactor was fabricated from PDMS, using UV-depth and soft lithography, and bonded to a glass bottom. The reactor design included a micronozzle which generated bubbles with diameters of a few hundred micrometres.

The authors reported a gas holdup lower than 30%. Rising bubbles enhanced mixing and prevented cell sedimentation. No mixing time values or analysis of mixing conditions was reported. Fiber optics and needle-type micro sensors allowed real time monitoring of OD and DO. A maximum $k_L a$ value of 0.14 s^{-1} (504 h^{-1}) was claimed.

Krull and Peterat (2016) studied the Crabtree effect in *Saccharomyces cerevisiae* cultivated aerobically in continuous mode. Mathematical modelling of the micro-chemostat culture based on stationary balance equations was presented. Dilution rates ranging between 0.14 and 0.42 h^{-1} were tested and samples for glucose and ethanol analysis by HPLC were extracted at each steady state. Wash-out was achieved at a dilution rate ~0.425 h^{-1}. The authors modelled the cellular growth considering two types of metabolism (purely oxidative metabolism and oxido-reductive metabolism). Several kinetic parameters were estimated (including the specific growth rate and the substrate saturation constant K_S) using the Lineweaver-Burk (Lineweaver and Burk 1934) and other linearization methods. A dilution rate of ~0.194 h^{-1} was identified as a limit value, where D < 0.194 h^{-1} was purely oxidative metabolism in which glucose was completely converted to biomass, and D > 0.194 h^{-1} was oxido-reductive metabolism with generation of ethanol under aerobic conditions (at the expense of biomass formation). No data on DO concentration was presented. Finally, Krull and Peterat (2016) compared kinetic parameters estimated in the microbioreactor with values reported in the literature for chemostat experiments with a 2.85 L bench scale bioreactor. Values of kinetic parameters were of the same order of magnitude at both scales.

Perez-Pinera *et al* (2016) used the device reported by Lee *et al* (2011) for the rapid and switchable production of two biologics using a genetically engineered *Pichia pastoris* strain. The device demonstrated production of near-single-dose levels of recombinant human growth hormone (rHGH) and interferon-α2b (IFNα2b). The manufacturing process was in continuous culture with sequential and controllable expression of the two proteins. After an outgrowth period of 24 h, medium was switched to produce interferon-α2b (IFNα2b), and after 48 hours of culture, medium was switched again to produce recombinant human growth hormone. The total average production of IFNα2b and rHGH was 19.73 µg per reactor and 43.7 µg per reactor, respectively. This was more than the daily dose needed in adults, so no bioprocess optimization was required to improve the production. Authors envisioned that the combination of the reactor system with analytical, purification and polishing technologies could lead to a small-scale, portable, personal biomanufacturing platform.

Table 1.3 summarizes the properties of the microbioreactors discussed in this section. Note that few microchemostats have been established, most of them growing *E. coli* or *S. cerevisiae,* and none of them applied to synthetic biology.

Table 1.3 A summary of microbioreactor systems reported in peer reviewed publications. Adapted from Kirk and Szita (2013).

Reference	Volume (µl)	Mixing method; oxygenation method	k_La (h^{-1})	Mixing time (s)	Measured (online)	Controlled	Cell type	Mode of operation	Notes
Zanzotto *et al* (2004)	5,50	Diffusion; PDMS membrane	60	NR	OD, DO and pH	T	*E. coli*	Batch	Scale up study
Zhang *et al* (2006a)	150	Magnetic stir bar; PDMS membrane	NR	NR	OD, DO and pH	T	*E. coli*	Continuous	Chemostat
Zhang *et al* (2006b)	150	Magnetic stir bar; PDMS membrane	75	30[*]	OD, DO and pH	T	*E. coli; S. cerevisiae*	Batch	Scale up study
Lee *et al* (2006)	100	Pneumatic peristaltic	360	5	OD, DO and pH	T, DO and pH	*E. coli*	Batch	Multiplexed (8 reactors)
Edlich *et al* (2010)	8	Diffusion; PDMS membrane	14	NR	OD and DO		*S. cerevisiae*	Continuous	Chemostat; optimized geometry
Lee *et al* (2011)	1000	Pneumatic Peristaltic	90	2	OD, DO and pH	T, DO, pH, and OD	*E. coli*	Batch and continuous	Chemostat and turbidostat
Kirk *et al* (2016)	100	Oscillating jet; PDMS membrane	170	7[**]	OD and DO	T and DO	*S. cerevisiae*	Batch	
Krull and Peterat (2016)	57	Gas sparging	504	NR	OD and DO	T and DO	*S. cerevisiae*	Batch and continuous	Chemostat; Parameter estimation

Nomenclature: DO: Dissolved Oxygen, OD: Optical Density. T: Temperature. NR: not reported. (*) at 180 rpm (**) determined using computational image analysis.

1.4   Research Objectives

Synthetic biology is an exciting new research area which offers new avenues to engineer strains to create novel biological products and enhance bioproduction yields. A few chassis have been explored although *Escherichia coli* has dominated the field until now (Adams 2016). *Staphylococcus carnosus*, for example, as a gram-positive bacterium and a chassis of well-characterized genome, has not been extensively explored, and can be genetically modified to produce preparative quantities of a variety of lantibiotics that anchor at the surface of pathogenic bacteria.

As categorized in Table 1.1 microfluidics has numerous advantages that provide what synthetic biology requires to blossom. Unsurprisingly, many topics have been advanced in meaningful ways. Phenotypic analysis, however, remains a challenge, which – if overcome – would accelerate the transition from establishing *de novo* strains to actual process improvements.

A tool that could maintain cells in steady-state conditions of metabolic activity (and by extension in controlled conditions of gene expression) would provide the necessary link between genetic engineering and quantifying product expression for subsequent bioprocess development. Chemostat is such a tool although its implementation using conventional systems comes with important challenges of operation and cost.

Miniaturization of bioreactors has altered process development and promises high-throughput experimentation at low cost. More recently, microbioreactors have emerged as potential tools for bioprocess development and continuous flow at the microfluidic scale has the potential to facilitate chemostat operation. In this thesis, I explored how microbioreactors can be made fit for synthetic biology by

carefully analysing reactor design parameters and how they affect oxygen transfer and mixing. Indeed, state of the art lacks detailed information about how to improve mixing and oxygen transfer in microbioreactors. Adequate characterization will facilitate an understanding of microbioreactor operation. Oxygen transfer is the most important phenomenon to characterize, as studies suggest that scaling-up based on constant volumetric oxygen transfer coefficient $k_L a$ is a valid approach (Garcia-Ochoa and Gomez 2009).

Once reactor characterization was complete, I characterized chemostat operation. Steady-state conditions obtained from chemostat operation can facilitate phenotypic analysis of strains and determination of biological parameters. As a model system, I chose *Staphylococcus carnosus* given its well characterized genome. This generated useful characterization data of a novel strain that could be further improved *via* synthetic biology.

Considering the above, the aim of this thesis was the development and engineering characterization of an instrumented microbioreactor system capable to operate in chemostat mode to aid scientists and engineers in the biological characterization of strains. Research questions addressed in this thesis are: what is the best reactor design and mixing method for chemostat studies? What are the best mixing conditions for chemostat culture? What process variables can be controlled during chemostat operation and what is their effect on cell growth?

2 MATERIALS AND METHODS

2.1 Fabrication of Microbioreactors

2.1.1 Microbioreactor Cassette

All components of the microbioreactor were designed using Solidworks (Solidworks Student Edition 2015, Solidworks Corp, MA, USA). Polycarbonate parts (RS components, UK) were fabricated using micromilling (M3400E, Folken Industries, CA, USA), Mastercam (3D CAD/CAM Mastercam X4, MA, USA) and HSMXpress (Solidworks, USA). Reactor body and lid were bonded *via* thermo-compression bonding (135°C, 45 N·m, 2 h).

The reactor chamber contained a recess that located an oxygen sensor spot and a central post that positioned a magnetic stir bar. Dimensions for these structures were measured using an Optical Interferometer (Contour GT-K 3D Optical Microscope, Bruker AXS GmbH, Karlsruhe, Germany).

Aeration membranes were made from polydimethylsiloxane (PDMS; Sylgard 184, Dow Corning, UK) at a 1:10 (catalyst/PDMS) ratio. Liquid PDMS was spin-coated onto a silicon wafer (P6708D, Specialty Coating Systems, USA) at different rotational speeds (depending on the desired thickness) and baked at 90 °C for two hours in an oven (UFP400, Memmert, UK). Membrane thicknesses were measured using a Dektak 8P (Veeco Instruments Inc, Woodbury, New York, USA) stylus profiler at a contact force of 5 mg and resolution of 111 nm. A PDMS membrane holder was fabricated by casting PDMS onto a micro-milled polycarbonate mould. PDMS holder and membrane were bonded using air plasma-assisted bonding (PDC-002, Harrick Plasma, USA).

2.1.1.1 Experimental Set-up

An aluminium incubator was fabricated for use with the microbioreactor cassette. The incubator was designed using Solidworks CAD and fabricated by the UCL fabrication workshop at the Department of Chemical Engineering. In addition, a fiber holder (for use with optical fibers) was designed using Solidworks CAD and fabricated by Finetech Engineering Limited at HertFordShire, UK.

A USB Temperature logger (EL-USB-1, Lascar Electronics, UK) was used to measure temperature changes inside the incubator. A standard thermometer probe (Habor, RS components, UK) was used to measure the temperature at the outlet channels of the incubator.

2.1.1.2 Mixing Methods

Two mixing methods were used with the microbioreactor cassette: a centrally fixed magnetic spin bar and a short, free-rotating magnetic spin bar.

A central post machined out from the bulk material of the reactor defined the axis of rotation of the centrally fixed bar. The magnetic bar was plated with nickel and coated with Parylene N50 (Super Magnet Man, Pelham, USA) to avoid oxidation.

The free-rotating bar was fabricated by inserting a 3 mm long and 0.5 mm diameter magnetized road into a fluoroethylene polymer (FEP) tube. The ends of the tube were sealed with silicon glue (RS Components, UK). Both types of magnetic stir bar were propelled using an electric motor (EC 32 Maxon EC motor, Switzerland). The motor was activated using a power supply unit (RS components, UK).

Confirmation of the rotational speed of the magnetic bars was performed by inspection of the reactor with a High-Speed Camera Photron FocusScope SV200-I (Photron, San Diego, USA) borrowed from the EPSRC Instrument Pool (Engineering and Physical Sciences Research Council, UK). Specially dedicated software (PFV Fastcam Viewer, Photron, San Diego, USA) was used in the analysis of images.

2.1.2 Suspension Microbioreactor

A suspension microbioreactor was fabricated in Poly (Methyl Methacrylate) (PMMA) via CO_2 laser machining (18X12 Epilog Laser, USA) with a 100 µm resolution. The bottom layer of the reactor chamber was fabricated using a raster scanning laser mode where the PMMA chip was locally thinned by a single passage of the laser beam.

Top and bottom layer of reactor were cleaned with RO water and dried with compressed air after fabrication. Parts were placed in a plasma cleaner chamber under vacuum conditions (PDC-002-, Harrick Plasma, USA) to remove all organic matter from the surface. An oxygen sensor spot (Presens Precision Sensing, Germany) was cut into a circle of 2 mm diameter and placed into a central hole at the bottom of the reactor chamber using non-toxic silicon glue (RS Components, UK). Once the silicone glue dried completely, the top and bottom layer of the reactor were attached together using a small amount of UV curing adhesive glue (Norland Optical Adhesive 61, Norland products, Inc., USA) to fill the bonding area. The device was then placed under a pre-heated UV lamp (UVP,

UK) for 10 minutes. Finally, to ensure complete bonding, the device was placed into an oven (Memmert, GmbH, KG, Germany) at 50 °C for an hour.

2.2 Characterization of Oxygen Transfer and Mixing

2.2.1 K_La Measurements

K_La experiments were carried out by placing the microbioreactors inside the aluminium incubator. The chamber was maintained at 37°C by flowing heated water coming from a water bath (Grant Instruments, UK) through the base.

Dissolved oxygen (DO) was measured using a Presens GmbH (Regensburg, Germany) PSt3 oxygen sensor membrane. The sensor was interrogated with a 2-mm optical fiber connected to a fiber optic oxygen transmitter (OXY4-mini, Presens GmbH). DO data was collected *via* PC and processed using a program written in MATLAB ™ (MATLAB R2015a, Mathworks).

The gassing-out method was used to determine K_La values (Suresh *et al* 2009). Oxygen concentration was recorded every 2 seconds and K_La values were obtained by fitting DO data (during the recovery stage) as a function of time to Equation 2.1.

$$DO(t) = 1 - \left[\left(\frac{1 - DO(0)}{1 - \tau_s k_L a}\right) \cdot \left(e^{-k_L a t} - e^{-\frac{t}{\tau_s}}\right) + (1 - DO(0)) \cdot e^{-\frac{t}{\tau_s}}\right]$$

Equation 2.1

Where $DO(t)$ is dissolved oxygen, $DO(0)$ is the value at which oxygen concentration starts recovering and τ_s is the value of the sensor response time.

By contrast, for the suspension reactor, the gassing-out method was not used. $k_L a$ was determined by provoking a step change in the concentration of dissolved oxygen in the inlet media. Two liquid solutions (saturated with oxygen and with zero dissolved oxygen) were used. The oxygen saturated solution was prepared by pumping compressed air into a 200-ml glass bottle containing fermentation media at 37 °C (for 20 minutes). The zero-oxygen concentration solution was prepared by dissolving 0.1 g/L of sodium sulphite powder in RO water at 37 °C. A hot plate (Jenway, UK) was used to heat up both liquid solutions.

1.5 ml of each solution was pipetted and dispensed into a 2 ml Eppendorf tube at the reactor inlet. First, the oxygen saturated solution was aspirated into the reactor at 21 µL/min. The solution filled the reactor until a constant DO value (close to 100%) was achieved. Second, the zero-oxygen solution was pumped into the reactor and the variation in dissolved oxygen monitored over time. $K_L a$ data was calculated from the decrease in dissolved oxygen concentration.

$k_L a$ values were determined three times per experimental condition and presented as the mean with one standard deviation.

2.2.2 Mixing Time

Mixing time was characterized *via* inspection of the reactor contents with a high-speed camera (Phantom MIRO4, Phantom, USA) borrowed from the EPSRC Instrument Pool (Engineering and Physical Sciences Research Council, UK). A syringe pump (KDS200, KD, Scientific, USA) was used to pump a coloured dye, 4 mM Allura Red (Sigma-Aldrich, UK), contained in a plastic syringe (Becton-Dickson, Fisher, USA) into the microbioreactor. The recorded videos were processed using a bespoke Python script (Python ™, Python Software Foundation, Delaware, United States) with NumPy (van der Walt *et al* 2011), SciPy (Oliphant *el al* 2007) and Matplotlib (Hunter 2007) modules. Mixing time was defined as the time required to achieve 95% of colour homogenization (as described in Kirk *et al* 2016). Mixing time values were determined three times per stirring condition and presented as the mean with one standard deviation.

For the case of the microfluidic suspension bioreactor, a USB camera (Edmund Optics, USA) was used determine mixing time by visual inspection. A neMESYS syringe pumping system (Cetoni GmbH, Germany) was used to pump the dye into the reactor.

2.2.3 Residence Time Distribution

A UV absorbance detector, Actipix™ D100 (Paraytec, UK) and a capillary tube (100 µm ID, SGE Analytical Science, Trajan Scientific, Australia) at the outlet of the microbioreactors were used in the determination of residence time distribution. A 1 g/L tryptophan, and 0.025 g/L allura red, solution was used as a

tracer (tryptophan for detection and allura red for visualisation of the moment the solution reached the reactor chamber). A 0.2 g/L and 0.025 g/L allura red solution was used with the circular chamber and diluted 4 times. The neMESYS syringe pumping system was used to pump reagents into the reactor.

The capillary tube was connected to the outlet of the reactors using a fluidic connector with 20 µL internal volume (Upchurch Scientific, UK) and plastic tubing (IDEX Health&Science, 500 µm ID, USA). For the circular reactor, the total volume at the outlet line was 100.4 µL. For the suspension reactor, the volume of the outlet line was 64 µL.

Absorbance data was related to Tryptophan concentration using a 4-point calibration curve. Data was smoothed by taking the moving average every 500 points.

2.3 Biological Characterization

2.3.1 Microorganism

The chloramphenicol resistant *Staphylococcus carnosus* TM300 (pCX-pp-gfp) was used in all experiments. The strain was kindly supplied by the University of Tubingen.

Complex media containing the following components was used:

- Tryptone 10 g/L, Yeast Extract 5 g/L, 5 g/L NaCl

- K_2HPO_4 0.684 g/L and KH_2PO_4 0.2741 g/L

- Glucose 1 g/L

- 0.01 g/L chloramphenicol

All medium components were from Sigma Aldrich. Components were sterilised by autoclaving at 121 °C for 20 minutes. Glucose was autoclaved separately from the rest of the components. Chloramphenicol was filtered with a Minisart ® NML syringe filter (Sartorius, Germany). Viscosity of the medium was measured using a rotational rheometer (Malvern Instruments, Kinexus lab +, UK).

2.3.2 Shake Flasks

Staphylococcus carnosus cultures were run in 250 ml shake flasks (Fisher Scientific, Loughborough, UK) using a shaken incubator (Adolf Kuhner Ag Schweiz) at 37°C and 200 rpm. Baffled flasks (4 baffles) were used exclusively. Flasks were filled to 20% volume (2 ml inoculum). 1 ml samples were taken every two hours. Three shake flasks were run independently. Data was presented as the mean with one standard deviation.

2.3.3 Minibioreactor

The compact Eppendorf DASGIP Parallel Mini Bioreactor System was used. The features of the system were the following:

- Number: 4 minibioreactors
- Material: Stainless steel
- Reactor volume: 300 ml
- Working volume: 200 ml
- DO sensing: polarographic oxygen probes
- pH sensing: pH electrodes
- Motor drive model SR02500DLS (2500 rpm maximum agitation speed)

Specially dedicated software (DASware® control software, Eppendorf International) was used in the control of the bioreactors.

During fermentations samples were taken as 1 ml every 2 hours for the measurement of OD, glucose and lactic acid. Reactors were autoclaved prior and after operation. Inoculum (%v/v) was 4%.

2.3.4 Procedure for Batch Fermentations with the Microbioreactor

2.3.4.1 Fluidic Aspects

For batch fermentations, two reactor inlets and one outlet were used. One input was connected to a 5-ml plastic syringe (Becton Dickinson, USA) containing the inoculum. The second inlet was connected to a 2.5 ml glass syringe (Hamilton, Switzerland) containing degassed RO water used to replenish the water that evaporated from the reactor. The evaporation compensation rate was 0.15 µL/min. Ethanol, water and media were entered to the reactor before fermentations following a calibration protocol as:

1. Reactor chamber was primed with 70% ethanol for disinfection of the system and the removal of all bubbles.

2. Reactor chamber was primed with reverse osmosis (RO) water. Voltage was recorded (1000 data points) while priming.

3. Reactor chamber was primed with media. Voltage was recorded (1000 data points) while priming.

4. Reactor chamber was primed with inoculum. Voltage was recorded (1000 data points) while priming.

5. Optical densities of RO water, media and inoculum were measured with a spectrophotometer (Ultrospec 500 pro, GE Healthcare LifeSciences, UK).

Averaged reactor OD values and spectrophotometer OD values were compared.

In parallel to the calibration procedure, two *Staphylococcus carnosus* precultures were run in shake flasks at 37°C and 200 rpm. A first preculture was inoculated with cells directly from the frozen stock (2 ml tube) and carried out for 24 hours. An aliquot from this (10 ml) was used to inoculate a second flask. Once a value of OD of approximately 0.5 (exponential phase) was achieved, an aliquot sample (5 ml) was taken, diluted with media by a factor of 2 and used to inoculate the microbioreactor. Once the reactor was primed with inoculum, the on/off valve at the outlet channel was turned off to keep the reactor closed. At this point, only evaporation compensation flow was on.

A neMESYS syringe pumping system (Cetoni GmbH, Germany) was used to introduce reagents into the reactor.

2.3.4.2 Monitoring of OD and DO

Optical density (OD) measurements were performed using a light emitting diode (LED) (L600-01V, Epitex Inc) which projected a ray of light through the reactor chamber. Light was emitted as a 2-kHz square wave signal and supplied using a function generator (FG100, Digimes). The transmitted light was detected using a photodetector (PDA36A, Thorslabs Inc, USA) located at the top of the reactor. Voltage signal from the photodetector was sent to a lock-in amplifier (SR 830, Stanford Research, USA) for further analysis. The data was stored using a

LabVIEW (Version 2014, National Instruments, USA) program and processed using a MATLAB™ script.

Voltage values were converted into OD values using Equation 2.2

$$OD = 8.33 \cdot \left[-log_{10} \left(\frac{V}{V_0} \right) \right]$$

Equation 2.2

Where OD is optical density, V is voltage, V_0 is the voltage of the chosen baseline (either water or media). 8.33 is a conversion factor to account for the path length of the reactor.

Similar than for k_La measurements, dissolved oxygen concentration was measured using a Presens GmbH (Regensburg, Germany) PSt3 oxygen sensor membrane. DO data was collected via PC every 30 seconds using specially dedicated PreSens software and processed using a program written in MATLAB™.

2.3.5 Procedure for Continuous Fermentations with the Microbioreactor

For continuous fermentations, two fluid inputs and one output were used. One input was connected to a 5-ml plastic syringe (Becton Dickinson, USA) containing the inoculum. The same input was connected later to a 10-ml glass syringe (Hamilton, Switzerland) containing media (feed). The second input was connected to a 2.5 ml glass syringe containing degassed RO water (evaporation

control). Both water and media/inoculum lines contained sections for bubble removal. The media/inoculum line contained a section for inoculum waste.

As with the batch protocol, the reactor chamber was first primed with 70% ethanol for disinfection and then water and media were entered to the reactor following the calibration protocol. After this, the system was primed with inoculum (volume added quantified as the sum of the reactor volume and the inlet tubing volume), and the on/off valve at the outlet channel was turned off to keep the reactor closed. At this point, only evaporation compensation flow was on. Initial batch fermentations were performed for three hours before continuous feed started.

The neMESYS syringe pumping system was used to pump media into the reactor at the desired flow rates.

Experiments at different dilution rates were performed independently, cleaning, disassembling and assembling the reactor in between.

2.3.6 Analytical Techniques

2.3.6.1 OD Measurements

OD samples were prepared to the appropriate dilution (1:2 to 1:10) and measured using the UV spectrophotometer (Ultrospec 500 pro, GE Healthcare LifeSciences, UK).

2.3.6.2 Glucose and Lactic Acid Measurements

Glucose and lactic acid samples were prepared to the appropriate dilution (1:2) and measured using the Bioprofile FLEX Analyser (NOVA ® Biomedical, UK).

3 EVALUATION OF MICROBIOREACTORS DESIGNS FOR BACTERIAL CELL CULTURE

In this chapter, two microbioreactor designs required evaluation to demonstrate bacterial cell culture potential. The first design was developed as a microfabricated cassette device and was based on the work of Dr. Matthew Davies (Davies *et al* 2013). The capacity to actively promote mixing was a central feature. The cassette device was compatible with two mixing mechanisms: a centrally fixed stirrer bar (CFB), positioned in a post at the centre of the reactor chamber, and a free-rotating stirrer bar (FRB). Mixing is not a simple operation at the microscale and the device needed to provide well-mixed, homogeneous conditions for cell growth.

The centrally fixed bar was thought to mimic stirring methods traditionally used in large scale bioreactors (specifically a paddle turbine). The concept was that similar mixing between the microbioreactor and larger scales could facilitate scale-up of fermentation results.

The free-rotating bar was thought to overcome deficiencies in the mixing obtained with the centrally fixed bar. Previous Computer Fluid Dynamics (CFD) evidence (Zhang 2006b) showed stagnant volumes at the corners of the microbioreactor when the centrally fixed bar was used. To reduce the volume of these zones, the free-rotating bar was intended to rotate around its vertical axis and to move around the floor of the reactor, hitting and ricocheting off the reactor walls.

Oxygen transfer was also an important feature, relevant for both aerobic and facultative anaerobic organisms. Oxygen supply was achieved by implementing a thin, gas permeable PDMS membrane. Features of the design considered a special structure designed to avoid deformation of the membrane.

The cassette device also considered aspects of disposability. The reactor was fabricated with polycarbonate which is cheap and allowed the reactor body to be disposable. Similarly, the PDMS aeration membrane was intended to be single-use, reducing sterilisation and cleaning costs.

The second design was developed by Professor Philippe Renaud (École Polytechnique Fédérale de Lausanne EPFL, Switzerland) as a microfluidic suspension bioreactor with liquid flowing from bottom to top. One important motivation for the design was to achieve mixing without the integration of moving parts which can be difficult and expensive to manufacture and can potentially exert stress on the cells. A second motivation was to create an uplifting flow to compensate for natural the sedimentation of the cells and to maintain them in suspension for very long periods (such as the length of time required for chemostat operation).

Key design features needed evaluating to ensure they were fit to purpose, including high oxygen transfer rates for optimal growth and scale-up and good mixing with a low percentage of stagnant volumes that could provide operation as a perfectly mixed reactor. An additional goal regarding mixing was choosing between the centrally fixed stirrer bar and the free-rotating stirrer bar. Critically the potential to culture bacterial cells in a microfluidic device needed to be demonstrated.

3.1 Results and Discussion

3.1.1 Microbioreactor Cassette Design

The microbioreactor cassette consisted of a top plate, a membrane frame, an oxygenation membrane, a reactor lid, the reactor body and a bottom plate (Fig. 3.1). Transparent and sterilisable materials were used in fabrication. Oxygenation membrane and frame were made from gas-permeable PDMS while the reactor body, the lid, the top plate and the bottom plate were made from autoclavable, ethanol-resistant polycarbonate. Transparent parts facilitated integration of optical instruments and allowed observation under a microscope camera.

The modular concept of design allowed easy insertion and removal of the reactor body and the membrane/frame structure. An important advantage of this was that changes in the reactor body/chamber did not require a complete re-design of the entire reactor, which would have been the case with a monolithic construct. Furthermore, with the modular structure the parts with a more complex design such as the top and bottom plates are kept separated from the simple parts (reactor body and membrane/frame structure) which have potential for large scale manufacturing. In this sense, to facilitate industrial manufacturing, it was thought that PDMS structures can be cast cheaply and quickly and replication processes (such as hot embossing) are commonly available for polycarbonate. Simple parts were intended as single-use.
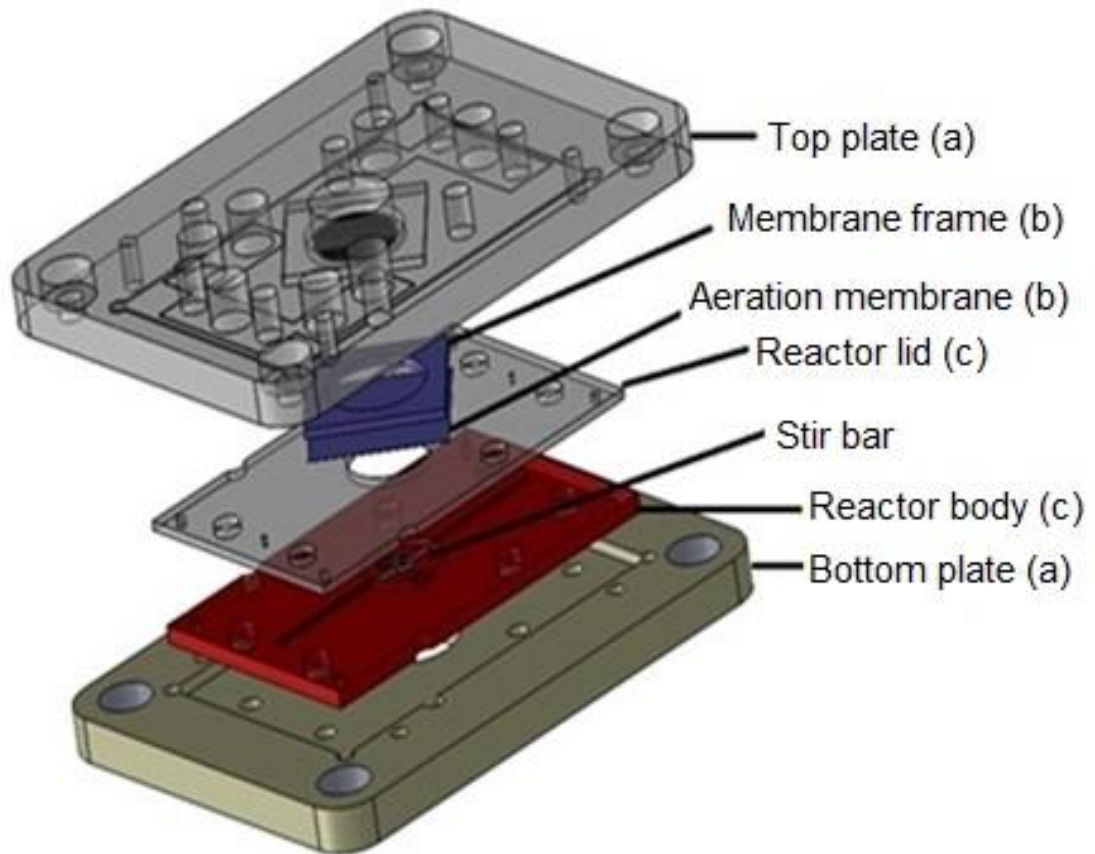
Figure 3.1. 3D view of the microbioreactor cassette highlighting individual parts. Components are grouped into a) cassette parts b) aeration membrane/frame construct, and c) reactor parts. The reactor body contained the fluidic channels and the reactor lid the fluidic ports. The top plate contained a grid structure (center). Cassette and reactor parts were made of polycarbonate. Aeration membrane and frame were made of PDMS.

The top plate of the device contained a set of threads compatible with fluidic connectors. The outer dimensions of the top plate were 70 mm long and 50 mm wide. The plate contained a central recess designed to hold in place the oxygenation membrane. It was noticed that it takes very little force of pressure to deform the membrane upwards and change the reactor volume. Bulging of the membrane threatened both chemostat operation and the accuracy of optical measurements. The degree of deflection of the membrane was modelled by the theory of Poison's small deflections of a circular plate (Qian *et al* 2016) where the deflection of the membrane is directly proportional to the applied pressure (by

flow) and inversely proportional to the thickness of the membrane. Reducing the operational flow rate was not possible since it would have affected continuous operation. Changing either the material or the thickness of the membrane was also not possible since it would have affected the oxygen transfer rate. A better choice was to design a grid structure to prevent the bulging of the membrane upwards and maintain the volume of the reactor as constant as possible. The grid structure was made of polycarbonate which is transparent and did not excessively prevent oxygen transfer due to the high number of perforations. The grid structure was part of the design of the top plate.

The thickness of the aeration membrane was chosen as 100 µm to minimise the diffusion length of oxygen through the membrane and improve oxygenation. As discussed in Chapter 4, a thickness of 100 µm allowed high oxygen transfer rates while maintaining the top of the reactor sealed. The degree of compression of the membrane was defined by the location and pressure provided by eight M3 screws that were used to clamp the top and bottom plates together. At very low membrane thicknesses values (< 50 µm) sealing of the top of the reactor was deficient and created leakage.

The bottom plate had the same outer dimensions as the top plate and contained a recess (50.1 mm long and 30.1 mm wide) designed to hold the reactor body. The reactor body was 49.8 mm long and 29.8 mm wide. An extra space of 0.3 mm accounted for variations in the milling of the reactor outer sections and facilitated removal of the reactor from the bottom plate.

The reactor body contained a chamber of cylindrical shape, which had a diameter of 10 mm and a height of 1 mm. When the reactor body was thermally bonded to the lid (1 mm thick) the total height of the chamber was 2 mm, accounting for a

chamber volume of 157 µL. Thermal bonding between the lid and the reactor sealed the microfluidic channels and allowed the delivery of reagents into the chamber *via* fluidics ports in the lid. Thermobonding at 135°C for 2 hours did not change the optical properties of polycarbonate. Additionally, the reactor body contained lateral incisions designed for removal (Fig. 3.2).

Two recesses in the floor of the reactor chamber were designed to position optical sensors. One of the recesses positioned an oxygen sensor spot. The other recess was kept available to position a pH sensor. The recesses were of 300 µm depth and 2.2 mm diameter. A 2-mm oxygen sensor spot was glued to the bottom of the recess using silicone glue (extra 0.2 mm in the recess provided room for the glue). The depth of the recess allowed rotation of the stirring bars without hitting the sensor. The recess was milled in 6 z-axis steps with settings as 100 mm/min for the feed rate of the tool and 50% horizontal overlap. These settings defined the roughness of the bottom of the recess so it did not affect optical measurements.

A
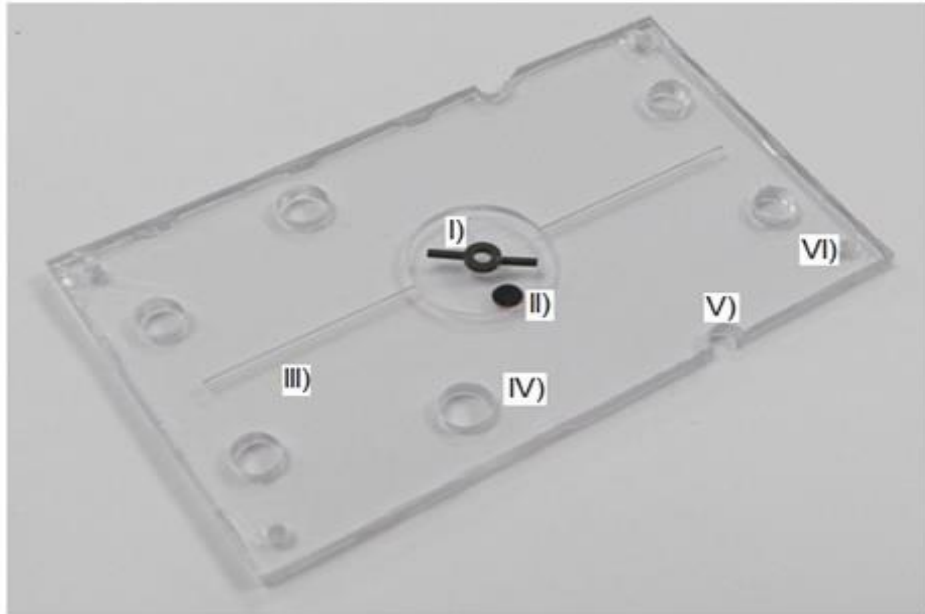
B
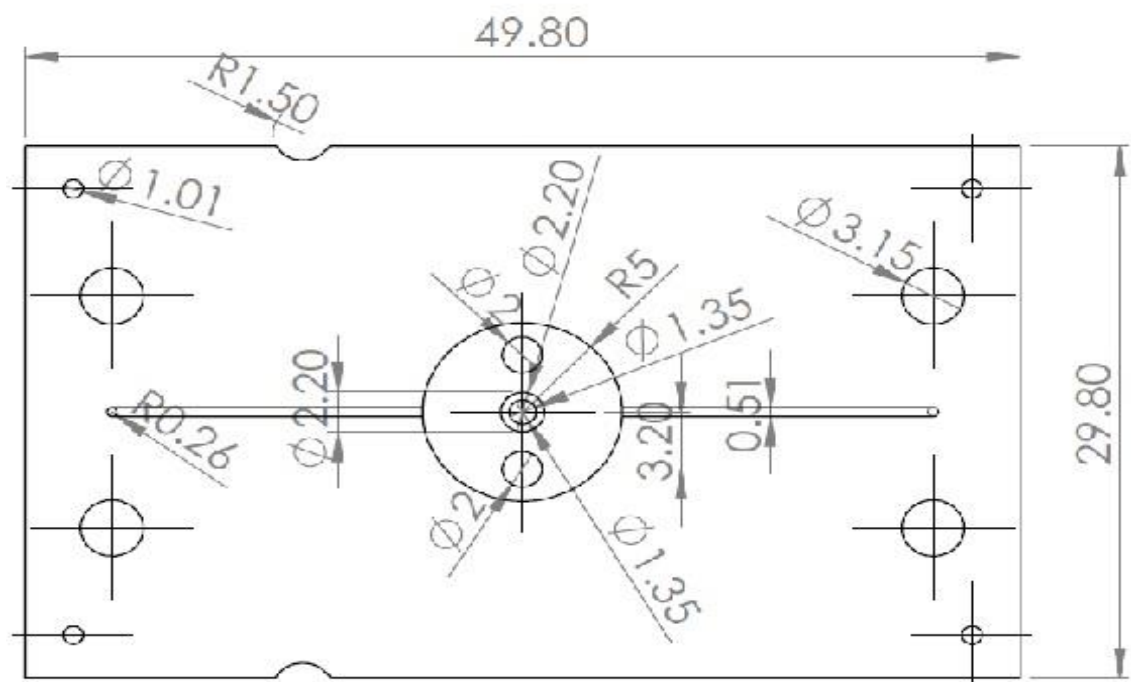
Figure 3.2. Photo of the reactor body seen from the top (A) and CAD design (B). Centrally fixed bar (I) positioned in central post. Oxygen sensor spot (II) in a recess (0.3 mm depth and 2.2 mm diameter). Fluidic channels (III) allowed the delivery of reagents into the chamber. Threaded holes (IV) allowed correct clamping of the reactor with cassette parts. Lateral incisions (V) allowed easy removal of the reactor body from the bottom plate (after clamping). Pin holes (VI) at the corners allowed correct alignment between the reactor body and the lid. Reactor body was made of polycarbonate.

The reactor channel dimensions were 500 μm wide and 500 μm depth. These dimensions were compatible with standard upchurch fittings and tubing that contained a through hole of 0.5 mm diameter. All inlet channels were located very close to the reactor chamber. The short residence time of the fluid between the fitting ports and the entrance of the chamber meant that fluids were introduced in the reactor with virtually zero delay. This was important for residence time distribution experiments discussed in chapter 4.

A central post included in the reactor body was used to hold in place a centrally fixed bar. The post was milled from the bulk of the reactor and its dimensions were precisely measured (see evaluation of microbioreactor cassette). When the post was not included in the reactor design, the free-rotating bar was used. A technical drawing of the reactor body can be found as supplementary information.

3.1.1.1 Incubator

Once the reactor design was established, a chamber that provided adequate gas and heat transfer to the reactor was needed. An incubator chamber (Fig. 3.3) made of aluminium was designed with a large volume and thermal mass for holding the temperature to a constant value. The large volume of the incubator compared to the reactor ensured that gaseous oxygen was supplied in excess compared to the oxygen that could potentially be consumed by the cells. Temperature of the incubator was controlled by flowing water through the base.
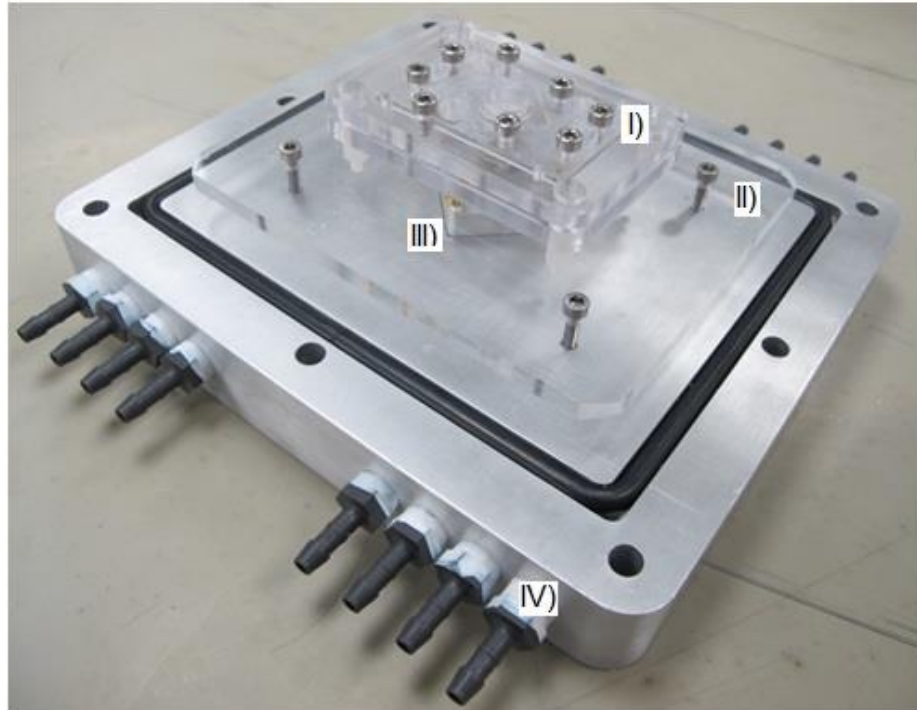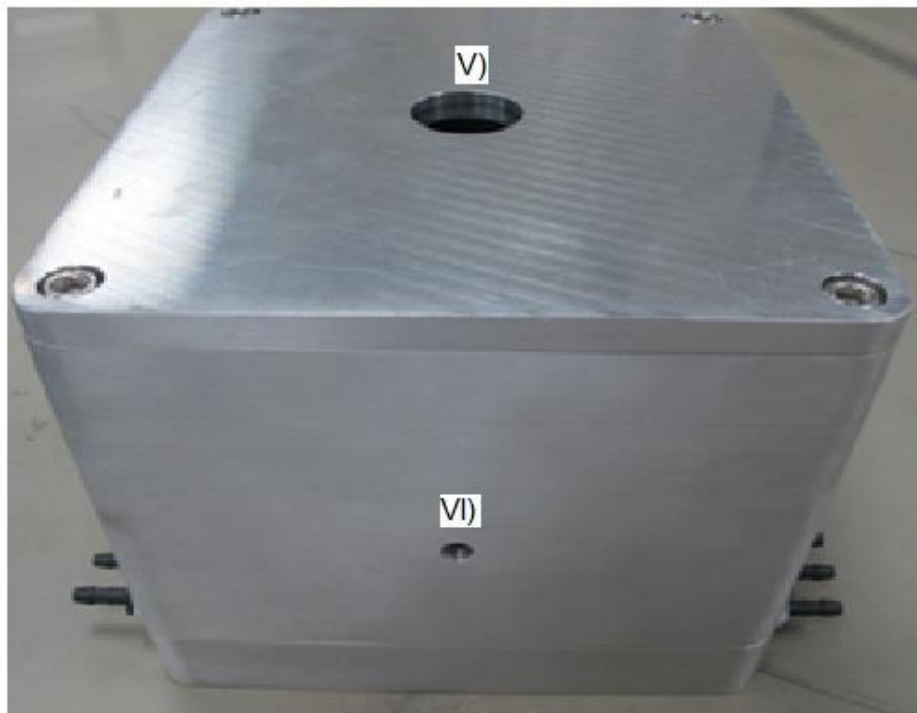
Figure 3.3. Photos of the aluminium incubator. On the inside (A) the microbioreactor cassette (I) was placed on a base plate (II) made of polycarbonate. A fiber holder (III) allowed the integration of optical fibers with the bottom of the reactor. Channels at the base of the incubator (IV) flowed water to provide heat transfer. When the incubator was closed (B) a hole in the lid (V) allowed the connection of an optical fiber (detector) to the top of the reactor. A port in the wall (VI) connected to a rotameter (gas flow).

Tests to the incubator demonstrated that the internal temperature can be kept constant (Fig. 3.4). For this, a USB Temperature logger was positioned inside the incubator at the same position of the microbioreactor. Data showed that it takes approximately 51 minutes to achieve a steady temperature inside the chamber. The aim was to maintain the internal temperature at 37 °C, which is the optimal growth temperature for *Staphylococcus carnosus*.
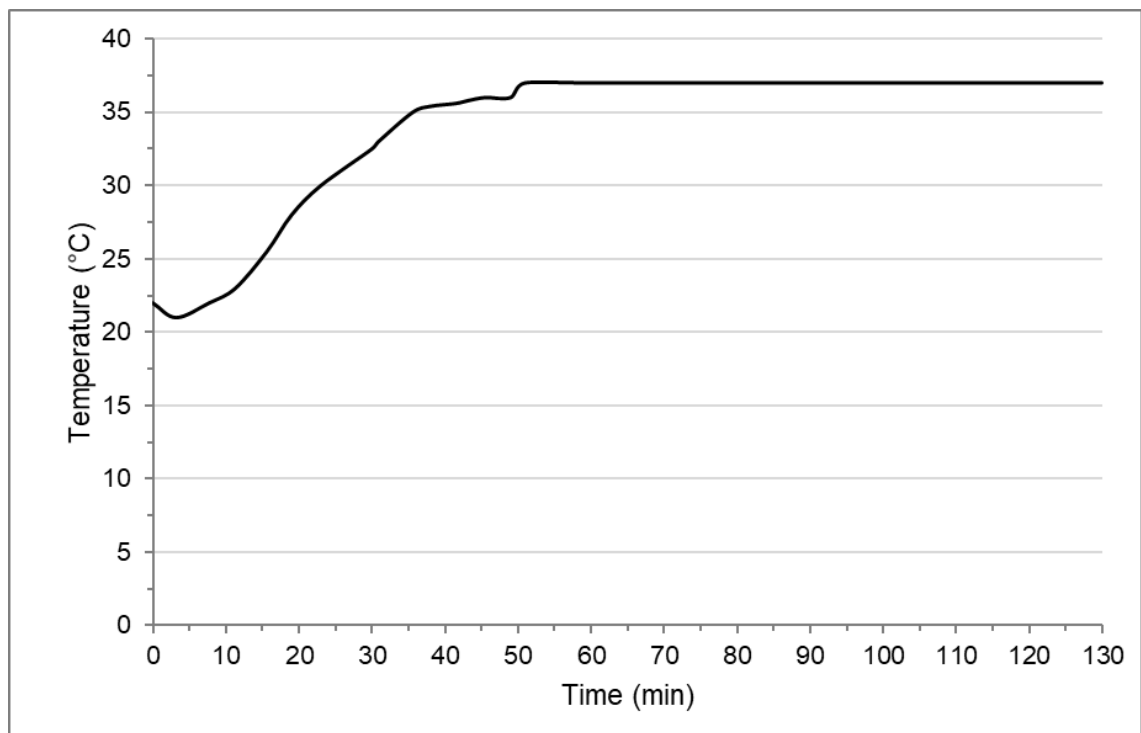
Figure 3.4. Temperature evolution inside the incubator after heating of the base started (time zero). A USB temperature logger was placed inside the incubator chamber to measure temperature. 51 minutes were required to achieve a steady value (37 °C). n=1 measurement.

Aluminium worked efficiently as a thermal conductor. The material provided rapid heat transfer and cooled the incubator quickly. Local changes in temperature were not measured as it was assumed that all points of the chamber were kept at a similar temperature due to the high thermal conductivity of aluminium.

In addition to heat transfer, the incubator chamber also provided optical access and optical isolation. Optical fibers were integrated at the top and the bottom of the incubator, directly above and below the reactor chamber, respectively. A fiber holder inserted at the bottom of the incubator (and below the reactor) contained three holes to locate optical fibers for the measurement of dissolved oxygen, optical density and pH (pH was not used). The internal design of the fiber holder allowed bending of the optical fibers (Fig 3.5a) up to 55° degrees. Additionally, a hole at the lower part of the connector allowed the positioning of a magnetic stirrer. Technical drawings of the internal sections of the fiber holder (top and bottom parts) can be found as supplementary information.

An additional component was a base plate attached to the base of the incubator (Fig. 3.3a). The base plate ensured that the reactor and the fiber holder for optical fibers were aligned together. Four threaded holes at the bottom of the incubator were used to attach the base plate.

The incubator chamber was placed directly above the magnetic stirrer to minimize the distance to the stir bars. This distance was 5 cm measured from the tip of the stirrer to the stir bars.

A
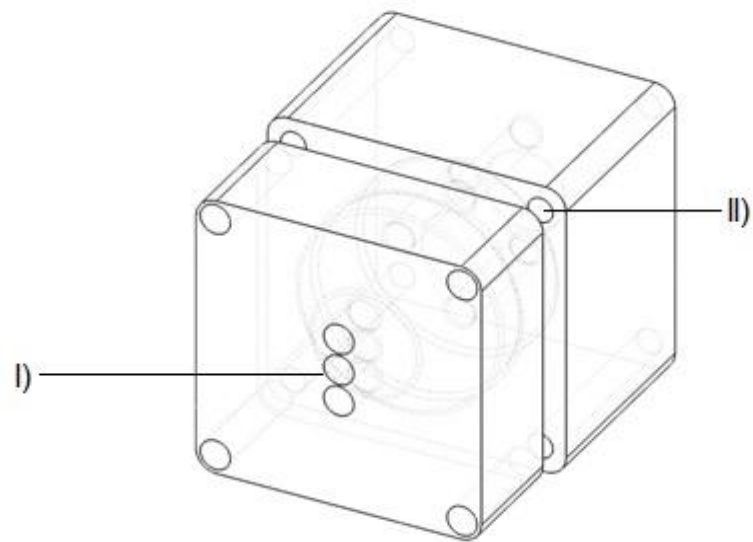
B
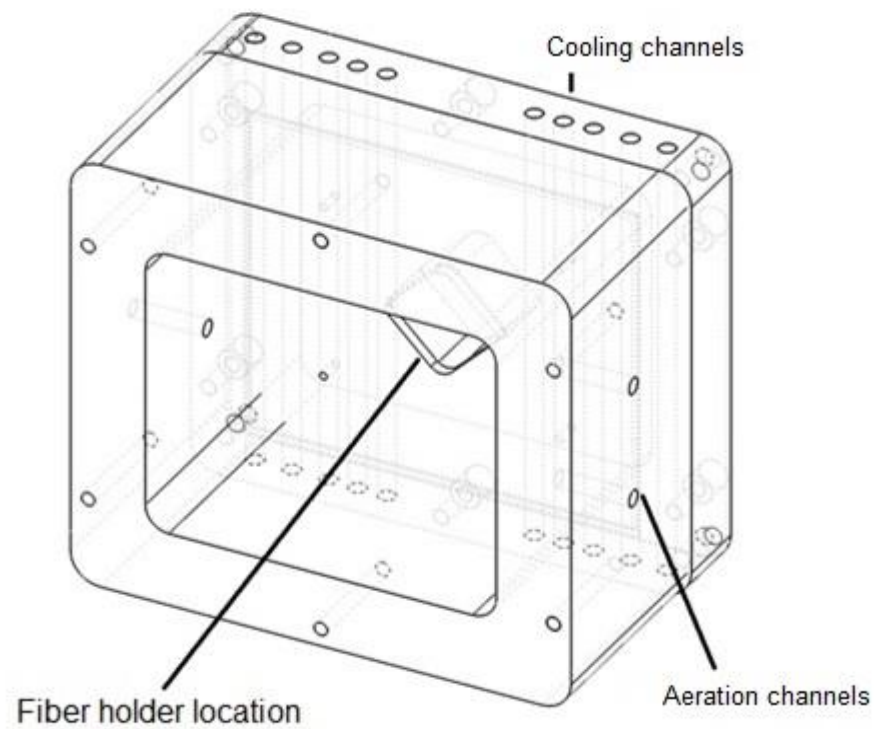
Figure 3.5. Design of the fiber holder (A) including three holes for optical fibers (I) and one hole (at the bottom back) for the stirrer motor. The two parts of the fiber holder were assembled together using threaded holes (II). The fiber holder was inserted in the specified location (B). An optical fiber (2 mm diameter) passed through the central hole of the fiber holder and through the base of the incubator (not shown).

The amount of heat needed for the incubator to be kept at 37 °C was calculated using a simple energy balance. A steady-state flow process (*i.e.* all properties of the system are invariant) was considered. Thus, there was no accumulation or change over time in the energy of the system, and an energy balance was applied. Appendix I shows that the energy required for the incubator to heat to 37 °C was 16.48 KJ/h.

Once the reactor design was defined, the cassette device needed a series of experiments to evaluate performance. First, tests were carried out to confirm appropriate reactor characteristics (*i.e.* size of internal structures and capacity of stirring). Second, mixing and oxygen transfer for the centrally fixed and free-rotating bar were described.

3.1.1.2 Measurement of the Reactor Internal Structures

The reactor internal structures needed verification of variances in fabrication during the milling procedure. With milling, structures of ~50 µm are possible although the accuracy of fabrication below this value is questionable due to changes in polycarbonate stock thickness, variations due to stock fastening technique (adhesive tape) and zeroing the tool in the z axis (Kirk 2013).

The central post (Fig. 3.6a) for the centrally fixed bar, the recess for optical sensors (Fig. 3.7a) and the microfluidic channel (outlet) next to the reactor chamber (Fig. 3.7b) were measured with an optical interferometer. Additionally, the internal diameter and the depth of the ring of the centrally-fixed stir bar (Fig.

3.8b) were also measured to verify any deviations from the design values and to confirm variances in fabrication indicated by the manufacturer (1.4 mm ± 0.1 for the diameter and 0.5 ±0.05 mm for the depth).
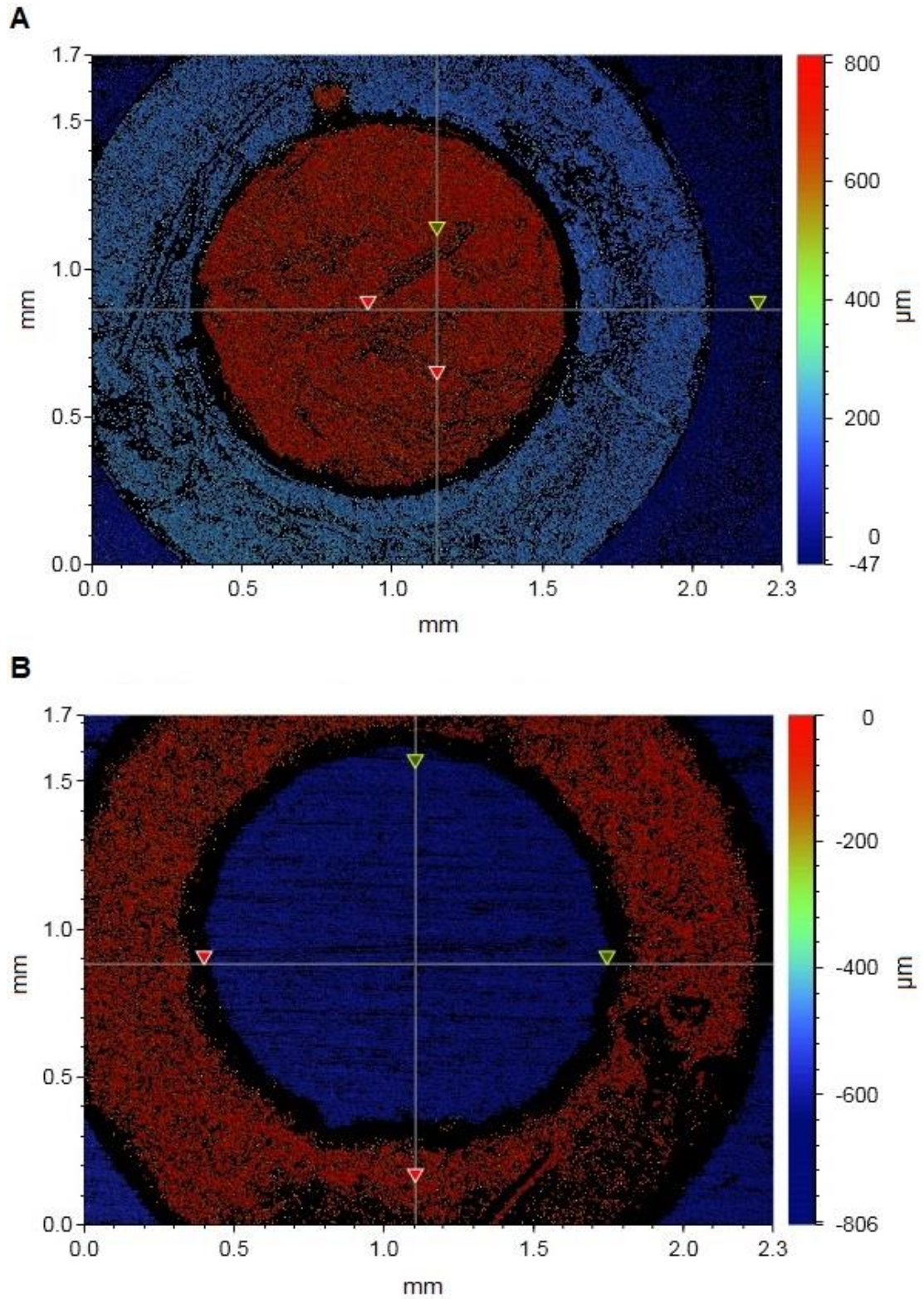
Figure 3.6. Interferometer measurements of the central post (A) and the ring of the stir bar (B). Diameter and depth for both structures were measured. For the ring, the internal diameter was considered. The coloured bar at the right of both figures represents the Z axis (depth). For the central post, Z=0 was the bottom surface of the chamber. For the stir bar, Z=0 was the top surface of the bar. Green and red triangles are cursor points for measurement along the X and Y axis using the software Vision64 part of Contour GT-K Optical Microscope. n=1 measurement per structure.
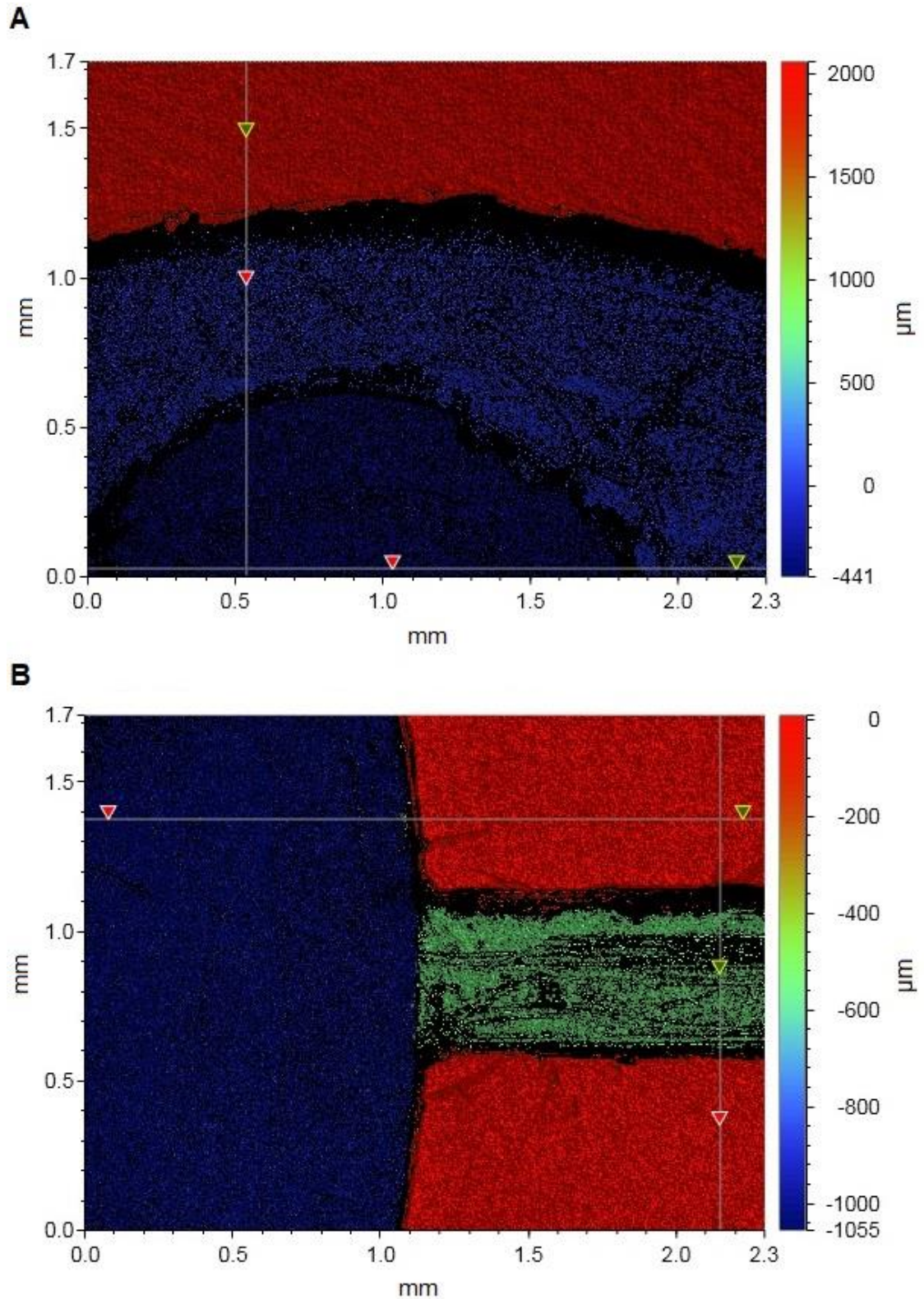
Figure 3.7. Interferometer measurements of the recess (A) and the outlet channel (B). Diameter/width and depth were measured for both structures. The coloured bar at the right of both figures represents the Z axis (depth). For the recess, Z=0 was the bottom surface of the reactor chamber. For the channel, Z=0 was the top surface of the reactor body. Green and red triangles are cursor points for measurement along the X and Y axis using the software Vision64 part of Contour GT-K Optical Microscope. n=1 measurement per structure.

Optical metrology technology allowed high-resolution measurements of the reactor internal structures. Interferometric microscopes enhance the resolution of the images obtained with an optical microscope due to holographic registration of several partial images. Every image is the recording of a light field (hologram). When several images are combined, a composite image with a resolution much greater than what could be obtained with a conventional optical system is created (Schwarz *et al* 2003).

In laser microscopy, a laser beam is split into two beams, one of them directed to the object of measurement and the other one used as a reference. The interferometer thus required of a reference value for the depth direction (z=0) before measurement. The reference plane was defined as either the top surface of the reactor body or the bottom of the reactor chamber.

Table 3.1. shows a good comparison between designed and measured values for the reactor internal structures. The greater differences between design and measurement were found for the stir bar. The smaller internal diameter of the stir bar could have affected its positioning in the central post, and subsequently the rotation of the bar. This was not the case in practice as the tiny 0.041 mm difference between the bar and the central post did not affect rotation of the bar. Similarly, the extra 0.035 mm in the depth of the recess did not affect the positioning of the oxygen sensor.

Measurements of the central post and the recess were performed before and after thermally bonding the reactor body to the lid. No differences in measurement were observed before and after the bonding which proved that two hours at 135°C and 45 N·m did not damage or changed the internal structures of the reactor.

Table 3.1. Interferometer measurements and design values for different internal structures of the microbioreactor cassette. n=1 measurement per structure. Reactor characterized was used later in fermentation experiments.

Structure	Design value (mm)	Measured value (mm)
Central post (diameter)	1.280	1.302
Central post (height)	0.800	0.822
Stir bar (internal diameter)	1.400	1.343
Stir bar (depth)	0.500	0.564
Sensor recess (diameter)	2.200	2.220
Sensor recess (depth)	0.300	0.335
Outlet channel (depth)	0.510	0.549
Outlet channel (width)	0.510	0.504

Measurements of the central post and the recess used as a reference plane the bottom of the reactor chamber. Measurement of the channels was carried out before bonding the reactor body to the lid. The reference plane was the top surface of the reactor body.

3.1.1.3 Confirmation of the Rotational Speed of the Magnetic Bars

Coupling between the magnetic bars and the stirrer motor needed confirmation. It was thought that factors such as friction forces at the bottom of the reactor, friction between the central post and the magnetic bar, or the gap (5 cm) between the motor shaft's tip and the magnetic bars could have influenced the mixing.

The set-up (Fig. 3.8) designed for the confirmation of the coupling included a high-speed camera at the top of the reactor. A digital multimeter was connected to the speed output of the motor electronics to monitor the rotational speed of the motor's shaft. The multimeter measured the frequency of digital signals (high/low) sent as six output pulses per mechanical revolution of the shaft. This allowed the calculation of the actual speed of the motor's shaft using Equation 3.3.

$$n_{actual} = 10 \cdot f_{monitored}$$

Equation 3.3

Where n_{actual} is the speed of the motor's shaft (rpm) and $f_{monitored}$ is the frequency at the speed monitor output (Hz).

Once the actual speed of the motor shaft was known, a comparison with the rotational speed of the magnetic bars was possible. The following rotational speeds were chosen to check the rotation of the magnetic bars: 0, 200, 580, 850 and 1350 rpm.
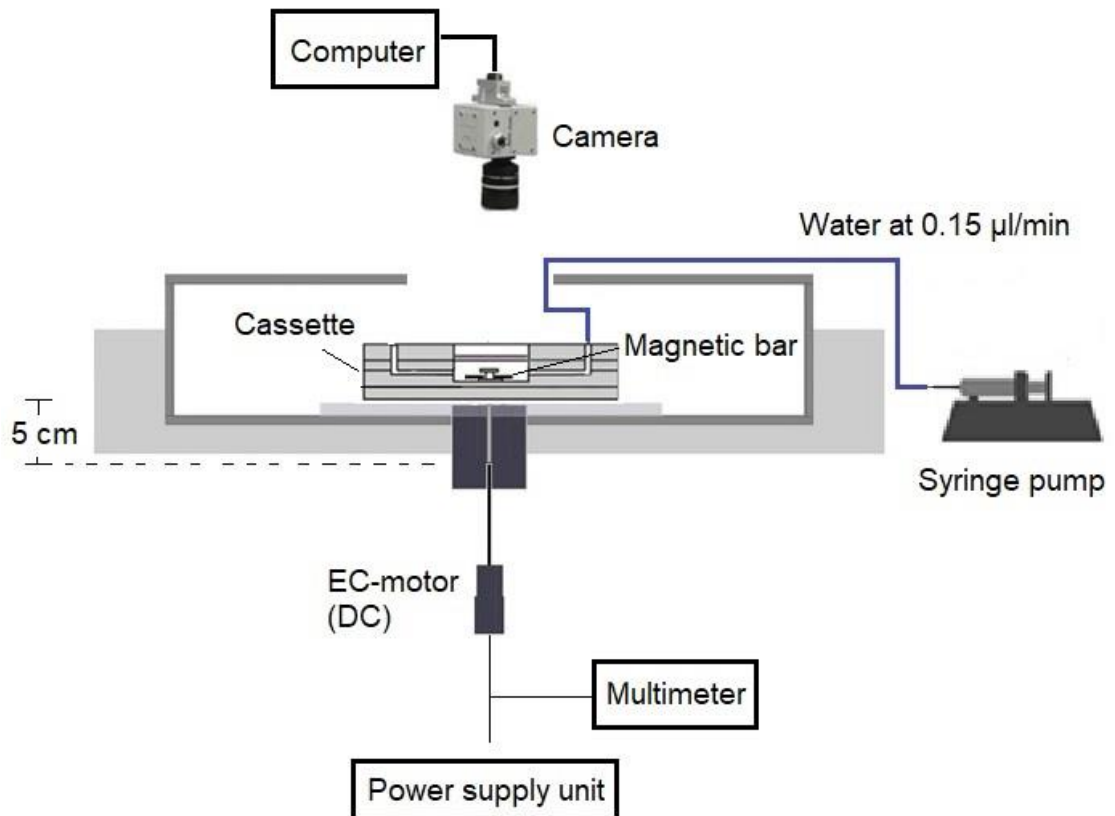
Figure 3.8. High speed camera set up for the confirmation of the coupling between the magnetic bars and the stirrer motor. A power supply unit was used to activate the motor and the magnet. A digital multimeter was used to monitor the rotational speed of the motor's shaft. Water was pumped to mimic reactor operational conditions during fermentation (evaporation control). Electronically Commutated (EC) motor was powered by direct current (DC).

Rotational speeds below 200 rpm were not possible due to limitations in accuracy of the speed controller of the motor. Rotational speeds higher than 1350 rpm were not possible due to wobbling. Excessive vibration beyond 1350 rpm was attributed mainly to the high speeds, since the magnetic bar and the motor's tip were aligned center to center.

The distance (5 cm) between the motor shaft's tip and the magnetic bars could have had an effect on the loss in the magnetic bar's balance. Nevertheless, keeping this distance as part of the set-up design was needed to ensure appropriate bending of the optical fibers (inside fiber holder).

High speed camera videos (Fig. 3.9) showed excellent coupling between the magnetic bars and the motor (Fig. 3.10) confirming that friction forces did not affect the rotation of the stirrer bars.
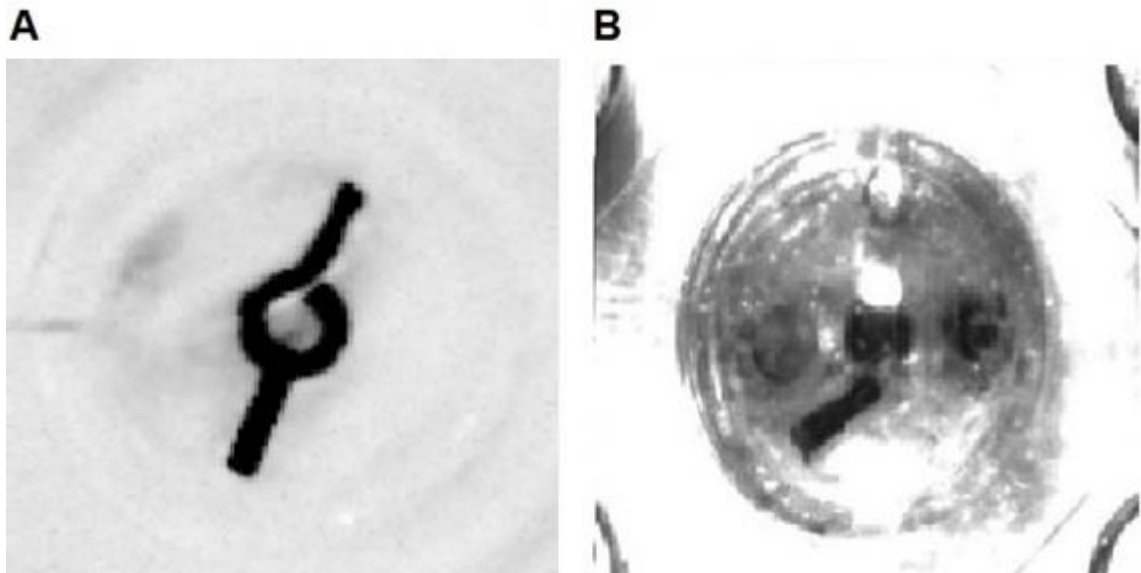
Figure 3.9. High-speed photos of (A) Centrally fixed bar and (B) Free-rotating bar. Light conditions created contrast between the floor of the reactor and the magnetic bars, allowing the counting of the rotation of the bars. Capture rate was 250 frames per second (fps) and shutter speed 1/4000 s. Original resolution of the images was 512x512.
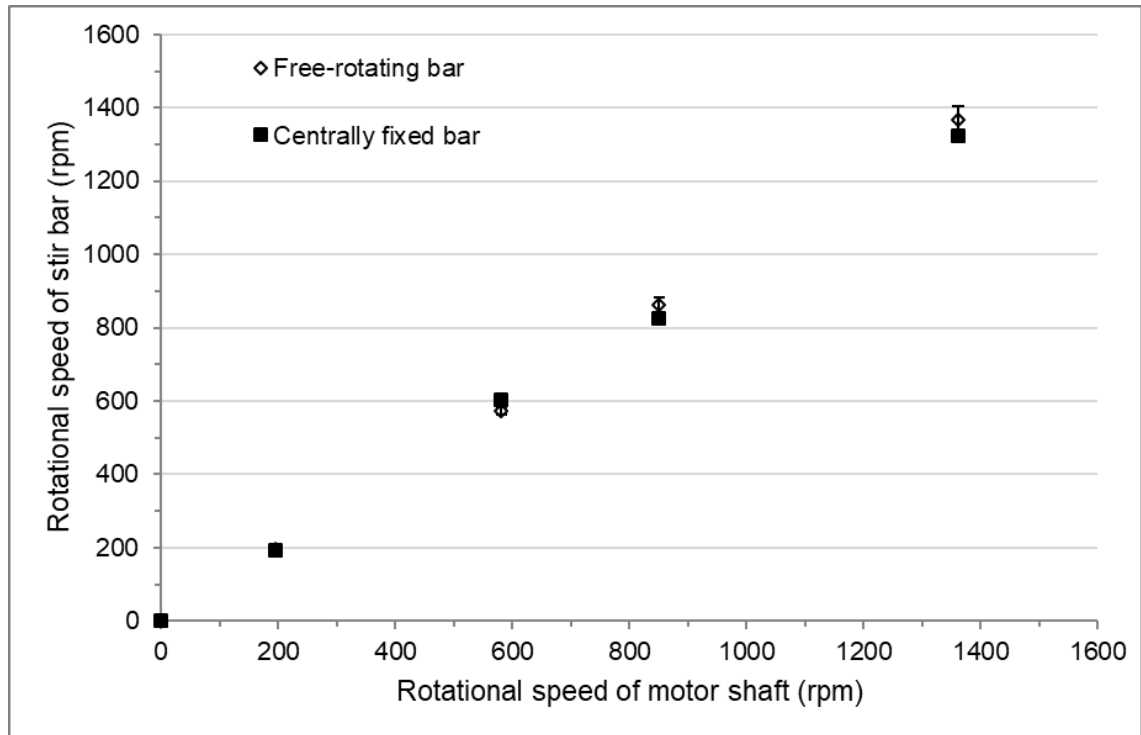
Figure 3.10. Coupling between rotation of stir bars and rotation of the motor's shaft (mean ± 1 standard deviation). The rotational speed of the motor's shaft was determined using a digital multimeter. The rotational speed of the magnetic bars was determined from high-speed videos. n=3 repetitions per rotational speed tested.

The actual rotational speed of the magnetic bars was determined by analysis of the videos with specially dedicated software PFV Fastcam Viewer. The software allowed decomposition of the videos into still images. When playing the images at very low rates (*e.g.* 25 frames per second) it was possible to visually count the number of rotations of the bars over time. The contrast between the stirrer bar (dark) and the bottom of the reactor chamber (clearer) facilitated the counting. Alternatively, for the centrally fixed bar which had a defined motion, it was possible to write a simple MATLAB™ script to count the rotation of the bars by focusing on the position of the tip of the bar with respect to the bottom corner of the reactor (Appendix 2). Results were very similar in both cases.

Standard deviations at 1350 rpm were the highest with +- 36 rpm for the free-rotating bar and +-17 for the centrally fixed bar. This represents a 2.7 % and 1.26% difference with respect to the nominal value (1350 rpm), respectively.

3.1.1.4 Evaluation of Mixing and Oxygen Transfer

Once confirmation of the reactor characteristics was performed, the centrally fixed stir bar (Fig.3.11a) and the free-rotating stir bar (Fig.3.11b) were evaluated. Typically, the flow regime is characterized with the Reynolds numbers which was the first part of the evaluation. Second, the volumetric oxygen transfer coefficient (k_La) was determined for both stirring methods.
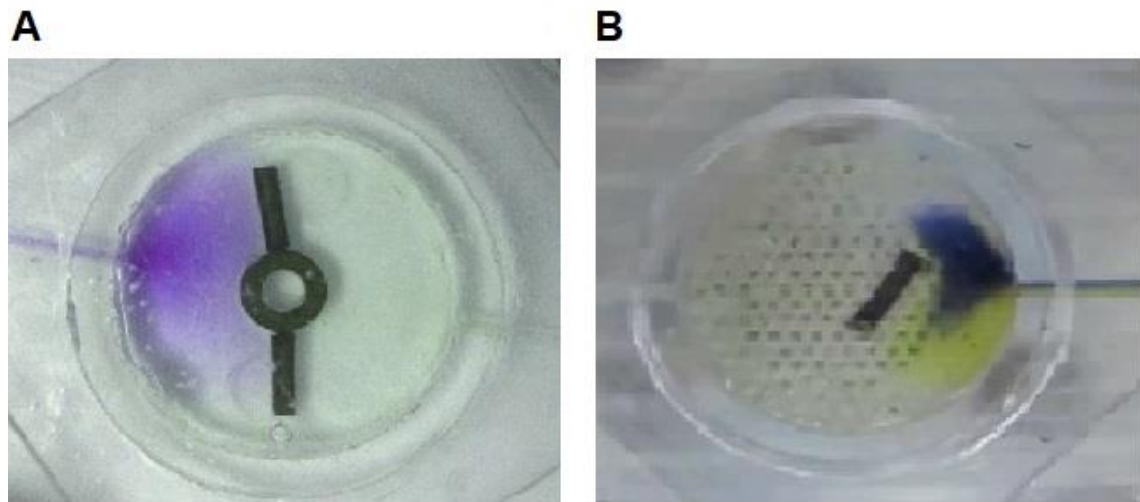
Figure 3.11. Mixing methods used with the microbioreactor cassette (A) Centrally-fixed bar and (B) Free-rotating bar. Dyes were used for the visualisation of mixing in each image. For the free-rotating bar the grid structure supporting the aeration membrane is shown.

Determination of Reynolds Number

When the cylindrical chamber of the reactor is stirred by the centrally fixed bar, the characteristic dimension is the diameter (D) of the stirrer bar. The maximum velocity of the bar relative to the fluid is (ND) where N the rotation speed. With this, Reynolds numbers (Re) for the centrally fixed bar were calculated as:

$$Re = \frac{D^2 N \rho}{\mu}$$

Equation 3.4

Notice that D is the length of the magnetic bar from arm to arm, μ the viscosity coefficient and ρ the density of the fluid.

Considering the viscosity of water at 37 °C (temperature of operation) as 6.9 x 10^{-4} Pa·s, the density of water as 993 kg·m^{-3} (International Association for the Properties of Water and Steam 2017)), Reynolds numbers for different stirring speeds were calculated (Table 3.2).

Table 3.2 Reynolds numbers[*] in the microbioreactor cassette for different stirring speeds of the centrally fixed bar

Stirring speed (rpm)	Reynolds number
200	173
580	501
850	734
1350	1166

[*] Reynolds numbers were calculated with the properties of liquid water at 37 °C

As expected, Reynolds numbers showed that convective inertial forces dominate over the viscous forces. Reynolds numbers ranged between the laminar and transitional flow regime in stirrer-tank reactors (Bin 1984; Blanch and Clark 1996). The values depend on the viscosity, which for fermentation media was measured using a rotational rheometer and shown to be a 15% percent higher than water. Reynolds numbers calculated with fermentation media were therefore slightly lower (~ 13%) for each stirring speed condition.

Mixing behaviour using the free-rotating bar is naturally more complicated and difficult to predict. The free-rotating bar follows a complex movement pattern where the bar rotates not only around its own axis but also move around the bottom of the reactor. Therefore, several components of velocity exist, including components of velocity in the *x* and *y* direction of the chamber.

Two assumptions were made to estimate Reynolds numbers for the free-rotating bar. First, that the fluid flow follows the maximum velocity of the bar relative to the fluid (*i.e.* the tip velocity) and second, that the characteristic dimension is perpendicular to the flow, which means that the flow 'grows' in the direction of the characteristic dimension. The second is the case for well-known examples of the calculation of the Reynolds numbers such as flow in a circular pipe where the internal diameter is the characteristic dimension.

With these assumptions, Reynolds numbers were calculated for the free-rotating bar similar than for the centrally fixed bar, with the diameter (*D*) as the characteristic dimension and *ND* as the velocity. Using Equation 3.4 for the free-rotating bar and considering a 3 mm diameter, Reynolds numbers ranging for 43 (200 rpm) to 291 (1350 rpm) were calculated, which falls in the laminar flow regime.

Notice that the first assumption would not be valid if the bar would move around the chamber more rapidly than it moves around its own axis. In this case, it would be necessary to track the movement of the bar around the chamber to calculate the maximum velocity, which could be performed using video analysis software.

In large scales, mixing is due to convective inertial forces. Therefore, high Reynold numbers (>10000) and turbulent conditions are associated with good mixing. In the microscale, although convective forces can provide active mixing,

Reynolds numbers are much lower due to the small dimensions. Mixing *via* diffusion, however, plays an important role and the general aim is to achieve efficient mixing with low Reynolds numbers.

Determination of Power Number

Electrical power was used to drive the stirring bars in the reactor. This raised the question of how much power was used to drive the stirring bars and create mixing.

Fig. 3.12. can be represented in terms of how much voltage needs to be applied to the armature of the motor to achieve a certain rotational speed of the shaft (and subsequently a certain rotational speed of the magnetic bars). Fig. 3.12 shows that the voltage applied to the armature of the motor is linearly correlated with the rotational speed of the magnetic bars. This was consistent with the information provided by the manufacturer, which indicates a linear relationship between the input voltage and the speed of the motor's shaft as:

$$n_{target} = V_{input} \cdot 600$$

Equation 3.5

Where n_{target} is the desired rotation speed and V_{input} the input voltage. Equation 3.5 is valid between 200 and 6480 rpm according to the manufacturer.
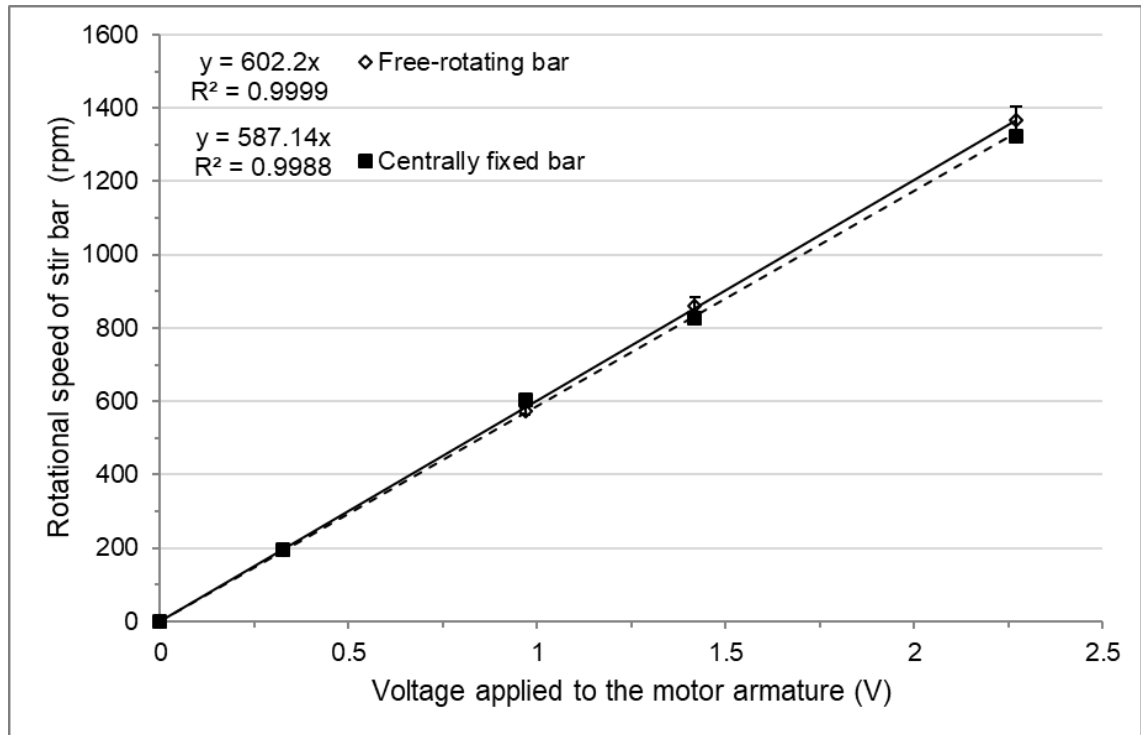
Figure 3.12. Correlation between voltage input and rotational speed of stir bars (mean±1 standard deviation). Linear regression confirms information provided by the manufacturer. The amount of voltage applied was measured using a power supply unit. n=3 repetitions per voltage value tested.

Since the effect of friction forces is almost negligible, the power to drive the magnetic bars is essentially the power required to drive the motor's shaft.

The output mechanical power (*i.e.* the amount of work that the motor does) can be calculated as Equation 3.6.

$$P_{out} = T \cdot \omega$$

Equation 3.6

Where ω is the angular velocity (rad/sec), T is the torque (($N \cdot m$)) and P_{out} the output power (Watts). (Simple Motors 2015).

Additionally, the angular velocity ɯ can be calculated as:

$$\omega = \frac{2 \cdot \pi \cdot N}{60}$$

Equation 3.7

Where N is the rotational speed of the motor's shaft in rpm.

The torque T can be calculated using the concept of efficiency of the motor E as:

$$E = \frac{P_{out}}{P_{in}}$$

or

$$P_{out} = E \cdot P_{in}$$

Substituting Equation 3.6 and considering $P_{in} = I \cdot V$

$$T \cdot \omega = I \cdot V \cdot E$$

Substituting Equation 3.7

$$T = \frac{I \cdot V \cdot E \cdot 60}{2 \cdot \pi \cdot N}$$

Equation 3.8

Where I is the current (Ampere) , V the voltage input and E the efficiency of the

motor.

Finally, the Power number (N_P) can be calculated using Equation 3.9.

$$N_P = \frac{P_{out}}{\rho N^3 D^5}$$

Equation 3.9

Where ρ is the density (Kg/m^3) and D the diameter of the impeller (m).

The calculation of the power number requires the value of the power output which at the same time requires the value of the torque. Calculation of the torque (Equation 3.8) assumes a value for the efficiency of the motor. The maximum reported efficiency for the miniature electric motor EC 32 is 54%. Considering this and a nominal current of 560 mA (0.56 A), the density of water at 37 °C as 993 kg·m^{-3} and the length of the centrally fixed stir bar as 6 mm (0.006 m), the torque, power outputs and power numbers for different voltages input values were calculated and indicated in Table 3.3.

For the free-rotating bar, assuming the fluid motion follows mainly the tip of the bar, all power numbers can be similarly calculated as shown in Table 3.4.

Table 3.3. Power output, power number and other parameters for the microbioreactor cassette using the centrally fixed bar at different stirring speeds.

Voltage input (Volts)	Rotational* speed motor (rpm)	ω** (rad/s)	Torque ($N \cdot m$)	Power output (W)	P_{out}/V*** (mW/µl)	Power**** number
0.33	200	21	0.005	0.10	0.64	1.63
0.97	580	61	0.005	0.29	1.86	0.19
1.42	850	89	0.005	0.43	2.73	0.09
2.25	1350	141	0.005	0.68	4.33	0.04

* Rotational speed of the motor was calculated using Equation 3.5. Equation was provided by the manufacturer (Maxon Motor 2017) for the motor version EC-32. The relationship is valid between 200 and 6480 rpm.

** Angular velocity. Calculated according to Equation 3.7.

***P/V is power per unit of volume. Where P_{out} is power output (milliwatt) and V the reactor volume (microliters).

**** Power number was calculated using Equation 3.9.

Table 3.4. Power output, power number and other parameters for the microbioreactor cassette using the freely rotating bar at different stirring speeds.

Voltage input (Volts)	Rotational[*] speed motor (rpm)	ω[**] (rad/s)	Torque ($N \cdot m$)	Power output (W)	P_{out}/V[***] (mW/µl)	Power[****] number
0.33	200	21	0.005	0.10	0.64	55.3
0.97	580	61	0.005	0.29	1.86	5.55
1.42	850	89	0.005	0.43	2.73	3.15
2.25	1350	141	0.005	0.68	4.33	1.23

Noticeably, an inverse relationship between the power number and the Reynolds numbers was found (Fig. 3.13) .This data is similar to the correlations developed by Rushton *et al* for Rushton turbines, marine impellers and paddles in bench-scale bioreactors (Rushton 1950) where an inverse relationship between power number and Reynolds numbers was found.
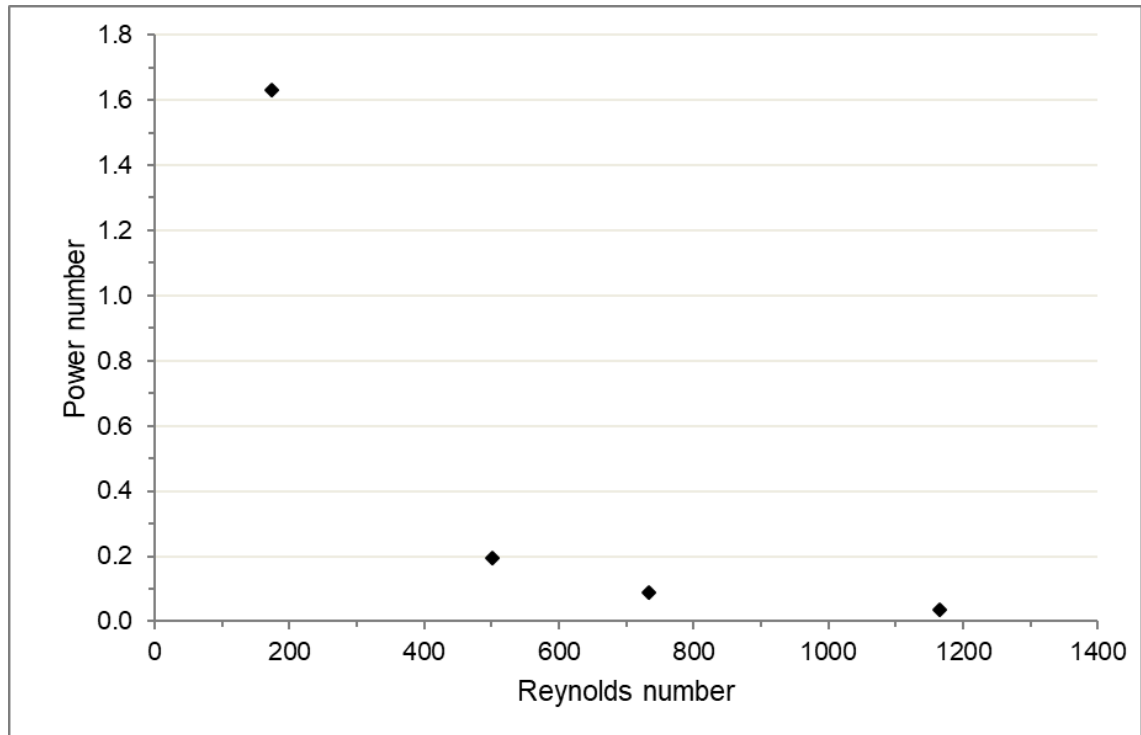
Figure 3.13. Relationship between power number and Reynolds number in the microbioreactor cassette with the centrally fixed bar as mixing mechanism. Power number was calculated using Equation 3.9 and Reynolds numbers using Equation 3.4.

Finally, Table 3.3 also indicates the ratio between the power output and the volume of the reactor or P/V. P/V is one of the most used criteria for the scale-up of cell culture processes (Platas Barradas 2011; Marques *et al* 2010; Doran 1995:154) and will be discussed in chapter 5.

Determination of K_La

Oxygen is a key substrate that needs to be homogeneously distributed for microbial consumption. If the same membrane thickness (100 μm) is used in the microbioreactor, variations in the oxygen transfer coefficient will depend exclusively on the mixing method employed and how well the liquid phase is mixed. The variation of k_La with the mixing method was then thought as a deciding factor to choose between the free-rotating bar and the centrally fixed bar.

Before starting k_La experiments, the optical sensor response time needed to be determined (Fig. 3.14). Thus, a step experiment where oxygen passed from 100% DO (air saturated water) to 0% DO (liquid solution with sodium sulphate and cobalt nitrate) was carried on in a stirred vessel at 37 °C.
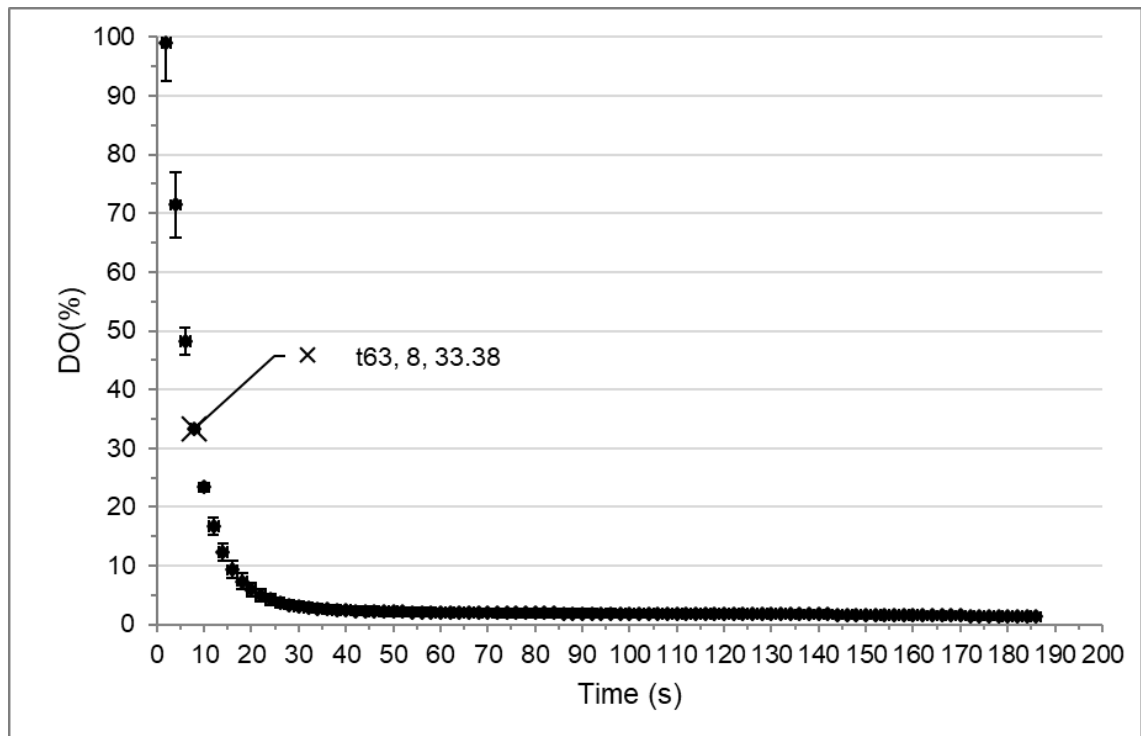
Figure 3.14. Determination of the oxygen sensor response (mean ± 1 standard deviation) at 37 °C. A step experiment where oxygen passed from 100% (air saturated water) to 0% (sodium sulphate and cobalt nitrate) was implemented. Sensor response was 8 s for 63% of the DO % response. n=2 repetitions for the step experiment.

Once the value of the sensor response was determined, Equation 2.1 (Materials and Methods) was used to measure k_La. The set-up for k_La determination (Fig. 3.15) included a rotameter which regulated the volumetric flow of gas that entered to the incubator. The gas entering was approximately 13 L/min which allowed efficient gas transfer. The gassing-out method was employed for k_La measurement. The culture liquid was first stripped of oxygen by flushing nitrogen

into the bulk of the incubator. Then, air was flushed which caused a rise of DO in

the liquid.
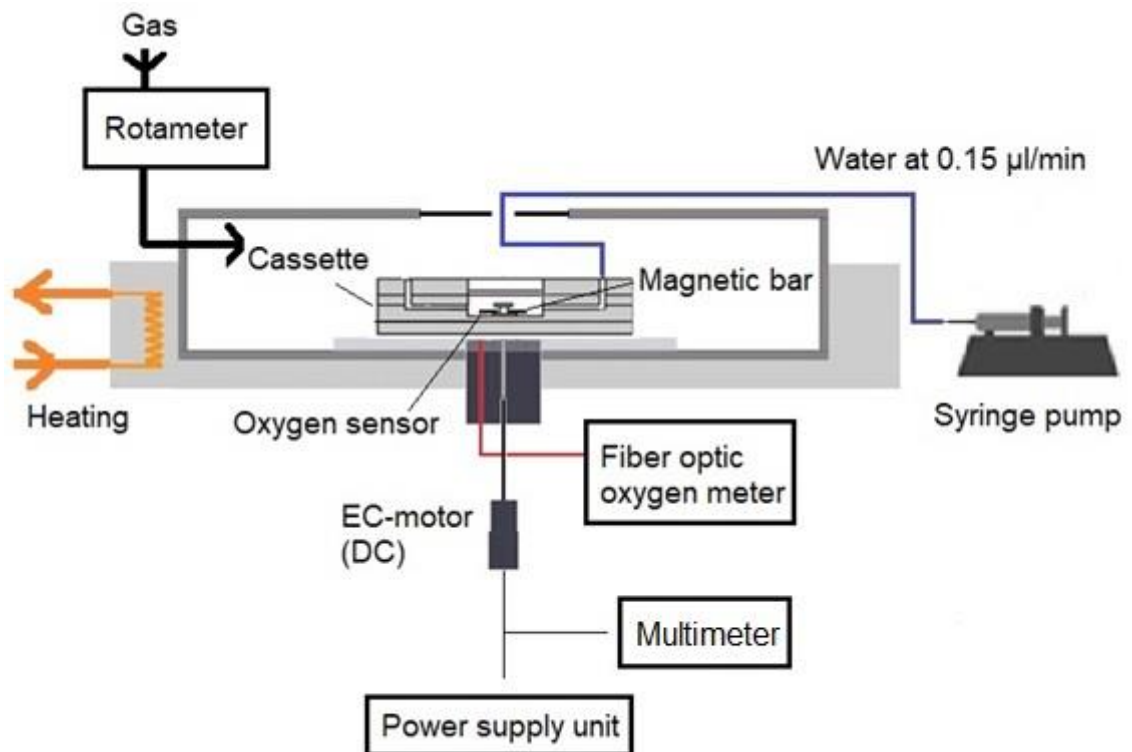
Figure 3.15. Device set up for the determination of the volumetric oxygen transfer coefficient (k_La) at 37 °C using the gassing-out method. Water was pumped to mimic reactor operational conditions during fermentation (evaporation control). A digital multimeter was used to monitor the stirring speed. Electronically Commutated (EC) motor was powered by direct current (DC).

Equation 2.1 included a modification that allowed the calculation of k_La when the

DO concentration at the beginning of the recovery stage was not zero. This

residual DO concentration was incorporated given that in practice it took a very

long time to achieve low DO values in the reactor (below %5), never really

approaching zero.

K_La values increased for both the free-rotating bar and the centrally-fixed bar when higher stirring speeds were used (Fig. 3.16). There was an important difference between k_La values (observed difference (between 40% (200 rpm) and 52% (1350 rpm)) observed difference (between 40% (200 rpm) and 52% (1350 rpm)) obtained with both systems for all stirring conditions, which suggested a lower efficiency of mixing for the free-rotating bar.
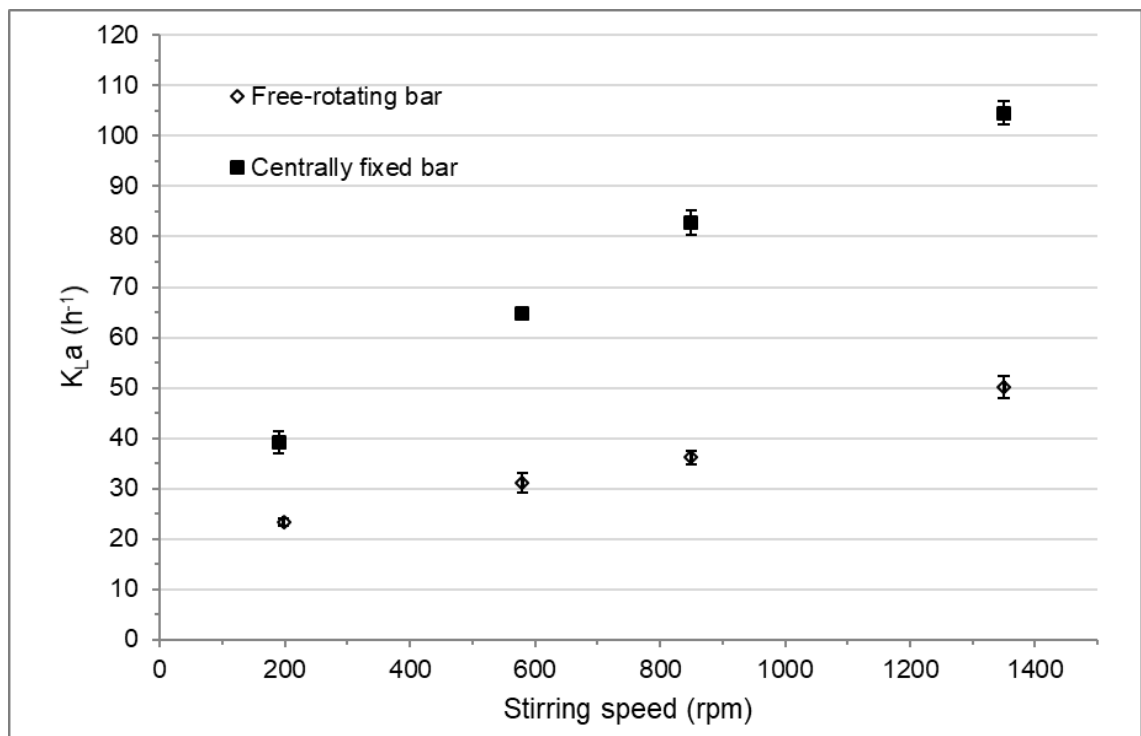
Figure 3.16. Measurements of the volumetric oxygen transfer coefficient (k_La) for the free-rotating bar and the centrally fixed bar in RO water at 37 °C (mean ±1 standard deviation). Aeration membrane was 100 µm thick. Reactor chamber was 2mm depth. n=3 measurements per stirring speed tested.

Mixing behaviour using the centrally fixed bar was simulated using Computational Fluid Dynamic (CFD) methods (Zhang 2006b). Two components of flow were identified: a horizontal flow in which the tip of the magnetic bar generated a circular mixing pattern (primary flow of high velocity), and a vertical flow which

created a toroidal mixing pattern (secondary flow of lower velocity). Zhang suggested that the component of vertical flow contributed to oxygen transfer from the internal edge of the PDMS membrane (top of the reactor chamber) to the bottom of the reactor (Fig.3.17). Zhang also showed that the secondary flow retained the same features with increases in rotation speeds but the values of flow velocity were higher. This information was not verified for the microbioreactor cassette, although it applies to this study since Zhang used a reactor chamber and a stirring bar of similar dimensions to the ones used here.

The free-rotating bar was designed to improve mixing in the horizontal direction. The method eliminates stagnant zones at the bottom corners of the reactor and keep cells in suspension, decreasing the sedimentation of strains such as *Saccharomyces cerevisiae* at the walls of the reactor (Schäpper *et al* 2010). Nevertheless, k_La measurements suggest that the method does not improve mixing in the vertical direction and therefore oxygen transfer. Additionally, since the free-rotating bar is shorter in diameter (3 mm) compared to the centrally-fixed bar (6 mm), the toroidal pattern of mixing with the vertical component of flow was probably not fully generated (or not generated with the same intensity as with the centrally fixed bar). This because the flow velocity depends on the tip speed, which is lower at shorter diameters.

As a final point, Schäpper *et al* 2010 achieved higher k_La values of ~63 h^{-1} using the free-rotating bar and a reactor of the same dimensions. The authors however used a specially dedicated aeration layer in the reactor design to improve oxygen transfer.
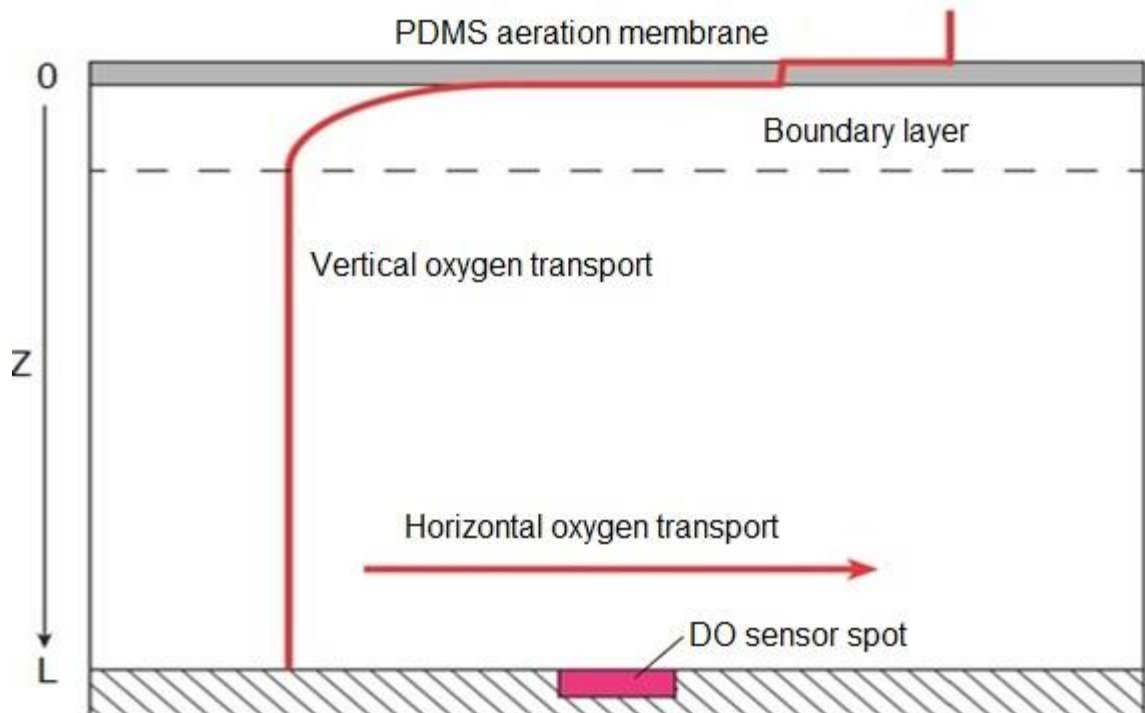
Figure 3.17 Oxygen transport in the microbioreactor chamber. Two concentration profiles are generated (vertical and horizontal). At the interfaces (air/PDMS/liquid) chemical equilibrium is assumed. L is the height of the chamber (2 mm). Adapted from Kirk and Szita (2013).

3.1.2 Suspension Microbioreactor

As mentioned at the start of the chapter the objective of the suspension microbioreactor was to provide a vertical flow capable of maintaining cells indefinitely (or at least for very long periods) in suspension. A reactor capable of vertical flow by aspiration was fabricated using PMMA (Fig 3.18a). The thickness of the chip was 1.5 mm and the volume of the reactor was 150 µL, which allowed direct comparison with the microbioreactor cassette. The chip comprised guiding structures at the bottom designed to hold it on top of an Eppendorf tube used as medium reservoir (Fig. 3.18b).

Transparent PMMA allowed the integration of optical sensors such as oxygen spots (DO). Transparency also provided the potential to add optical fibers for illumination and detection of cells. The reactor was fabricated very rapidly using laser technology (less than 2 minutes). Noticeably, PMMA is not compatible with ethanol which suggested other methods for sterilisation/disinfection (thermal or UV).
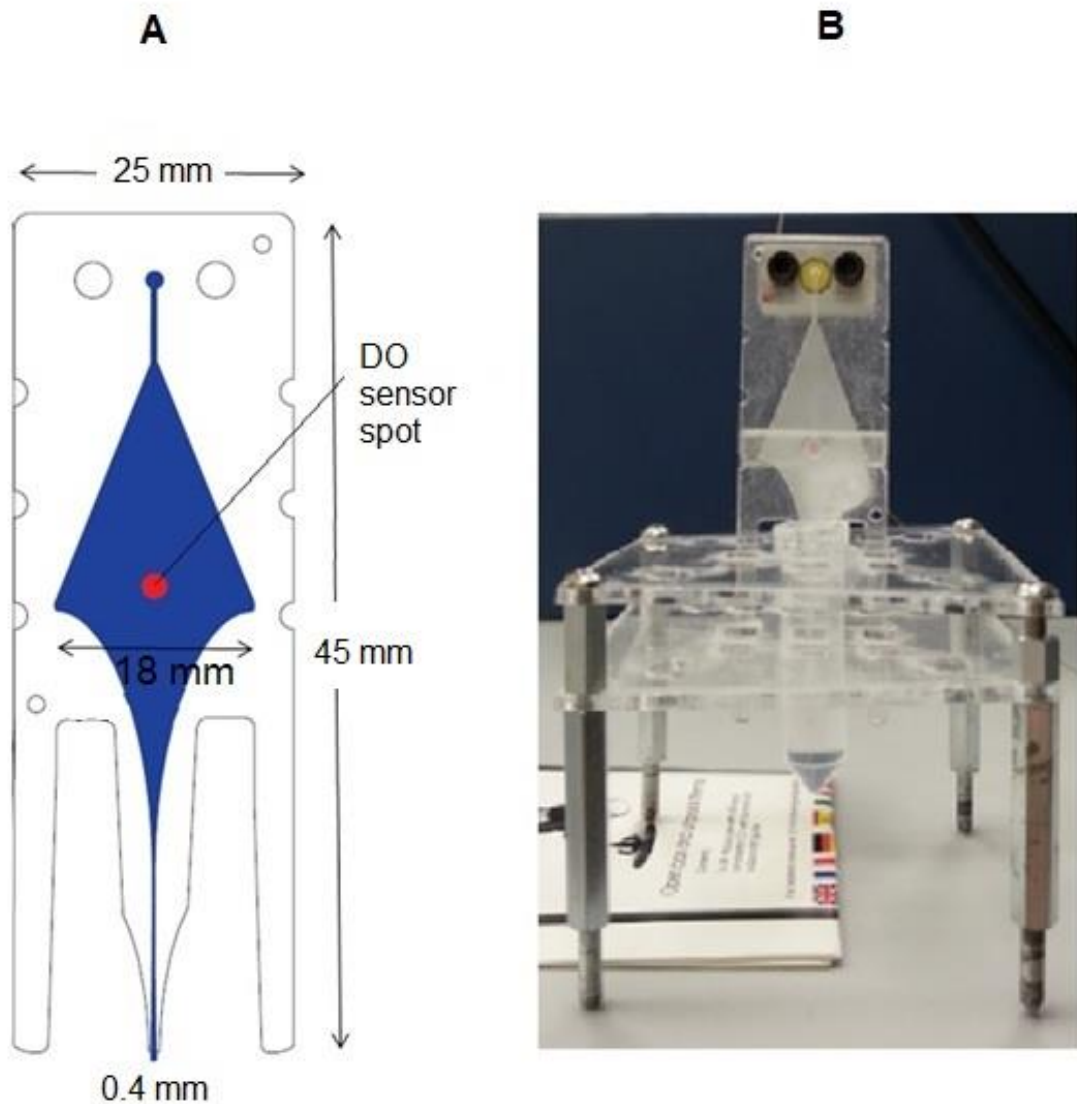
Figure 3.18. Microfluidic suspension reactor stating key dimensions (A). The material of the reactor was PMMA. A dissolved oxygen (DO) sensor (2 mm diameter, 300 μm depth) was placed in the centre of the reactor. (B) Suspension microbioreactor on top of guiding structures and feed reservoir.

The general concept of design was based on the Hele-Shaw Chamber where the width of the reactor is much larger than the depth. The widest section of the chamber was 18 mm, and the depth was 200 μm. The shallow chamber was designed to provide enough shear near the walls to lift cells.

The concept of operation was that cells will be suspended at a given height of the chamber where the average flow speed is equivalent to the sedimentation speed.

The chamber was designed with a variable width so cells of different size (or cell aggregates) will be suspended at a given height. Cells of a large size or cell aggregates will sediment at the entrance of the chamber (where the flow is the highest) and smaller cells will be suspended at the widest section (where the flow is the lowest).

The sedimentation speed of cells depends on the size and the buoyancy. Under the assumption of cells as perfect spheres immersed in liquid, the sedimentation velocity was derived using the Stoke's law for the frictional force in a viscous fluid. The final expression for the sedimentation velocity (reached when the frictional force combined with the buoyant force balances the gravitational force) is given by Equation 3.1 as:

$$v_s = \frac{2}{9} \cdot \frac{(\rho_p - \rho_f)}{\mu} \cdot g \cdot R^2$$

Equation 3.1

Where g is the gravitational acceleration (m·s^{-1}), R is the radius of the spherical particle, ρ_p is the mass density of the cells (kg·m^{-3}), ρ_f is the mass density of the fluid (kg·m^{-3}) and μ is the dynamic viscosity (Pa·s).

Considering the viscosity of water at 37 °C (temperature of fermentation) as 6.9 x 10^{-4} Pa·s, the density of water as 993 kg·m^{-3} (International Association for the Properties of Water and Steam 2017), the density of cells as 1160 kg·m^{-3} (Godin M *et al* 2007), g as 9.831 m·s^{-1}, and a particle of 1.5 μm such as *Staphylococcus carnosus* (Schliefer and Fischer 1982) or *Escherichia coli*, the sedimentation velocity is approximately 0.3 μm/s.

In addition, the required flow velocity to suspend cells in the chamber is equal to the sedimentation velocity. For a flow rate F, the flow velocity can be related to the width (w) and depth (d) of the chamber as:

$$v_f = \frac{F}{w \cdot d}$$

Equation 3.2

Considering $v_f = v_s$ and for a width of 18 mm and a depth of 200 μm, the flow velocity required to suspend cells of 1.5 μm diameter is: 0.06 μL/min.

Operation of the suspension microbioreactor

The designed protocol to use the suspension microbioreactor (Fig. 3.19) involved inoculation using the feed reservoir underneath the reactor. The reactor was designed so very few cells will grow in the widest section of the chamber. At the same time, the narrow entrance was designed to ensure no cells were lost in the culture phase.
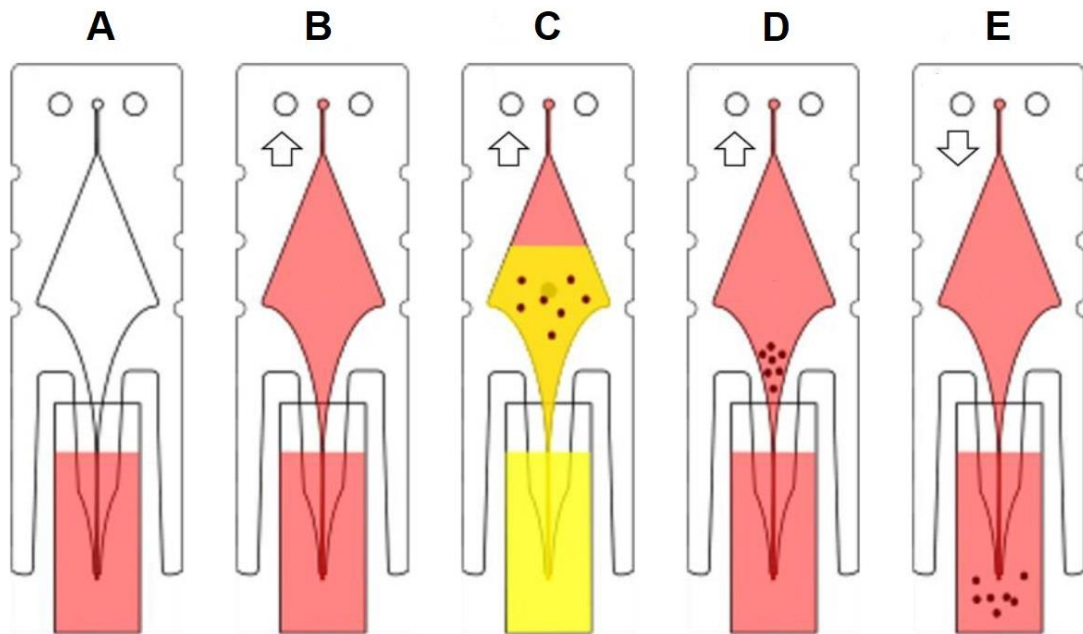
Figure 3.19. Operation of the microfluidic suspension bioreactor. (A) The reactor inlet is immersed in medium. (B) The reactor is primed with medium (C) the reactor is inoculated with cells (D) the reactor is perfused with fresh media at the sedimentation flow rate (E) Cell culture is finished and cells are recovered. Image adapted from Renaud 2015.

Analysis of the suspension microbioreactor started with the evaluation of mixing. For this, the measurement of mixing time and residence time distribution were used. After this, exploration of oxygen transfer in the device followed.

3.1.2.1 Evaluation of Mixing

Mixing is an important operation since cells must be kept in suspension and equal access to nutrients must be ensured. As discussed in the introduction (mass transfer and mixing), there are usually two common methods for mixing at the microscale: passive methods and active methods. Active methods involve the use of moving parts whereas passive methods rely on molecular diffusion and chaotic advection.

Passive mixing in the suspension microbioreactor relies on molecular diffusion and advection (transport of matter by flow). This requires large interfacial areas, gradients and diffusion coefficients to achieve good mixing.

Mixing occurs when the fluid flow travels from bottom to top of the reactor. Video records (Fig. 3.20) with allura red dye (4 mM) as indicator showed that the reactor contents get mixed as the fluid (dye) front advances towards the top. Very little vertical mixing occurred and mixing on the horizontal direction depended on the diffusion distances. Thus, mixing was quicker at the bottom part of the reactor (entrance) where the chamber is narrow and the local flow rate was the highest. Mixing by diffusion was slower at the widest part of the reactor.
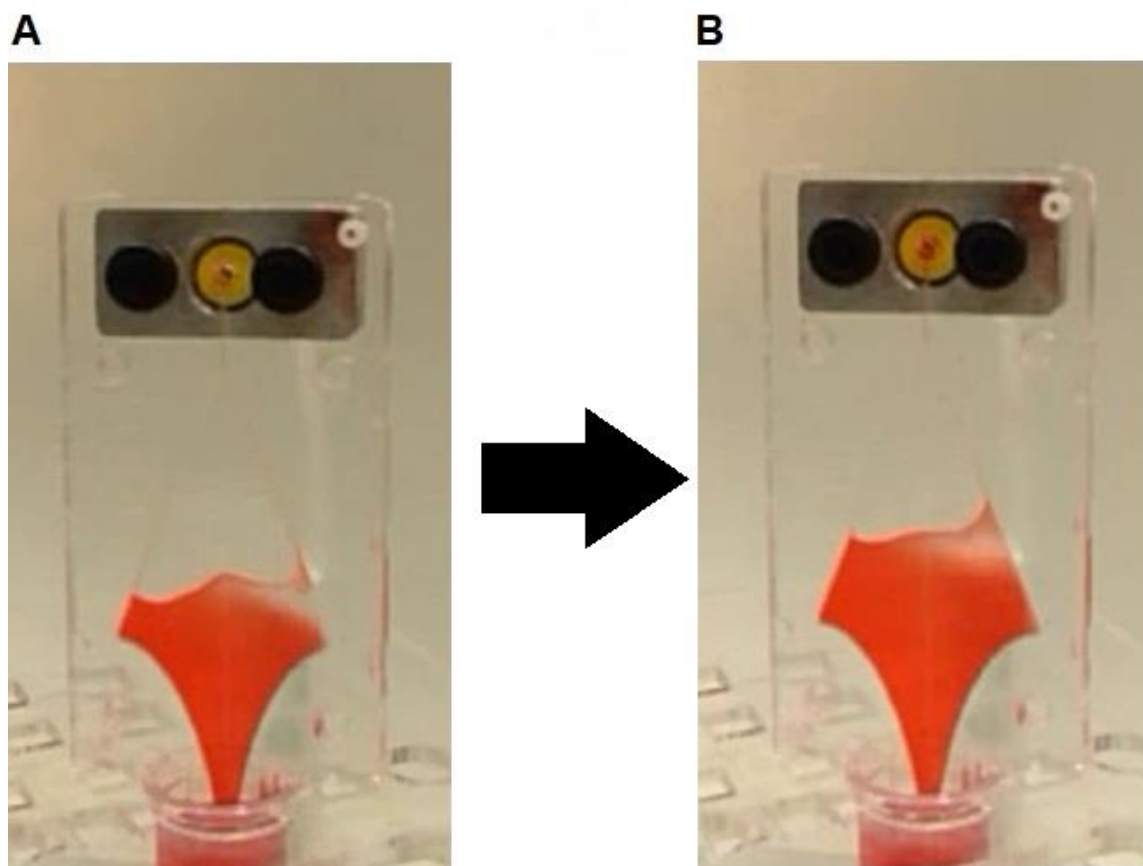
Figure 3.20. Mixing behaviour in suspension microbioreactor. (A) still image at time zero where the dye was flowing towards the top. (B) still image at time two minutes. Allura red 4 mM dye was used for visualisation. The reactor was primed with water before the dye was introduced.

Mixing quality in the suspension microbioreactor can be improved by increasing the flow rate (Table 3.5). This was reflected by an increase in the Reynolds numbers which accounts for magnitude of the convective inertial forces. Reynolds numbers were calculated at the point of the reactor chamber with the largest cross-sectional diameter (18 mm). At this point the lowest velocity was achieved.

Table 3.5. Reynolds numbers and mixing times for the suspension microbioreactor operating at different flow rates. Allura red dye 4 mM was used in the visual estimation of mixing time. n=1 repetition per flow rate tested.

Flow rate (µL/min)	Reynolds number	Mixing time (min)	True residence time (min)
1	0.14	150	150
3	0.28	70	50
5	0.56	30	30
11	1.11	18	13.6
21	2.23	10	7.1

The concept of mixing time can be used as an indicator of the efficiency of the mixing. For the purposes of this study, mixing time was defined as the time required for the complete homogenisation of the Allura Red dye in the reactor chamber. Mixing times were estimated by visual inspection of the reactor contents.

Given the mass transfer characteristics of the system, mixing time was overall slightly higher than the true residence time of allura red in the reactor. The value

of mixing time decreased approximately 93% when the flow rate was increased twice times.

The concept of mixing time as described here provided only a superficial understanding of the mixing process. For this reason, a more detailed study that considered the percentage of stagnant volumes, was performed next.

3.1.2.2 Residence Time Distribution Analysis

One way of describing mixing in the reactor is to consider imperfect mixing and the non-idealities. This is achieved by means of the residence time distribution (RTD) analysis. Residence time distribution is as a function that describes the amount of time an element of fluid spends in the reactor and it is usually applied to diagnose operational problems (Fogler 2006:868; Davis ME and Davis RJ 2003).

For the suspension microbioreactor, the following assumptions were considered valid (Dudukovic and Felder 1983):

- The reactor was at steady state

- Transport at the inlet and outlet took place only *via* advection of materials

- The flow was incompressible

Additionally, the RTD analysis required the insertion of an inert substance into the reactor (tracer). This substance needed to be non-reactive, easily detectable, have physical properties (*i.e.* viscosity and density) like the ones of the liquid mixture, be completely soluble, and not absorb into the reactor walls (Fogler

2006:871). Tryptophan was selected as tracer since it meets all these properties. Tryptophan is soluble in water (solubility of 11.4 g/L at 25 °C as reported by O'Neil 2006a) and has a maximum absorbance in dissolved water at 280 nm (Weast RC, 1979).

A UV area imaging system (ActiPix^{TM} D100 UV) was used to measure tryptophan concentration. A fine glass capillary column at the outlet of the reactor was a central part of the detection unit and allowed the measurement of absorbance by visualisation of the capillary's internal structure.

Before RTD experiments, a calibration curve (Fig. 3.21) was created using a battery of different concentrations of Tryptophan and a concentration in the linear range of measurement was chosen. Linearity between absorbance and tracer concentration was important since it was not possible to measure the tracer directly.
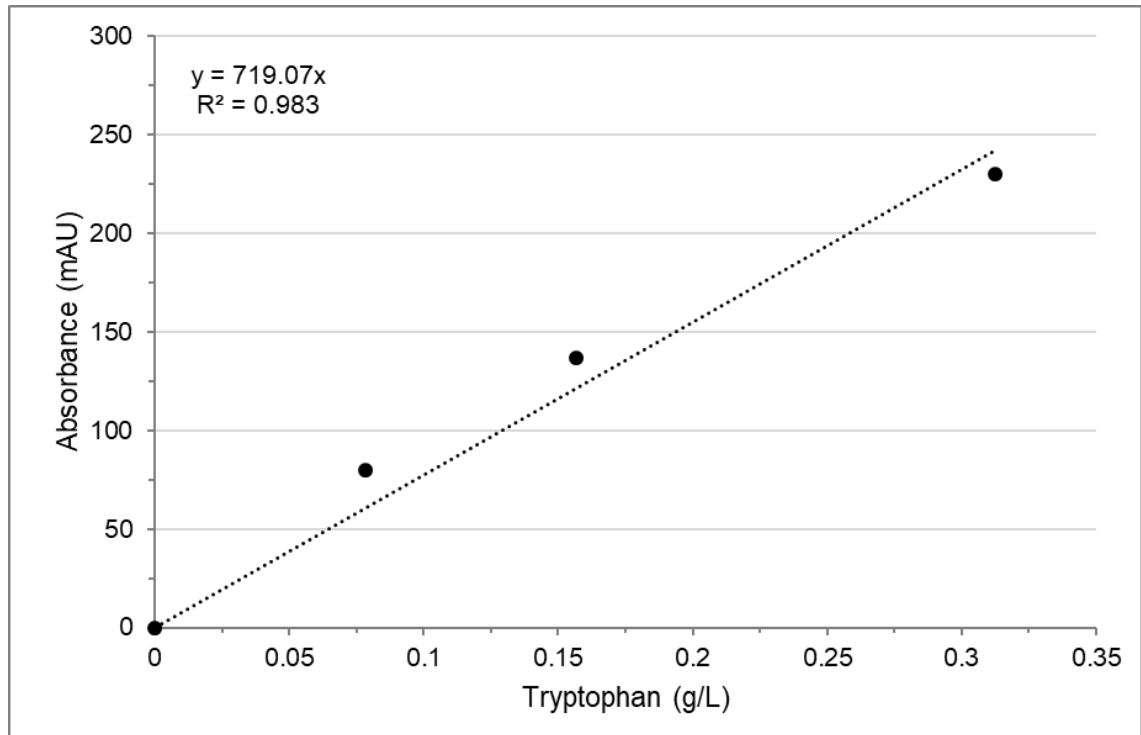
Figure 3.21. Calibration curve of tryptophan for its detection in residence time distribution experiments. Four concentrations of tryptophan were in the linear range of absorbance. n=1 measurement of absorbance per tryptophan concentration.

Absorbance data followed the Beer's law in which absorbance is directly proportional to the concentration of Tryptophan in the sample.

The tracer solution also included a small amount of Allura Red (0.025 g/L or 0.05 mM) which was used for the determination of moment the tracer touched the reactor for the first time.

Two methods were considered for the injection of the tracer in the reactor: the pulse input and the step input. In a pulse input a certain amount of tracer is suddenly injected into the reactor in a very short time, and the outlet concentration measured as a function of time (Fogler 2006:871-872).

The other option was the step experiment. This involves a constant flux of tracer initiated at time zero (Fogler 2006:876). The tracer is pumped until the outlet concentration cannot be distinguished from the inlet concentration.

Step input experiments are normally easier to carry out in laboratory conditions. A step change involves a simple change in the feed stream that is maintained over time. Nevertheless, it is necessary to avoid dilution at the immediate entrance of the reactor. In the set-up for the suspension reactor (Fig. 3.22), this was easy to do since it only involved a quick change of the media reservoir from the priming solution (degassed RO water) to the tracer solution. Thus, the reactor was immediately put in contact with the tracer solution and a true step was performed.
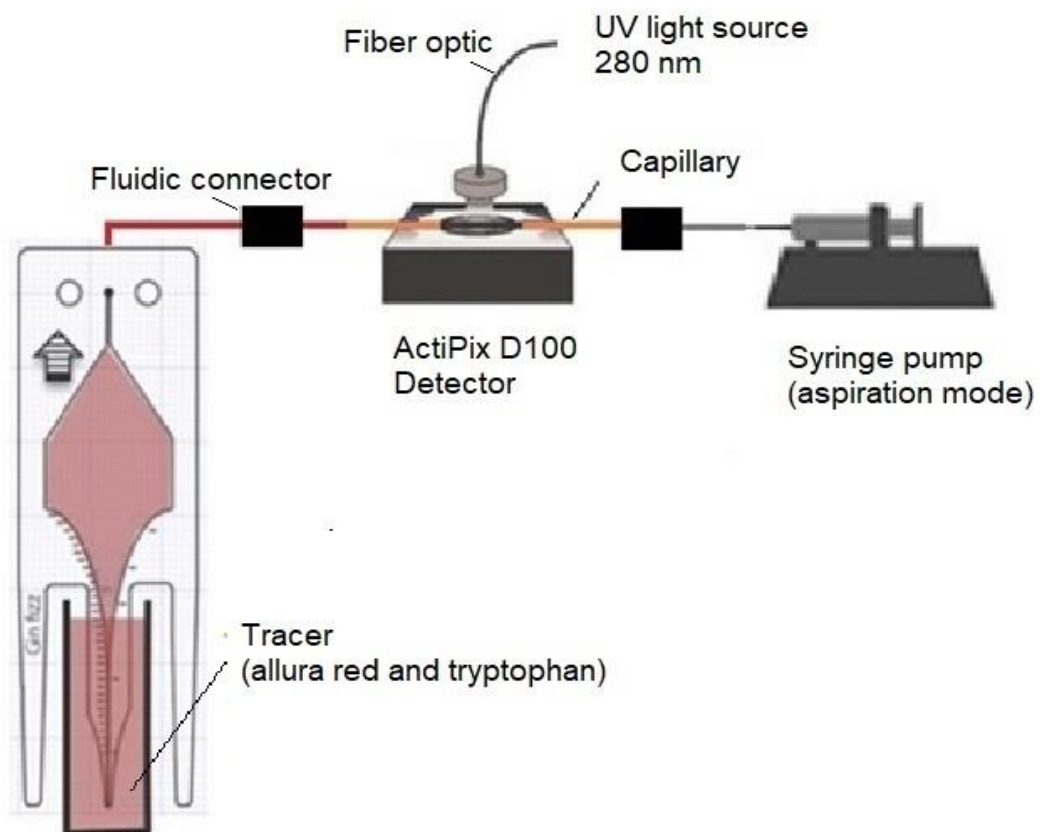
Figure 3.22. Experimental setup for the measurement of residence time distribution in the suspension microbioreactor. The device and outlet pipeline were first flushed with degassed RO water which was used as a base line. After this a tryptophan/allura red solution was used as a tracer. ActiPix D100 UV detector allowed real time detection of tryptophan at 280 nm.

RTD experiments were designed so the liquid was aspirated from the top of the reactor to the capillary tube and read by the UV detector. The reactor was first primed with ethanol 70% to make sure all volumes were 'bubble free'. Following this, the device was flushed with degassed RO water which was used as a baseline.

Absorbance values were determined by the UV detector and converted into concentration values by using the calibration curve. Concentration values were then used to calculate a cumulative distribution function $F(t)$ as Equation 3.10.

$$F(t) = \frac{C(t)}{C_0}$$

Equation 3.10

Where $C(t)$ and C_0 are the concentration of tracer at the outlet of the reactor and at the inlet, respectively.

The cumulative tracer concentration is also called normalised tracer concentration as it represents a fraction of the tracer concentration at the inlet.

Residence time distribution experiments at different flow rates (Fig. 3.23) showed that the time required to achieve a steady concentration of tracer at the outlet of the reactor, after a step input, is inversely proportional to the flow rate employed. Thus, the lower the flow rate the more time was spent in the outlet line (dead volume with no mixing).

Noticeably, the total volume of the system was: reactor (150 µl) + outlet tubing (66 µl) + connector (2 µl). The volume of the outlet line (68 µl) was considered in the analysis.
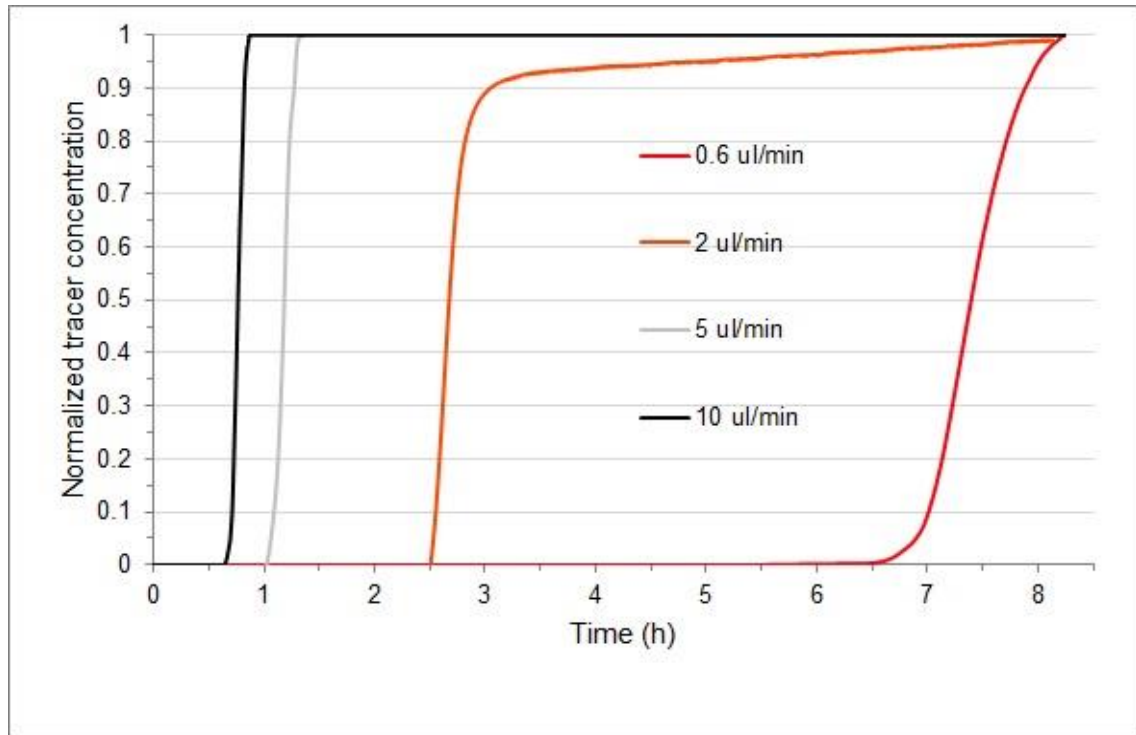
Figure 3.23. Residence time distribution of the suspension microbioreactor at four different flow rates. n=1 repetition per flow rate.

Additionally, the percentage of stagnancy for each flow rate was calculated using Equation 3.8, Equation 3.9 and Equation 3.10.

$$t_E = \int_0^\infty (1 - F(t))$$

Equation 3.8

$$\tau = V/F$$

Equation 3.9

$$PS(\%) = \left[\frac{\tau - t_E}{\tau}\right] \times 100$$

Equation 3.10

Where PS (%) is the percentage of stagnancy, t_E is the apparent residence time, τ is the true residence time (h), V is the reactor chamber volume (150 µL) and F is the aspiration flow rate (µL/min).

The apparent residence time was calculated by using the trapezoid rule for approximating a definite integral for the curve normalized tracer concentration versus time.

Table 3.6 shows the percentage of stagnancy as a function of the flow rate. The data showed that mixing in the suspension microbioreactor is poor with a high percentage of stagnant volumes. Additionally, the number of stagnant volumes decreased as the flow rate increased. Thus, mixing was more efficient at higher flow rates (although the number of stagnant volumes was over 10%).

Microbioreactor data in terms of percentage of stagnancy was also compared to an ideal laminar flow reactor (a long tube with constant diameter) of the same volume. Equations used for the laminar flow reactor were the following:

$$F(\theta) = 0$$

for $\theta \leq 1/2$

$$F(\theta) = 1 - \frac{1}{4\theta^2}$$

for $\theta \geq 1/2$

Equation 3.11

Where θ is normalized residence time $\theta = t/\tau$

Table 3.6. Effect of the flow rate on the percentage of stagnancy for the suspension microbioreactor and the theoretical laminar reactor. n=1 repetition per flow rate.

Flow rate (μL/min)	PS* Suspension reactor (%)	PS Laminar reactor (%)
0.6	35	40
2	29	31
5	15	16
10	10	11

*Percentage of stagnancy for each flow rate was calculated as Equation 3.10

Lower flow rates, such as the one required to keep cells in suspension (0.06 μL/min) were not used due to impossibility to produce flow rates lower than 0.15 μL/min. Nevertheless, the overall trend showed that the percentage of stagnancy would have been higher than 35% for such a low flow rate, which is prohibitive for the operation of a chemostat reactor.

Data in Table 3.6 showed that operation of the suspension microbioreactor is very similar than a laminar flow reactor where a parabolic flow profile exists. This is consistent with passive mixing that relies only on diffusion mechanisms.

3.1.2.3 Evaluation of Oxygen Transfer

Most industrial bioprocesses are aerobic and take place in aqueous solutions containing salts. To demonstrate potential to culture bacterial cells, the suspension microbioreactor needed to provide high oxygenation rates.

The suspension reactor design did not incorporate membranes or any active methods for oxygenation. In this sense, oxygen transfer was passive and relied mainly on diffusion and transport of the oxygen contained in the inlet media. Thus, high oxygenation rates were not expected.

In a simple experiment, the oxygen transfer coefficient was estimated by creating a negative step change in the concentration of oxygen at the inlet. Thus, dissolved oxygen passed from 100% (solution of air saturated media) to 0% (solution of sodium sulphite). The reactor was placed in the aluminium incubator at 37 °C for this.

1.5 ml of each solution was aspirated into the reactor at 21 µL/min (high flow rate to improve mass transfer). First the air saturated solution filled the reactor until a constant DO value (close to 100%) was achieved. After this, the zero-oxygen solution was pumped into the reactor and the variation in dissolved oxygen monitored over time. K_La data was calculated from the decrease in dissolved oxygen concentration using Equation 2.1 (Materials and Methods).

Oxygen transfer was found to be extremely slow with k_La values of 0.22 ±0.03 h^{-1}. (mean ± 1 standard deviation, n=3 measurements). From this, it was clear that oxygen transfer rates were not suitable to sustain cellular bacterial growth, which typically needs much higher rates.

3.2 Conclusions

Two microbioreactor designs were designed and fabricated based on the work of Dr. Matthew Davies and Prof. Phillipe Renaud. Two mixing mechanisms were studied with the microbioreactor cassette, and several flow rate conditions tested with the suspension microbioreactor. The aim was to evaluate which reactor design was capable to deliver well-controlled, uniform culture conditions that were suitable for chemostat fermentation.

A few tests were carried out to confirm appropriate reactor characteristics, namely appropriate dimensions for the reactor internal structures and adequate capacity for stirring. Measurements with an optical interferometer showed a good comparison between design and measured values for the reactor internal structures. Additionally, high speed camera videos showed excellent coupling between the rotational speed of the stirring bars and the rotational speed of the motor's shaft, confirming that friction forces did not affect the rotation of the stirrer bars.

Comparison between the free-rotating bar and the centrally fixed stir bar showed that the last one was the best method for mixing. Reynolds numbers showed that the reactor operated in the laminar flow regime and were higher for the centrally fixed bar compared to the free-rotating bar, which accounted for the relative magnitude of the convective inertial forces that created mixing. Additionally, low oxygen transfer rates were measured for the free-rotating bar (~ 50 h^{-1}) at the highest stirring speed (1350 rpm). This suggested that the free-rotating bar does not improve mixing in the vertical direction (which is associated with oxygen transfer) and only in the xy plane and corners of the reactor. The centrally fixed stir bar, on the other hand, achieved high k_La values of ~ 105 h^{-1} for a 1350 rpm

stirring speed. This high k_La value was attributed to a high velocity, secondary vertical flow that aided oxygen transfer.

It would have been interesting to perform a residence time distribution analysis of the free-rotating bar to determine the existence of stagnant volumes slowing oxygen transfer (at the top corners of the reactor). k_La measurements, however, were considered as compelling evidence against the use of the free-rotating bar. The centrally fixed bar, on the other hand, showed k_La values close to the ones obtained with bench scale bioreactors at the lower end of the operation. This was promising for scale-up studies (chapter 5).

A second design option, the suspension microbioreactor, was also evaluated. This design achieved mixing of the reactor contents with no moving parts. The suspension microbioreactor was evaluated in terms of mixing time and residence time distribution. Mixing time values were slightly higher than the residence time value. Mixing times were high in magnitude, which was expected since the suspension microbioreactor relied only on molecular diffusion and advection (transport of matter by flow) for mixing.

The residence time distribution analysis showed that the efficiency of mass transfer was low. Mixing was deficient with a high percentage (over 10%) of stagnant volumes for all flow rates tested. RTD evidence was considered compelling against the use of the suspension reactor in future fermentation studies, particularly chemostat, since the chemostat mode of operation demands good mixing and distribution of substrates and cells in the reactor. Additionally, oxygen transfer rates were extremely low (~0.22 h^{-1}) since there were no aeration membranes or other methods of oxygenation. This confirmed that that the

suspension microbioreactor was not suitable for fermentations where a high oxygen supply was needed.

In summary, two microbioreactor designs were compared in terms of mixing and oxygen transfer. Analysis showed that the microbioreactor cassette device with the centrally fixed bar was the best option for the culture of bacterial cells in suspension. This sets the scene for a more detailed characterization study of the cassette device, in which design parameters and their effect on performance is considered. This will allow finding the best conditions for scale-up and chemostat studies.

4 ENGINEERING CHARACTERIZATION OF THE MICROBIOREACTOR CASSETTE

Data in chapter 3 showed that the microbioreactor cassette design had multiple beneficial design features. Among the most important ones were the use of the centrally fixed stir bar and the PDMS aeration membrane. The use of the centrally fixed bar together with the PDMS membrane resulted in good mixing behaviour and high oxygen transfer rates. This was found promising and incentivised a more detailed study of the microbioreactor.

The cassette design was studied in the following key areas: 1) effect of design parameters on oxygen transfer capability 2) effect of stirring speed on mixing time 3) residence time distribution analysis. This chapter will address the study of these areas. The overall aim was to find the best operational conditions for fermentation studies.

4.1 Results and Discussion

4.1.1 Oxygen Transfer Characterization

4.1.1.1 Effect of Membrane Thickness on Oxygen Transfer

The cassette design proved high oxygen transfer rates in chapter 3 but the impact of design parameters was not assessed. A design parameter that had the potential to affect oxygen transfer rates was the thickness of the aeration membrane.

Four PDMS membranes of different thicknesses were fabricated *via* spin-coating at defined rotational speeds. The individual thicknesses were measured using a DekTak stylus profilometer. Half of the PDMS contained in the silicon wafer (Materials and Methods 2.1.1) was removed, so each membrane was cut at three different diameters (n=3). The measurement was performed as a step with the stylus, at a contact force of 5 mg. The diamond stylus was moved vertically and then horizontally across the membrane cut (Fig. 4.1).
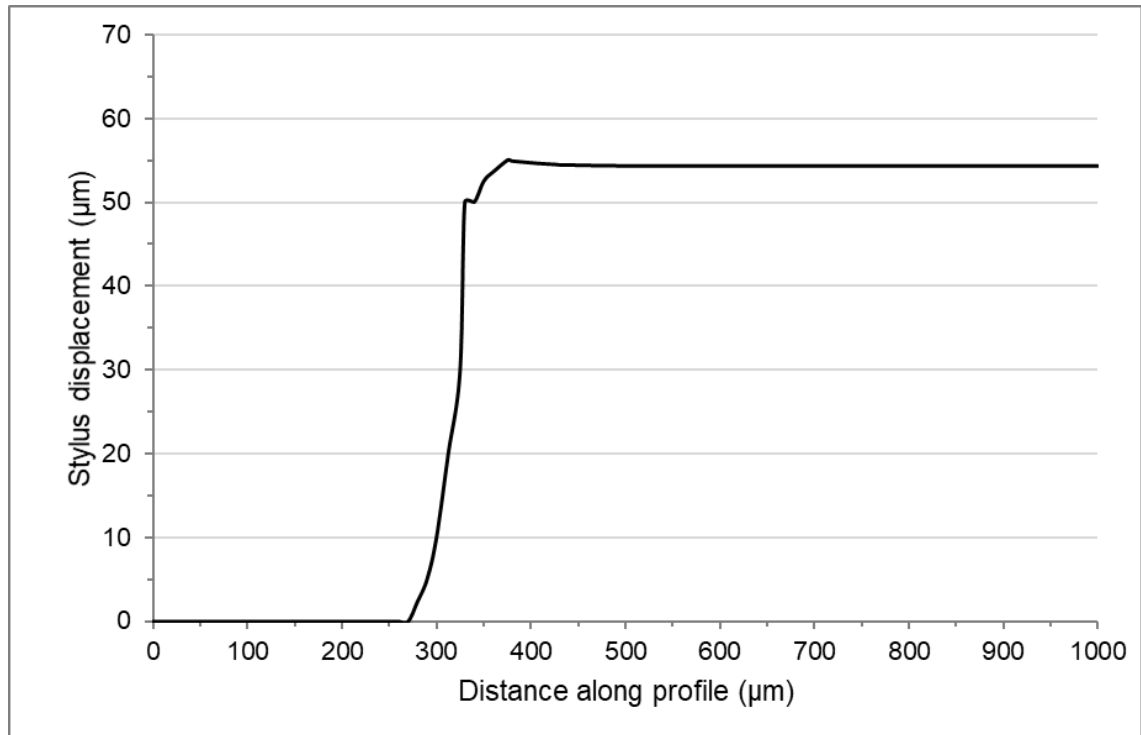
Figure 4.1. Single measurement of membrane thickness using the DekTak stylus profilometer. A contact force of 5 mg was used. The measured thickness of the membrane was 54 µm. n=1 repetition.

Each membrane was cleaned thoroughly with compressed air before measurements in a clean room facility. Measurement results are summarized in Table 4.1.

Table 4.1. Measurements of membrane thickness for different rotational speeds of the spin coater (mean and standard deviation). n= 3 measurements per rotational speed of the spin coater. CV is coefficient of variation (standard deviation divided by the mean).

Speed spin coater (rpm)	1st measure ment (nm)	2nd measure ment (nm)	3rd measure ment (nm)	Mean (nm)	Standard deviation (nm)	CV
250	136049	138589	143794	139477	3224	2.31
500	120385	120379	122379	121048	941	0.77
1000	100129	101705	100657	100830	655	0.64
1500	54303	54722	54439	54488	175	0.32

Overall results showed that the thickness of the membrane can be measured accurately with little variation (standard deviations ranging from 0.17 to 3.22 µm). Note that standard deviations decrease at higher stirring speeds (spin coater) as demonstrated by the coefficient of variation.

Once the thickness of the membrane was rigorously measured, the effect of the membrane thickness on K_La was quantified (Fig. 4.2). K_La values were determined using the set up described in chapter 3 (Fig. 3.17) and the gassing-out method (Materials and Methods 2.2.1). k_La was measured for each membrane over a 200 -1350 rpm range of stirring speeds. The effect of stirring speed on K_La was quantified for each membrane.

As expected, both stirring speed and membrane thickness influenced k_La. Overall, the influence of stirring speed was higher than the influence of membrane thickness.
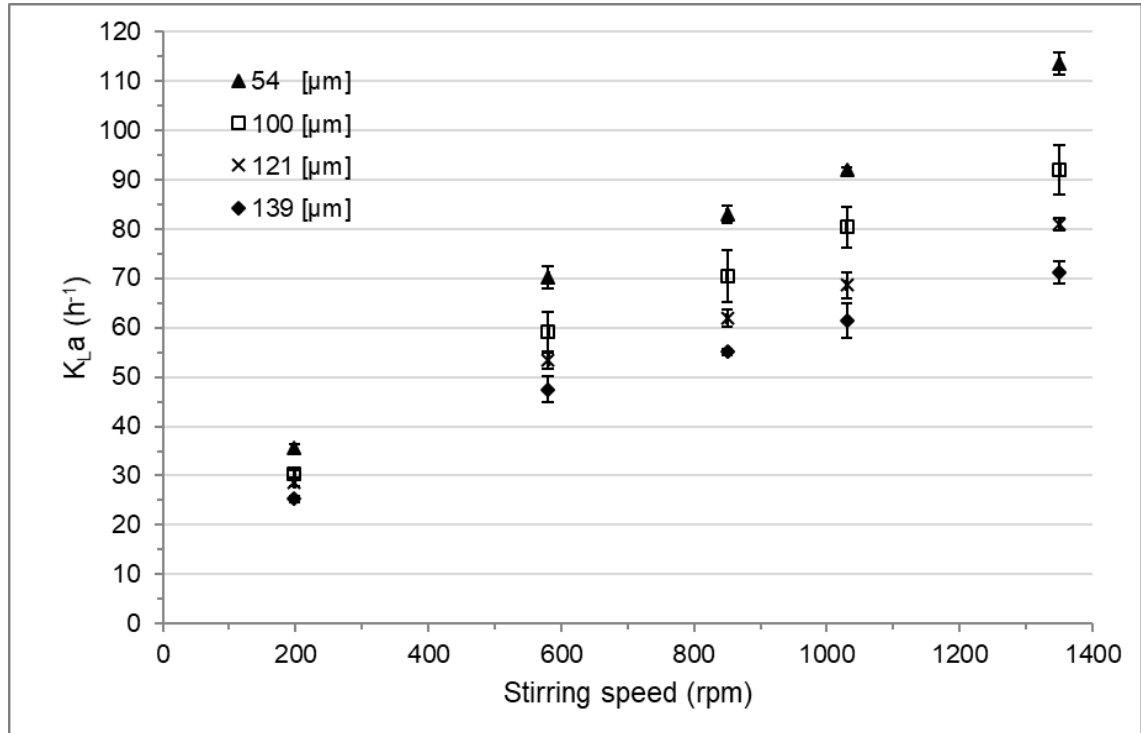
Figure 4.2. Measurements of the volumetric oxygen transfer coefficient (k_La) using different membrane thicknesses and stirring speeds (mean ± 1 standard deviation). The centrally fixed bar was used for mixing. Liquid medium was RO water at 37 °C. Reactor chamber was 2mm depth. n=3 measurements per stirring speed tested.

The influence of stirring speed and membrane thickness was better understood using Equation 4.1 which evaluates the relative importance of the different resistances to oxygen transfer (Bird 2002; Zhang 2006b). The overall oxygen mass-transfer resistance $\frac{1}{K_{L,overall}}$ is the sum of three resistances:

$$\frac{1}{K_{L,overall}} = \frac{1}{K_L} + \frac{\delta}{D_{PDMS}H} + \frac{1}{K_G}$$

Equation 4.1

Where $\frac{1}{K_L}$ represents the resistance to oxygen transfer in the liquid phase, $\frac{\delta}{D_{PDMS}H}$ is the resistance to oxygen transfer in the PDMS membrane, $\frac{1}{K_G}$ the resistance to oxygen transfer in the gas phase, δ is the membrane thickness, D_{PDMS} the diffusivity of oxygen in PDMS, and H the Henry's constant.

If we consider that the diffusivity of oxygen in air is very high compared to the diffusivity of oxygen in water (Cornell Science and Engineering 1996) and PDMS, $\frac{1}{K_G}$ can be neglected from Equation 4.1.

Data showed that when high stirring speeds were used the effect of a change in membrane thickness was more important than at lower stirring speeds (average distance of 9.6 h^{-1} between 54 µm and 139 µm at 200 rpm, and average distance of 42.3 h^{-1} between 54 µm and 139 µm at 1350 rpm). The resistance of the liquid phase $\frac{1}{K_L}$ was thus reduced due to convective forces provoked by high stirring speeds, making the relative importance of the membrane resistance higher.

In the theoretical case in which no resistance from the liquid exists, $K_{L,overall}$ can be represented as $\frac{D_{PDMS}H}{\delta}$. If we consider a PDMS membrane with a thickness (δ) of 100 µm, a diffusivity of oxygen in PDMS D_{PDMS} of 3.4×10^{-5} cm^2/s (Merkel et al 2000), a Henry's constant (H) of 7 (Zhang 2006b), an available area for oxygen transfer of 78.5 mm^2 (area of the cross section of the chamber) and a reactor volume of 157 µL, the theoretical maximum value calculated for K$_L$a is 450 h^{-1}. This value is almost five times higher than the highest k$_L$a value obtained with the microbioreactor and highlights the importance of the liquid resistance in practical experience.

One factor with potential to reduce the magnitude of the resistance offered by the membrane was the diffusivity of oxygen in PDMS. Merkel *et al* 2000 determined the diffusion coefficient from permeability and sorption data of oxygen in PDMS at 35 °C. The diffusion coefficient of oxygen in PDMS was a function of transmembrane pressure difference. They found that diffusivity decreases slightly (in fact it stays almost constant) with increases pressure. Considering this information, experiments involving changes in the internal pressure of the incubator chamber were not performed here since it was thought that changes in pressure would not provoke great changes in D_{PDMS}.

Another factor with potential to reduce the resistance offered by the membrane was the Henry's constant. At a constant temperature, H can be expressed as the ratio of solubilities between the solubility of oxygen in PDMS and the solubility of oxygen in water. Thus, to increase the value of H it is necessary to either increase the solubility of oxygen in PDMS or to decrease the solubility of oxygen in water.

Increasing the solubility of oxygen in PDMS implies increasing the porosity of the polymer. Porous PDMS is a great gas-liquid interface due to its high porosity and hydrophobicity. Studies show that is possible to produce porous PDMS and use it as a gas liquid interface and increase the absorption of gases. For example, Ren *et al* (2017) fabricated porous PDMS thin films using porous rice paper and a sugar leaching fabrication method. The authors report fast absorption rates for carbon dioxide in the films. Unfortunately, oxygen was not evaluated.

Another way is to decrease the solubility of oxygen in water. As the Henry's law states, one way to do this would be to increase the pressure of the headspace above the liquid. However, this does not apply to the microbioreactor used here which has no headspace.

Another approach was changing the oxygen transfer rate (OTR) not by changing

k_La but by increasing the mol fraction of oxygen dissolved in the media (*i.e.*

increasing $C_S - C_L$). Equation 4.2 shows the relationship between k_La and OTR

for the reactor in the absence of biomass:

$$OTR = k_L a \ (C_S - C_L)$$

Equation 4.2

Where C_S is the concentration of oxygen at saturation conditions and C_L is the

concentration of oxygen in the liquid phase.

One thought was to increase the value of both C_S and C_L by using

perfluorocarbons (Pilarek *et al* 2013; Dias *et al* 2004; Ju *et al* 1991).

Unfortunately, pure perfluorocarbons have very high densities *e.g.* ranging from

1.7 to 2 g/cm^3 and when applied in low-shear, gently mixed systems (such as the

microbioreactor) they tend to sediment into the bottom of the reactor. The use of

pure perfluorocarbon was tried experimentally but its efficiency in oxygen transfer

was unacceptably low due to sedimentation.

To correct this, perfluorocarbon emulsions need to be prepared. It would be

interesting to integrate the microbioreactor device with different microfluidic

channels geometries to produce droplets (for example a T-shaped junction, a

cross junction or a cross junction followed by a constriction in the channel).

k_La data in this section demonstrated that decreasing the thickness of the aeration membrane had an important effect on the oxygen transfer rate. Its effect, however, it is generally less important than the effect of stirring.

Increase in stirring speeds increases k_La. Increasing stirring speeds, however, must be in compromise with increasing shear stress which can detrimental for the growth of cells, especially sensitive cells with no protective cell wall.

4.1.1.2 Effect of Surface Area to Volume Ratio on Oxygen Transfer

The surface area to volume ratio was another relevant factor with potential to change oxygen transfer rates in the reactor. Higher surface area to volume ratios can lead to enhanced oxygen transfer.

In the microbioreactor (Fig. 4.3), the surface area to volume ratio can be calculated as Equation 4.3:

$$\frac{S}{V} = \frac{\pi \cdot \frac{D^2}{4}}{\pi \cdot \frac{D^2}{4} \cdot H} = \frac{1}{H}$$

Equation 4.3

Where S is the surface area available for oxygen transfer (78.5 mm^2). S is the cross section of the chamber. V is the chamber volume (157 μL), D is the diameter of the chamber (10 mm) and H is the chamber height.

If a constant diameter is assumed, the surface area to volume ratio can be changed by changing the chamber height.

Figure 4.3. Chamber dimensions of the microbioreactor cassette. H is the chamber height, D is the chamber diameter, and H_l is the height (thickness) of the stir bar (0.5 mm). 1 mm from the reactor lid was considered in the total magnitude of H.

Two surface areas to volume ratios (related to two different chamber heights) were considered here:

Case 1: height of 2 mm (S/V=0.5., V=157 µL)

$$\frac{S}{V} = \frac{1}{H} = \frac{1}{2} = 0.5$$

Case 2: height of 1.5 mm (S/V=0.67; V=118 µL)

$$\frac{S}{V} = \frac{1}{H} = \frac{1}{1.5} = 0.67$$

The decision of keeping a constant diameter was merely practical since changing the reactor diameter implied changing and milling new versions of the top plate of the cassette, which is of complex design.

K_La values did not differ greatly in the range of chamber heights considered (Fig 4.4). A very small enhancement in K_La was, however, expected as reduced volumes (at the same surface area) facilitate oxygen transfer.
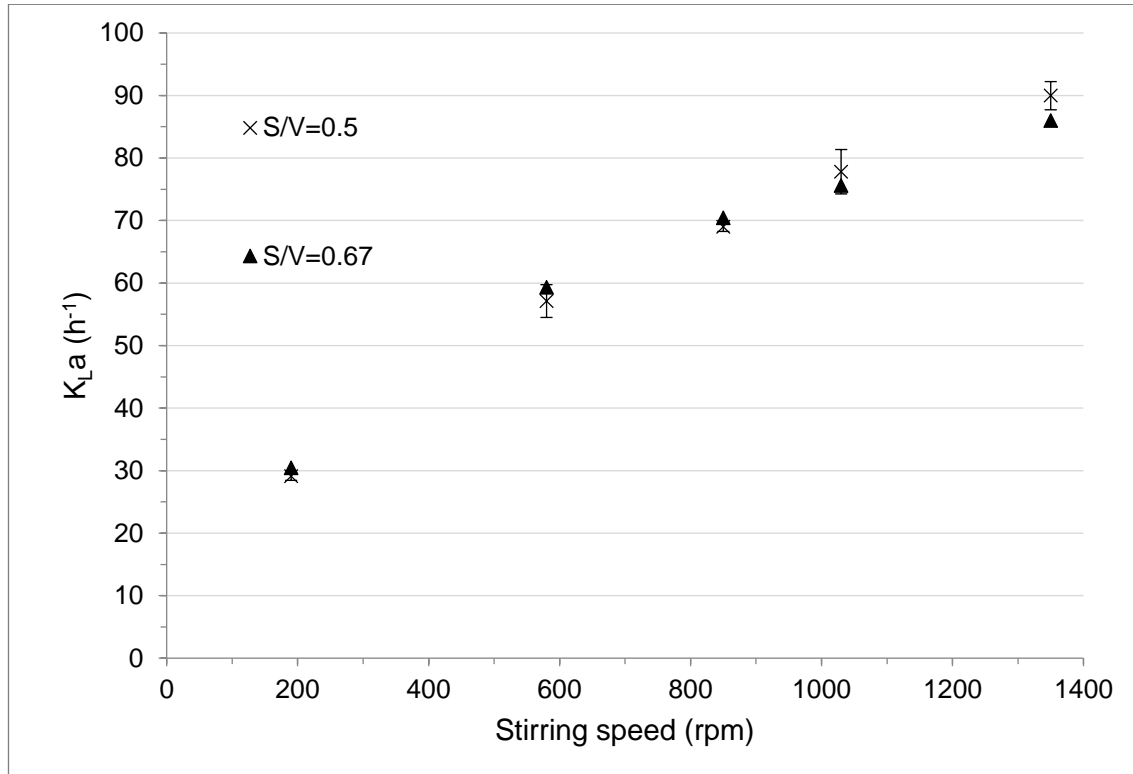
Figure 4.4. Measurements of the volumetric oxygen transfer coefficient (k_La) using different surface area to volume ratios (S/V) and stirring speeds (mean ± 1 standard deviation). The centrally fixed bar was used for mixing. Liquid medium was RO water at 37 °C. Oxygenation membrane was 100 μm. n=3 measurements per stirring speed tested.

Not all changes in reactor dimensions were feasible given the reactor design. For example, if the diameter was increased two times, but the volume aimed constant at 157 μL, the chamber height would need to decrease four times. A four times reduction in height, however, would imply a chamber height of 0.5 mm, which is not feasible due to the thickness of the stirring bar (0.5 mm).

Changes of more than two times the diameter are not possible if the volume is aimed constant. If volume is to be changed, however, it is important to keep working with values of the order of microliters (< 1 ml).

K_La values in Figure 4.4 compare favourably to k_La values obtained with larger bioreactors in which surface aeration was used as aeration method. For example, Kamen *et al* (Kamen *et al* 1995) reported K_La values of 52 h^{-1} for a 3.5 L surface baffled bioreactor.

4.1.2 Mixing Time Characterization

Once oxygen transfer in the reactor was fully characterized, mixing needed detailed characterization.

In the circular chamber both stirring and molecular diffusion occur simultaneously. Stirring here is the advection of materials blobs being mixed without any diffusion action (Suh and Kang 2010).

A series of mixing time experiments were performed to measure the efficiency of mixing. Mixing time was characterized after the analysis of a series of images taken by a high-speed camera (Fig.4.5) at 500 frames per second (fps).

The potential choice of dyes for mixing time measurements was vast. After a revision of the literature, Allura red dye was selected due to its linear absorbance in the visible light spectrum (Werts *et al* 2012). Allura red is soluble in both water and ethanol and has a maximum absorbance at 504 nm (Rappoport 2004:921).

The reactor set-up also included a series of LED strips to illuminate the reactor so clear images were obtained.
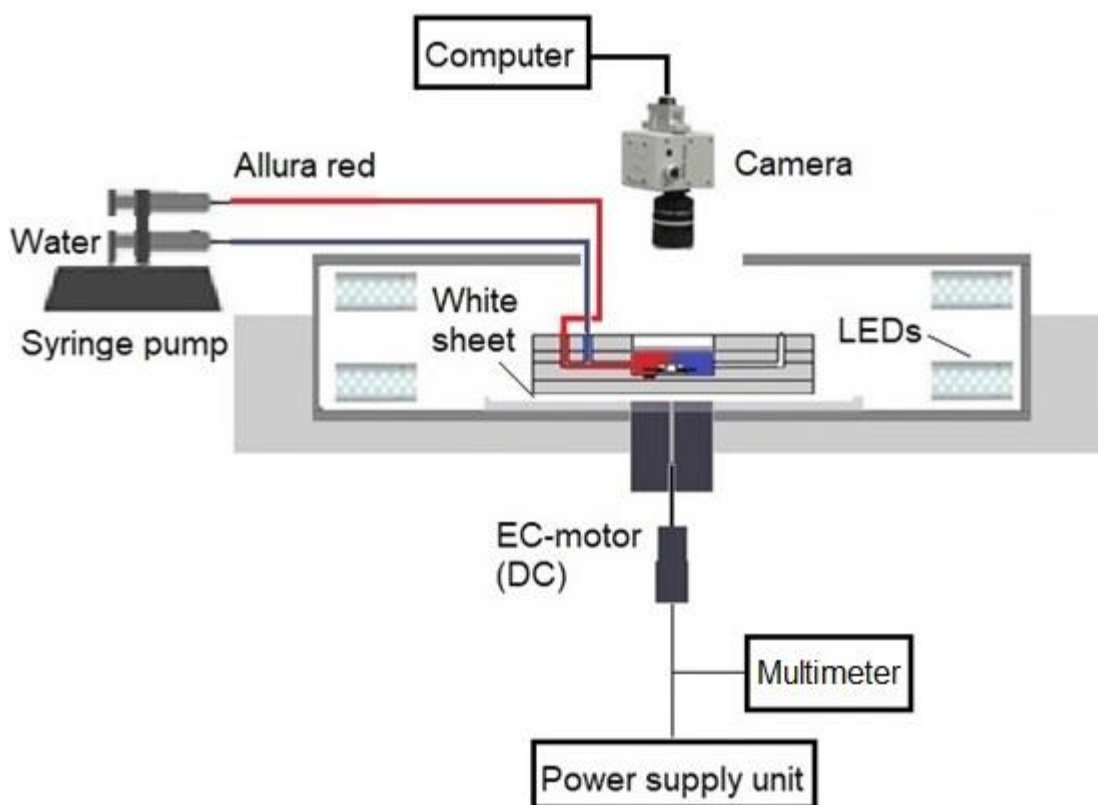
Figure 4.5. Set up for the characterization of mixing time. Allura red was used as an indicator of mixing. A high-speed camera recorded 16 seconds of video per mixing experiment. LED strips were used to illuminate the reactor chamber. A white paper sheet was used as background so to obtain clear images. First, water was pumped as a baseline. After this the flow was maintained at 0.15 µL/min to mimic reactor operational conditions during fermentation (evaporation control). A digital multimeter was used to monitor the stirring speed. Electronically Commutated (EC) motor was powered by direct current (DC).

The reactor had the ability to change mixing by changing the stirring speed. This feature was important since mixing time varied with stirring speed.

Mixing time experiments were conducted as follows: the reactor and all fluidic channels were first primed with ethanol 70% to make sure all volumes were 'bubble free'. After this, the reactor was flushed with RO water. Once priming was complete, water flow was reduced to 0.15 µL/min (simulating the effects of evaporation control) while allura red 4 mM was pumped at a rate of 50 µL/min until 50% v/v of the reactor chamber was filled. The filling of the chamber was judged by reference to the liquid achieving consistent points at the periphery of

the chamber. The measurement of mixing time was performed for the following stirring speeds: 200, 580, 850 and 1030 rpm.

Correct priming of the circular reactor was a difficult step. This was due to the formation of bubbles which appeared after the formation of a meniscus (at the interface water/air). More precisely, once one edge of the meniscus became 'pinned' due to the circular geometry, a bubble was trapped (Tan *et al* 2015). Addressing this issue required orientating the reactor vertically during priming to allow bubbles to achieve the outlet channel.

Images from the high-speed camera were analysed using a bespoke computational script (Fig. 4.6) written on Python programming language. This script was a modified version of the work reported by Pallipurath Radhakrishnan (2016). High-speed images (Multi-TIFF format) were loaded on to the script and addressed individually by copying pixels into arrays.

Features in the image array were labelled and the centre of mass of the reactor chamber was calculated. A circular mask was then overlaid on the centre of the chamber to ignore pixels outside the chamber. The stirrer bar was identified *via* a contour-finding algorithm and masked. The remaining pixels in the array corresponded only to the liquid in the reactor chamber (Fig. 4.7). Pixel values were averaged for the entire reactor area, left side (near the inlet) and right side (near the outlet) respectively. The value of standard deviation was also calculated for the whole reactor, the left side and the right side. Mixing time was considered as the point in time (or frame) where the standard deviation was within 5% (95% of colour homogenization).
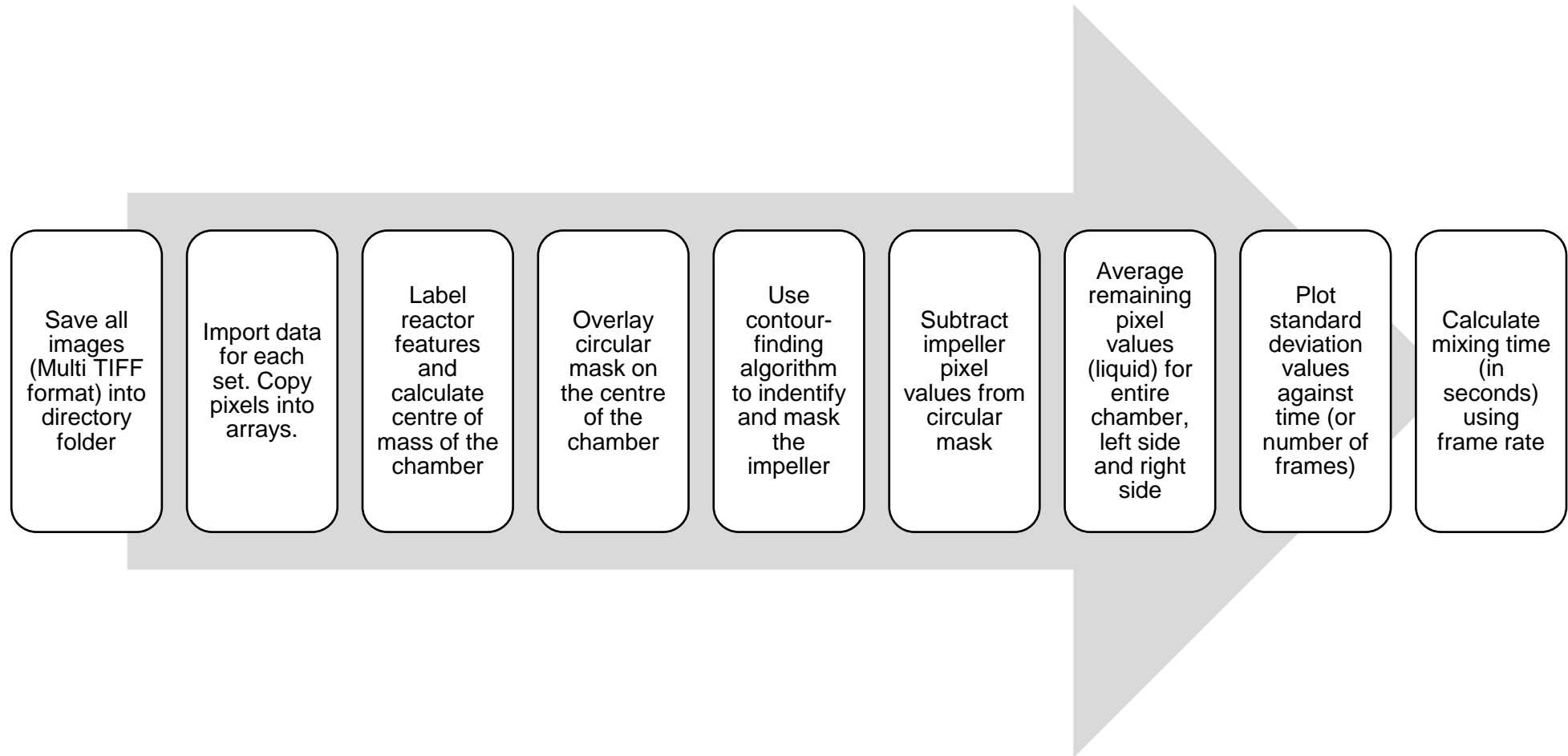
Figure 4.6. Flowsheet indicating necessary steps to determine mixing time. Python 3.2 packages were used in the processing of the files.
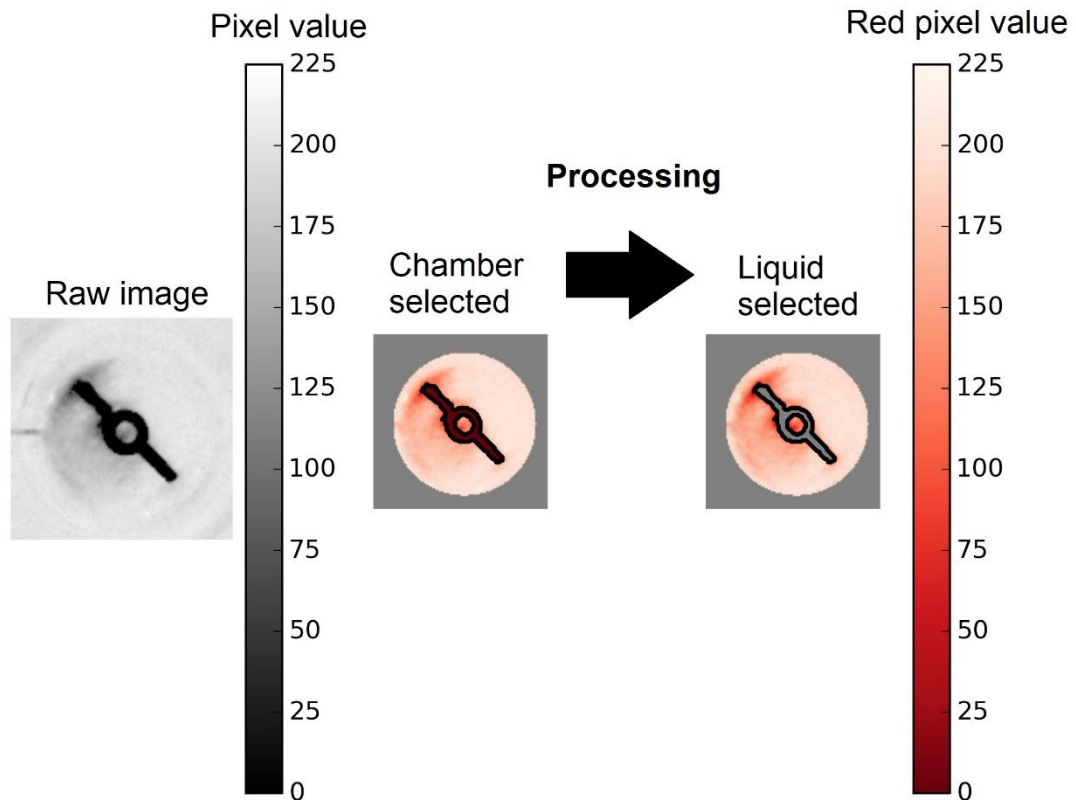
Figure 4.7. Summary of key steps in the processing of high speed photos. The processing of the images removed pixel information from the stir bar and the reactor contours. The relevant pixel information (reactor liquid) was then processed into a red pixel value scale (right). Raw image (left) was taken before the stir bar started rotation.

Standard deviation values converged to a stationary value as the mixing in the reactor progressed (Fig. 4.8). Mixing time was obtained by calculating the point where the standard deviation was within 5% of the final value achieved (average of last 1000 frames). Standard deviation was considered for the right side of the reactor (Kirk *et al* 2016) in mixing time calculation since this side experienced the maximum variation, as the dye was introduced the farthest away from this area (the inlet channel was next to the left side).
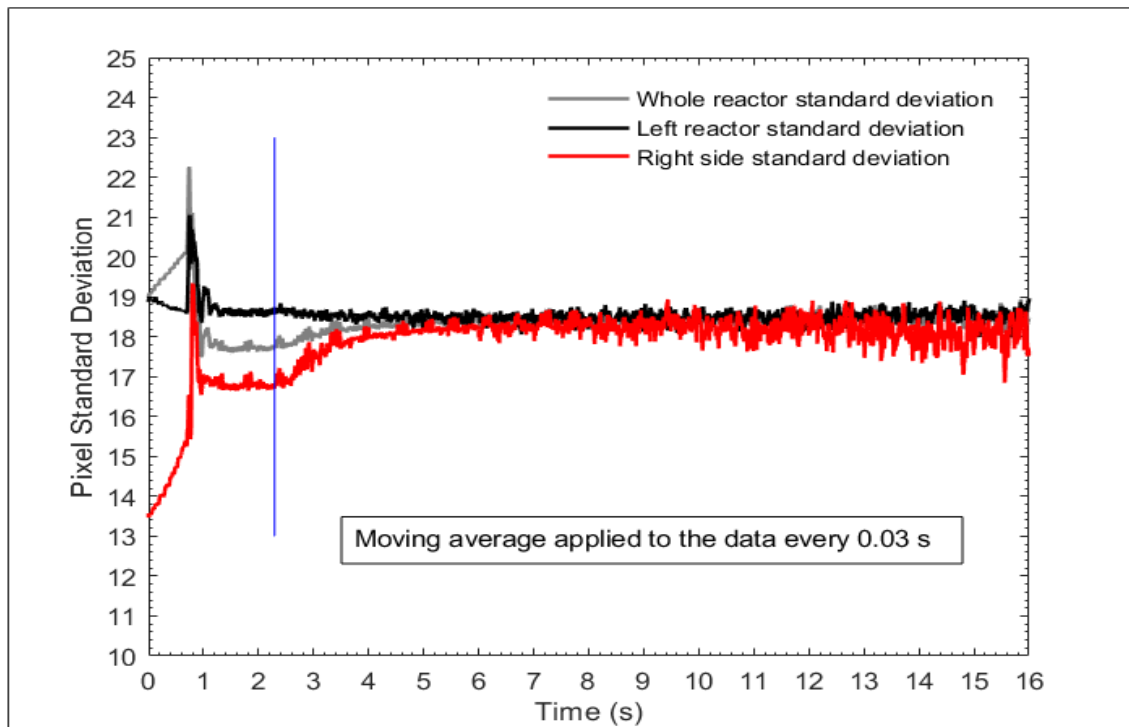
Figure 4. 8. Time profile of the variation of pixel standard deviation during a mixing time experiment. Grey: whole reactor standard deviation, black: left side reactor standard deviation, red: right side reactor standard deviation. Camera starts recording at t=0 s. Stirring bar started rotation at 0.72 s. Standard deviation was within 5% at 2.29 s (blue line). Mixing time calculated as: 2.29 s-0.72 s=1.57 s. Data for 1030 rpm. n=1 measurement. Data was processed using the simple moving average every 15 frames (0.03 s).

Mixing time results for different stirring speeds (Table 4.2) demonstrated the efficiency of the magnetic stir bar as a mixing mechanism (all mixing times below 10 s). Notice that variability among triplicates (standard deviation) tends to decrease at higher stirring speeds (as demonstrated by the coefficient of variation).

Table 4.2. Measurements of mixing time for the microbioreactor cassette using the centrally fixed bar at different stirring speeds (mean and standard deviation). Mixing time was determined using a Python script. n= 3 measurements per stirring speed. CV is coefficient of variation (standard deviation divided by the mean).

Stirring Speed (rpm)	1st Measurement (s)	2nd Measurement (s)	3rd Measurement (s)	Mean (s)	Standard deviation (s)	CV
200	9.54	7.80	3.83	7.1	2.4	0.34
580	2.30	4.80	4.08	3.7	1.0	0.28
850	2.85	1.79	5.26	3.3	1.5	0.44
1030	1.57	1.09	0.99	1.2	0.3	0.21

Allura red in the microbioreactor was mixed by stirring first and next *via* diffusion towards the periphery of the chamber (Fig. 4.9). The darkest red pixel value of the chamber was 140 (allura red 4 mM concentration) and the clearest red pixel value was 203 (water).
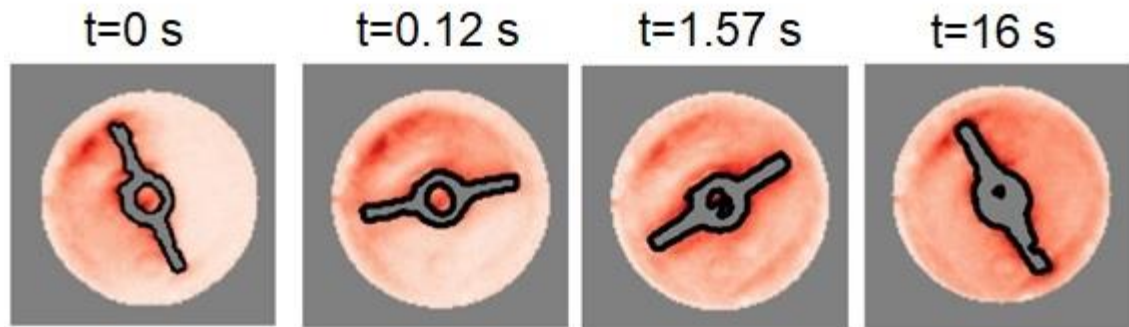
Figure 4.9. Time evolution of the mixing dynamics inside the microbioreactor.t is time. At t = 0 s, the dye filled approximately 50% of the reactor chamber and the stirring bar initiated its rotation. At t = 0.12 s, two full rotations of the stirrer bar were completed. At t = 1.57 s, 95% of the reactor contents were homogenized. At t = 16 s, 100% of the reactor contents were homogenized). Data for 1030 rpm. n=1 measurement.

Mixing time values presented in this section compare favourably with other mixing systems (Kirk *et al* 2016; Tan *et al* 2015; Davies *et al* 2013; Lee *et al* 2011; Schäpper *et al* 2010; Lee *et al* 2006). The results differ significantly, however, from the values reported by Zhang *et al* (2006b).

Zhang, Z. *et al* (2006b) reported mixing time in a microbioreactor of a similar volume (150 µL) and with a stir bar that had the same dimensions of the one used here (6 mm). The authors reported complete mixing within 30 s for a stirring speed of 180 rpm. This result differs significantly of the values reported here. Reasons that might explain this difference are: first, Zhang *et al* used phenol red dye as a mixing indicator. This compound is often used as a pH indicator and is not as soluble in water as allura red. Phenol red dye has a solubility of 0.77 g/L in water at 25 °C (as reported by O'Neil 2006b) compared to allura red which has a much higher solubility of 225 g/L at 25 °C (O'Neil 2006c). It is possible that phenol red dye took more time to dissolve and create a homogeneous mixture with water, which affected the measurement. Second, and more importantly, Zhang *et al* (2006b) determined mixing time by visual inspection of the reactor contents. This

has an inherent degree of subjectivity and inevitably increases the error in mixing time measurements. Additionally, measurement by visual inspection limits the reproducibility and the comparability of the results between laboratories. Finally, bulging of the PDMS membrane (upwards) in Zhang's reactor could also had affected mixing time measurements.

Schäpper *et al* (2010) reported mixing time in a microbioreactor of 100 µL and similar chamber dimensions (2 mm height, 8 mm diameter) but with a free-rotating bar (3 mm long) as a mixing mechanism. Authors reported mixing times of 1.2 s at 500 rpm with bromothymol blue solution as a mixing indicator. They observed mixing by adding a base to the reactor contents which changed the colour from yellow to blue (the amount added was not specified). Adding a volume of base to a chamber with no head-space, however, may provoke liquid displacement which can affect the accuracy of the measurement. Additionally, Schäpper *et al* (2010) determined mixing time by visual inspection.

Lee *et al* (2006) reported mixing times of 5 s in a flat form 100 µL microbioreactor with a 'peristaltic' mixer. Authors also used bromothymol solution as mixing indicator and determined mixing time by visual inspection.

Davies *et al* (2013) reported a mixing time of 1.5 s in a chamber with 10 mm diameter and 2 mm depth. The authors also used a free-rotating bar (3 mm long) to mix the reactor contents. They conducted experiments with water blue and yellow food coloured dyes. Davies *et al* (2013) determined mixing time by visual inspection.

Tan *et al* (2015) reported mixing within 4.5 s using an electromagnetically actuated bead. The authors used a water-soluble dye and a method similar than the one presented here but considering the simple moving average of the

normalized standard deviation. Authors reported the use of the simple moving average of the normalized standard deviation to mitigate noise effects created by their inability to illuminate the reactor chamber.

Finally, Kirk *et al* (2016) report mixing times of ~7 s using an oscillating jet-driven microbioreactor of 100 µL. Mixing was achieved by an eccentrically oscillating jet which infused and withdrew liquid from the chamber. The authors used methylene blue dye and a similar method to determine mixing time than the one described here.

4.1.3 Residence Time Distribution Analysis

As mentioned in chapter 3, mixing time is not the only method to describe mixing. The behaviour of the reactor can also be described in terms of how closely resembles idealised reactors such as the perfectly mixed, continuously stirred reactor. This is particularly useful when an estimation of the percentage of stagnant volumes in the reactor is needed.

Chapter 3 (RTD analysis of the suspension microbioreactor) stated the rationale for selecting tryptophan as a tracer for residence time distribution experiments. The chapter also stated that a step change in tracer concentration was chosen as a method of injection since it is experimentally easier to carry out. Additionally, a step input had the added benefit that the amount of tracer injected did not need to be known. Furthermore, wasting large amounts of tracer to maintain the step was not an issue at the microbioreactor scale.

One important point that was not discussed is that, for a true step experiment, there must be a negligible amount of dispersion between the point of injection and the entrance of the reactor. This is difficult to achieve in microbioreactors since laminar flow and dilution occur in the inlet tubing. If the tracer dilutes over the length of the tubing of the inlet stream, the step will not be a step but will 'smear' in the inlet channel. Therefore, the amount of inlet tubing needs to be minimized as much as possible.

The setup for RTD experiments (Fig. 4.10) included separate tryptophan and water inlet lines. Like RTD experiments in chapter 3, the ActiPix^{TM} D100 UV Area Imaging System was used for the measurement of tryptophan, and allura red dye was used to visualise the moment the tracer first arrives to the reactor chamber.
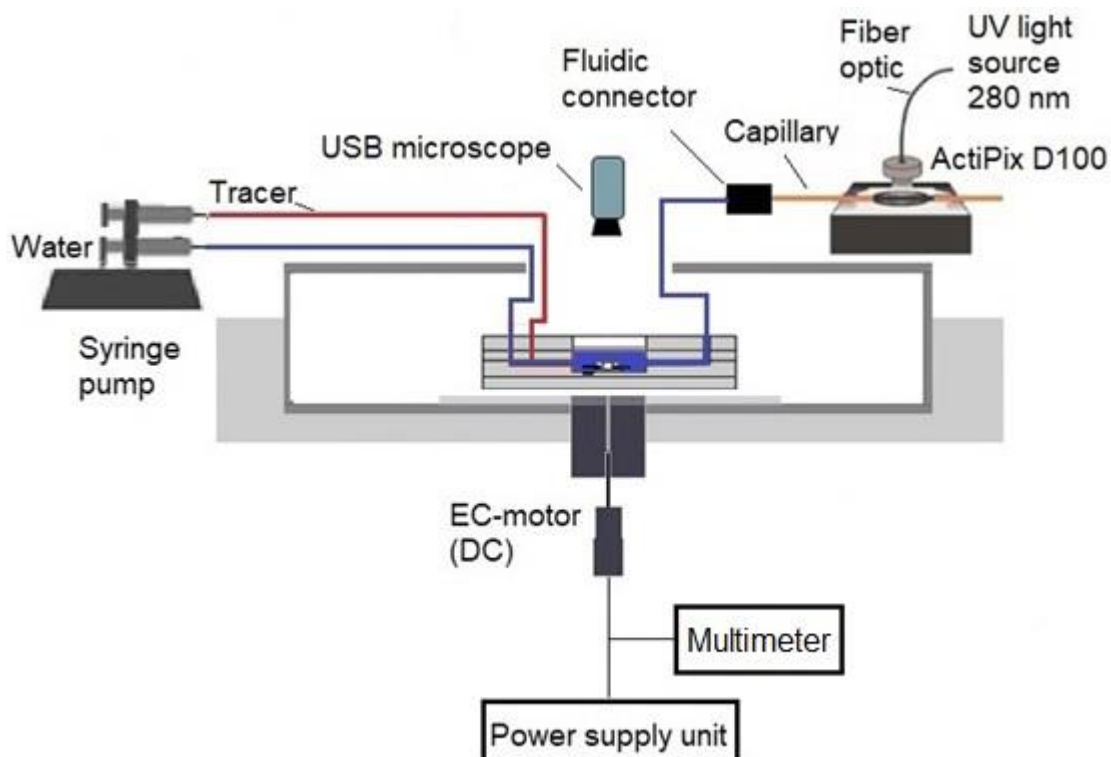
Figure 4.10. Set up for the measurement of residence time distribution in the microbioreactor cassette. The detection unit (ActiPix D100) was connected to the outlet of the reactor using a fluidic connector (internal volume 20 µL). The volume of the outlet line was minimised to 100.4 µL. Allura red dye and a USB camera were used to identify the moment the tracer first reached the reactor chamber (time zero). Water was pumped as a baseline (0% tracer concentration). A digital multimeter was used to monitor the stirring speed. Electronically Commutated (EC) motor was powered by direct current (DC).

To be able to introduce the tracer in the reactor at time zero in a precise manner, two reactor inlets were used (Fig. 4.11). The reactor design offered the functionality of switching between inlet flows. The inlet microchannel (right after the junction between the tryptophan and water lines, and at the left of the chamber) facilitated the introduction of the tracer with negligible dilution effects. This channel was 10 mm length, 510 µm wide and 510 µm depth, accounting for a volume of 2.6 µL (~1.66 % of the reactor volume).
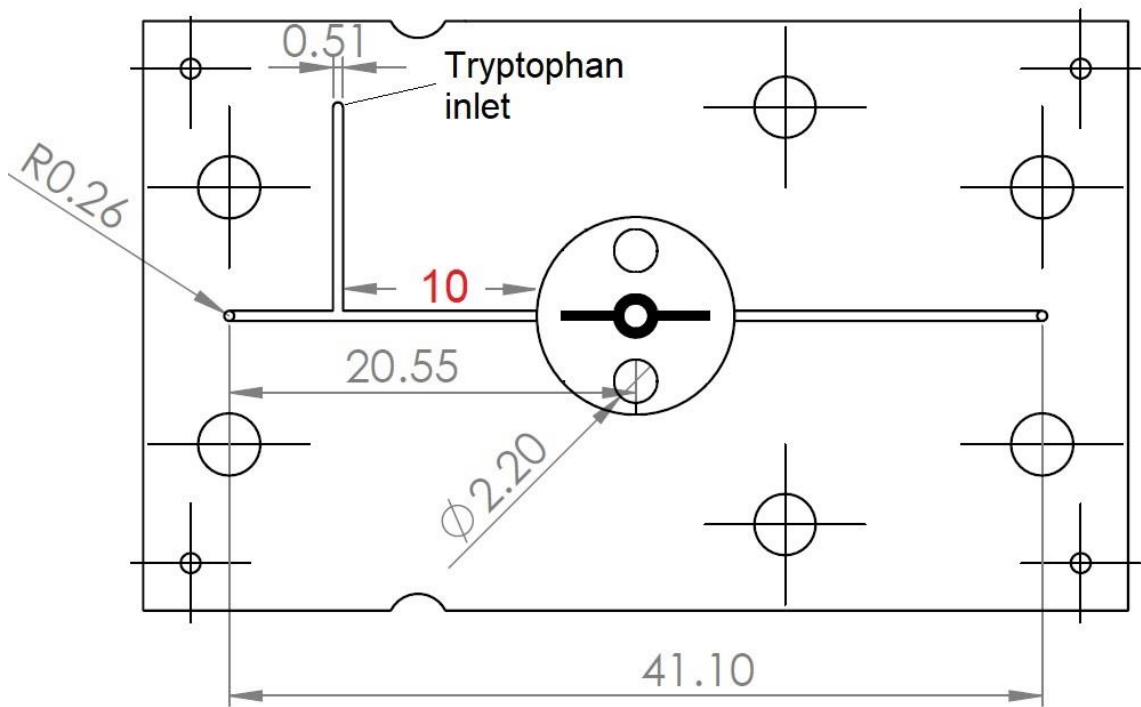
Figure 4.11 Technical drawing of the reactor design with two inlets for switching between inlet flows in a residence time distribution experiment. Dimensions are in mm. The inlet microchannel of 10 mm (red) facilitated the introduction of the tracer with negligible dilution effects.

In addition, distances at the reactor outlet (including tubing) were also minimized as much as possible. The outlet line constituted a stagnant or ineffective volume for mixing, however it was needed in the connection to the detection unit.

The total volume of the system was: 157 µL (reactor)+100. 4 µL (outlet line) +20 µL (connector)=277.4 µL. The volume of the outline was considered in the analysis.

The normalized tracer concentration was defined as before (Equation 3.10 in chapter 3). Normalized concentration $F(\theta)$ and normalized times θ will be used in this section. $\theta = t/\tau$, with t as regular time and τ as the true residence time V/F (V the reactor chamber volume and F the flow rate).

In the reactor, the normalized concentration is also the cumulative residence time distribution function. $F(\theta)$ can be understood as the fraction of the outflow that has been in the reactor for less than a time θ (and it is therefore detected out of the reactor). $1 - F(\theta)$ represents then the fraction of the outflow that has not been detected (or that stays in the reactor for longer time than θ). $F(\theta)$ is used in the determination of RTD when a step change is performed. (Dudukovic and Felder 1983).

Additionally, it is important to make a distinction between the true residence time and the apparent residence time. The true residence time is defined as above and represents the time the liquid spends in the reactor. Nevertheless, since mixing is not perfect, not all reactor volume is effective and ineffective or stagnant volumes exist. If we consider the effective volume of the reactor (V_e) as the total reactor volume minus the stagnant volume, we can calculate the apparent residence time (t_e) as Equation 4.4:

$$t_e = \frac{V_e}{F}$$

Equation 4.4

The concept of apparent residence time was a used in chapter 3 (Equation 3.10) to calculate the percentage of stagnancy and will be used again in this chapter. The apparent residence time was calculated by using the trapezoid rule for

approximating a definite integral for the curve normalized tracer concentration versus time.

Two types of idealised chemical reactors are relevant for comparison with the microbioreactor: The Laminar Flow Reactor (LFR) and the Continuous Flow Stirred-Tank Reactor (CSTR).

As mentioned in the introduction (1.1.4) the LFR uses laminar flow (parabolic profile) and can generally be considered as a long tube with constant diameter (Fogler 2006:888; Levenspiel 1999). Equations to describe the LFR were stated in chapter 3 (Equation 3.11) but are shown here again out of relevance.

$$F(\theta) = 0$$

for $\theta \leq 1/2$

$$F(\theta) = 1 - \frac{1}{4\theta^2}$$

for $\theta \geq 1/2$

A CSTR, on the other hand, assumes that the flow coming from the inlet of the reactor is instantly mixed with the internal contents. Therefore, the concentration of the tracer at the effluent is identical to the concentration of tracer in the chamber (Fogler 2006:887). In practical experience, however, it is impossible to achieve such a perfect mixing and stagnant volumes influence the increase in tracer concentration at the outlet.

The equation to describe the CSTR after the step input can be deduced by means of a material balance for the tracer. The resulting expression is Equation 4.5.

$$F(\theta) = (1 - e^{-\theta})$$

Equation 4.5

A set of RTD experiments were performed for the microbioreactor at different stirring speeds (Fig 4.12). Time zero was the moment the tracer arrived at the entrance of the reactor and pushed the liquid at the outlet to exit (the reactor had no headspace).

When the reactor was not stirred (0 rpm) it behaved like a laminar flow reactor (LFR) close to the end of the experiment. The reactor chamber was obviously geometrically different to the classic long tube with constant diameter, which accounts for the initial discrepancy between the data and the LFR model (between 0.5 and 1.5 normalized time). The chamber thus acted as an 'expansion zone' where the velocity profile was non-parabolic and natural mixing by diffusion occurred. Once the liquid was constrained to the outlet tubing, however, the flow regime was purely laminar (parabolic velocity profile) and therefore the experimental data fits the LFR model.
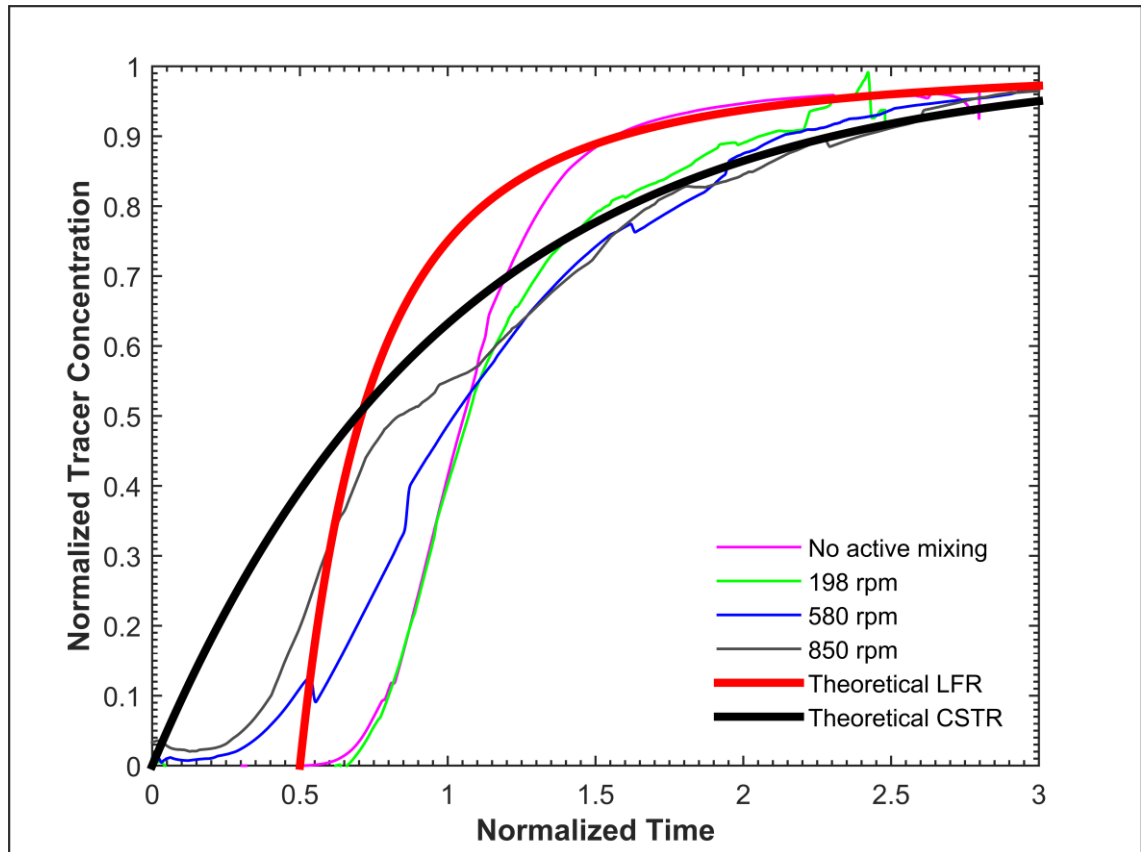
Figure 4.12. Residence time distribution analysis of the microbioreactor cassette. Flow regime was found between a Laminar Flow Reactor (LFR) and a Continuous Flow Stirred-Tank Reactor (CSTR) depending on stirring conditions. LFR and CSTR curves were calculated for a theoretical reactor of 157 µL. 'No active mixing' means 0 rpm stirring speed. Time zero was the moment the tracer reached the reactor chamber. Tracer was pumped into the reactor at 1 µL·s^{-1}. n=1 repetition per stirring condition.

When stirring commenced and speeds increased, mixing in the reactor improved. The better the mixing the more the flow approached to a continuous stirred-tank reactor (CSTR). In a theoretical CSTR the flow at the inlet would be completely and instantly mixed with the rest of the reactor contents. This did not happen here due to imperfect mixing which forced particles to spend longer times in the reactor (in stagnant volumes) before coming out. Stagnant volumes were located at the periphery of the reactor as shown by video analysis.

As mixing time results demonstrated, mixing improves when stirring speeds are increased. Similarly, stirring decreases the percentage of stagnant volumes. Table 4.3 shows the percentage of stagnancy (%) as a function of the stirring speed.

Table 4.3. Effect of stirring speed on the percentage of stagnancy for the microbioreactor cassette using the centrally fixed bar. n=1 repetition per stirring speed.

Stirring Speed (rpm)	Percentage of stagnancy[*] (%)
0	21.2
200	3.3
580	2.4
850	1.1

* Percentage of stagnancy for each condition was calculated as: $((\tau - t_e)/\tau) \times 100$. Where τ is true residence time and t_e is the apparent resident time (Equation 4.4).

One relevant point is that theoretically it takes 3 reactor volumes (or three residence times) to achieve a steady concentration at the outlet with a 95% of the concentration in the inlet. This was demonstrated with a mass balance to the tracer in the reactor as Equation 4.6:

$$\tau \cdot \frac{dM}{dt} = C_0 - M$$

Equation 4.6

Where C_0 is the concentration of tracer at the inlet, M the concentration of tracer at the outlet, and τ the residence time. Equation 4.6 assumes perfect mixing in the reactor (*i.e.* concentrations of tracer in the reactor and at the outlet are equal).

When Equation 4.6 was integrated for the initial condition $M = 0$ at time zero and the final condition $M = 0.95 \cdot C_0$ at time t, it was found that $t = 3\tau$. Results in Figure 4.12 were close to 3τ for the steady concentration values of the tracer.

Most studies in the literature describe RTD in microfluidic channels or capillary arrays, few describing RTD in microreactors. One exception is the work of Mo and Jensen (2016) who used a set of actively mixed cascade minibioreactors for the study of solid forming reactions. The reactor chambers were relatively big (18 mm diameter and 10 mm height, volume of 2.54 ml) and maintained solid products in suspension using 9.5 mm long magnetic stir bars. Authors reported nearly ideal CSTR mixing behaviour of each of the six individual units. Authors used the pulse technique to measure RTD, and methylene blue as a tracer (measured *via* spectroscopy).

4.2 Conclusions

In this chapter the microbioreactor cassette with the centrally fixed bar was characterized in terms of oxygen transfer and mixing. This was briefly explored in chapter 3, however, a more detailed study considering of the effect of design parameters on performance was needed.

Data on oxygen transfer studies showed that the most influential parameter on oxygen transfer was the stirring speed. An increase in stirring speed directly affected oxygen transfer by decreasing the thickness of the boundary layer at the membrane/liquid interface. This resembled behaviour at large scale reactors where stirring speed is the most influential parameter in oxygen transfer, followed by the type and the number of stirrers and the gas flow rate (Karimi *et al* 2013).

If mixing *via* stirring plans to be improved further, work should concentrate in developing impellers such as propellers or turbines that can increase mixing in the vertical direction, aiding oxygen transfer. Axial flow impellers could be difficult to fabricate as they require a high level of detail in the blades. Some work, however, where high resolution (25 μm) in fabrication was achieved, has been reported (Tian *et al* 2010).

The second most influential parameter was the thickness of the aeration membrane. Oxygen transfer *via* natural diffusion through the membrane was the only oxygenation method. In this sense, the effect of the thickness of the membrane (diffusion length) on oxygen transport was clear. The effect was even more noticeable when the reactor was well-stirred and the relative importance of the liquid resistance was reduced.

To improve oxygen transfer in the microbioreactor shorter diffusion lengths are needed. To do this, while maintaining appropriate compression and sealing of the top of the chamber, changes in the design of the top plate of the cassette are needed. Another improvement would be to actively compress and deflect the membrane, although the equipment necessary for this would increase the complexity and cost of the design and reactor set-up.

Changes in the surface area to volume ratio did not affect K_La results within one decimal figure. Greater changes in the ratio would imply important modifications of the reactor design and dimensions.

Of the conditions tested, the one that resulted in higher k_La values (~113 h^{-1}) was 1350 rpm stirring speed and a PDMS membrane of 54 μm thickness.

An automated methodology for the measurement of mixing time was developed and implemented. This represented a substantial improvement in accuracy, reproducibility and comparability of the results compared to measurement by visual inspection. One limitation of the method, however, it is that it only considers measurements of the spatial variation of the dye in the xy plane while the z direction is neglected.

Mixing times decreased at higher stirring speeds. Rapid mixing (~1.2 s) was found at 1030 rpm which compares favourably with the existing literature.

Residence time distribution analysis demonstrated that the reactor can operate at nearly ideally mixed conditions (*i.e.* as a continuous flow stirred-tank reactor). This is particularly relevant to chemostat operation where good mixing conditions are required.

Stagnant volumes decreased at higher stirring speeds. A low percentage of stagnant volumes (~1%) was found at 850 rpm. This was chosen as the most suitable stirring condition for chemostat experiments in the next chapter.

5   ASSESSMENT OF THE FERMENTATION CAPABILITY OF THE MICROBIOREACTOR CASSETTE

Review

A microbioreactor cassette design with a centrally fixed bar for mixing was introduced in chapter 3. The cassette was compared to other alternatives for aerobic bacterial culture and was found the most promising. Among the attractive features of the cassette was the capacity of inserting different reactor designs (chambers) with inlets and outlets. This aids bacterial culture because each inlet and outlet can offer a specific functionality (*e.g.* addition of reagents during fermentation). More importantly, the design allowed the insertion of a PDMS aeration membrane. This membrane provided oxygen transfer rates compatible with the growth of aerobic bacteria. Finally, both the reactor and the membrane material resist autoclave conditions (121 °C) and are ethanol resistant. This made the cassette design easy to sterilise and/or disinfect.

Chapter 4 addressed two important questions related to reactor operation: what is the effect of design parameters on oxygen transfer and mixing? and is the reactor capable of operating at perfectly mixed conditions? The answer to the first question is that the most influential parameter on both oxygen transfer and mixing is the stirring speed. Both oxygen transfer and mixing improve at higher stirring speeds. Stirring speed was a readily adjustable parameter and allowed the selection of the right conditions for chemostat and scale-up studies.

The answer to the second question is that the reactor can effectively operate at nearly ideally mixed conditions (*i.e.* as a continuous flow stirred-tank reactor) using a stirring speed of 850 rpm. This was important because good mixing conditions are a requirement for chemostat operation.

Next Steps

Following the answer to these questions the next step was to prove that the microbioreactor cassette can culture bacterial cells using both batch and chemostat operational modes. Only fermentation results could validate the potential of the microbioreactor to adequately characterize strain behaviour. Additionally, comparison of the microbioreactor with other bioreactor types was also important and addressed here.

5.1 Results and Discussion

5.1.1 Benchmarking studies of the Fermentation of *Staphylococcus carnosus*

The genetically modified, chloramphenicol resistant, *Staphylococcus carnosus* TM300 (pCX-pp-sfgfp) strain was used in fermentation experiments. This strain was chosen given the well-characterized nature of its genome. The strain is a gram positive, coagulase negative and low-GC content microorganism.

Cellular growth and substrate consumption profiles needed to be characterized. Two benchmark tools for comparison with the microbioreactor were used for this: baffled shake flasks and a 200 ml minibioreactor.

5.1.1.1 Shake Flask Study of the Fermentation of *Staphylococcus carnosus*

Baffled shake flasks (4 baffles) were first used as a bench mark. Lysogeny broth (LB) medium was used as specified in Materials and Methods (2.3.1). Glucose (1 g/L) was chosen as the growth-limiting substrate which was reflected in the microorganism's kinetics (Fig. 5.1a). Data showed that *Staphylococcus carnosus* ceased to grow once glucose was consumed. Lactic acid (and lactate) were produced (Fig. 5.1b). Given the formulation of the medium (which contains yeast extract), trace elements of carbon sources might be present. However, none of them seemed to affect Staphylococcus *carnosus* growth.
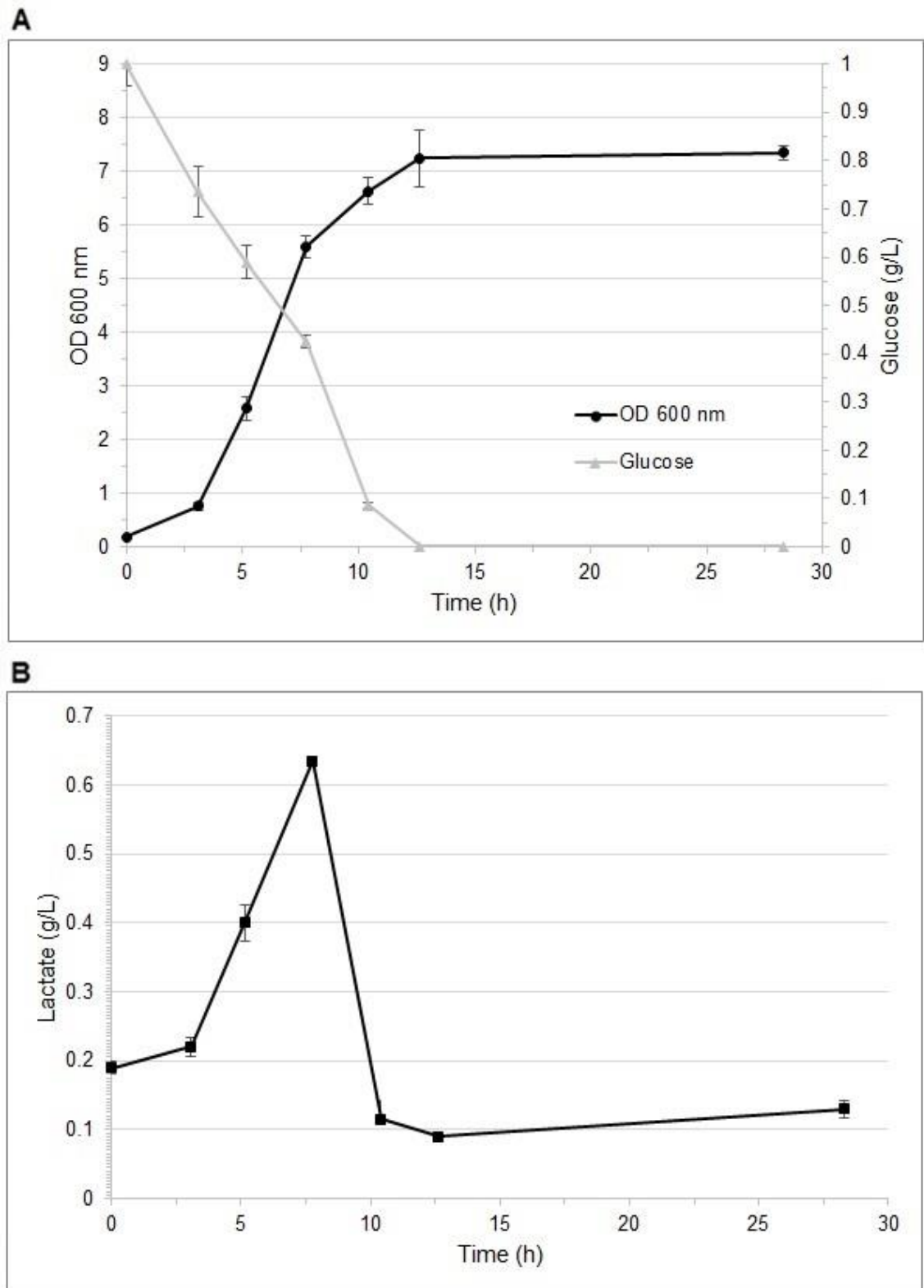
Figure 5.1. Batch fermentation of *Staphylococcus carnosus* TM300 in shake flasks (4 baffles). (A) OD and glucose profiles (mean ± 1 standard deviation) (B). Lactate profile (mean ± 1 standard deviation). Experimental conditions were 37°C and 250 rpm, with 20% v/v filling volume and 2% v/v inoculum. Initial OD was 0.19. n= 3 independent runs.

The value of OD at the stationary phase was ~7. This value was affected only by the concentration of glucose in the medium (1 g/L). Initial conditions were: initial inoculum added (OD=0.19) and the percentage of filling of the flasks (20%). The conditions were chosen based on laboratory experience. Because of the good inoculation protocol, *Staphylococcus carnosus* started to grow quickly without long lag phases.

If we assume balanced growth (*i.e.* all bacterial cells are dividing regularly by binary fission, and are growing by geometric progression), the increase in the natural logarithm of OD is proportional to the increase in time. The proportionality constant is the specific growth rate μ, which can be calculated by plotting the logarithm of OD (normalized by the initial value) versus time (Fig. 5.2). This method will be used to calculate the specific growth rates with other reactors in the rest of the chapter.

The calculated specific growth rate μ_{max} was 0.45 h^{-1} which corresponds to a doubling time of 1.54 hours. This value was expected for a rapidly growing bacterium. As a point of comparison, specific growth rates for *Escherichia coli* growing in LB media are approximately 2.5 h^{-1} (0.29 h doubling time) (Berney *et al* 2006) and for yeast values about 0.3 h^{-1} (2.3 h doubling time) (Gateway engineering education coalition 2017).
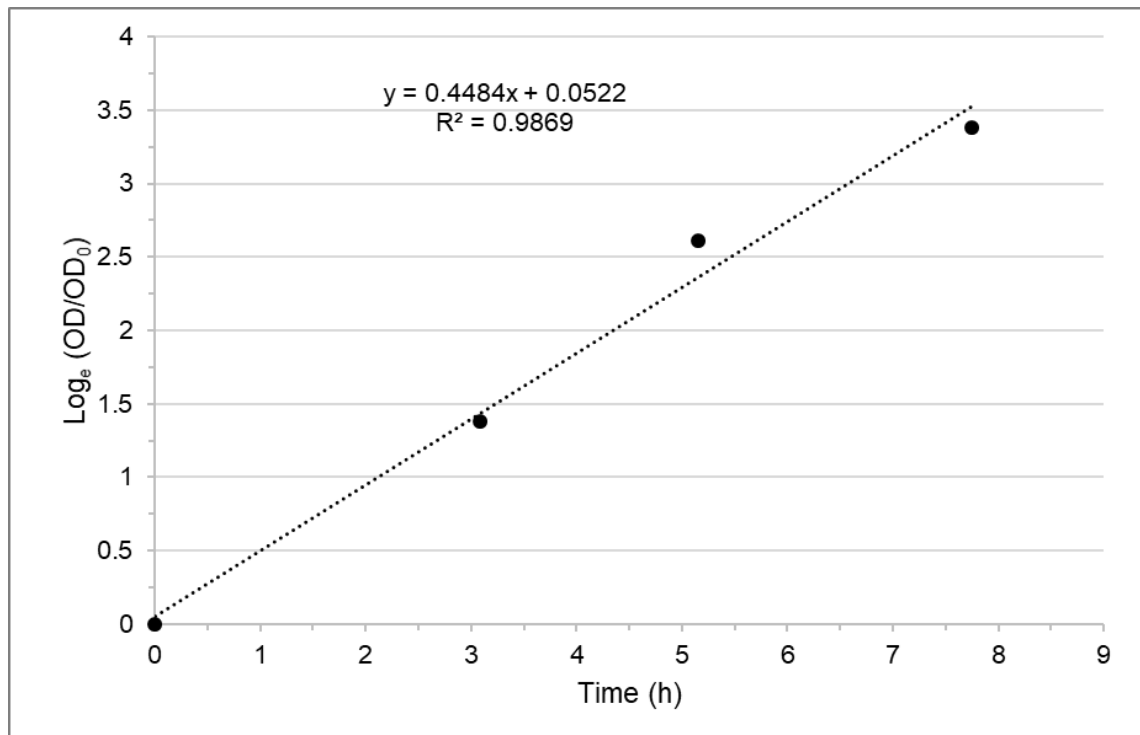
Figure 5.2 Calculation of the specific growth rate of *Staphylococcus carnosus* TM300 in shake flasks. OD_0 was the OD value at time zero (0.19). Mean values of OD during exponential growth were considered in the calculation. The specific growth rate was the slope of the trend line.

Lactic acid and lactate were produced due to the metabolism of *Staphylococcus carnosus*. When lactic acid loses one proton it becomes lactate which was measured by the enzymatic sensor of the Bioprofile FLEX Analyser. Lactic acid did not decrease the pH (7.5) since potassium phosphate buffer was included in the medium.

Notice that lactate (Fig. 5.1b) was consumed during growth. A decrease in lactate concentration after the end of the exponential phase may imply that L-lactate was metabolized to pyruvate (after glucose consumption) by the action of the enzyme L-lactate dehydrogenase (LDH) which is part of the enzymatic pool of *S. carnosus* (UniProt 2002). LDH aids the reaction of lactate with the oxidized form of Nicotinamide adenine dinucleotide (NAD+) to produce pyruvate and NADH.

Measure of oxygen in the flasks would have provided more information about the growth of *Staphylococcus carnosus*. To obtain this, an instrumented minibioreactor capable of reliably measuring oxygen will be used as benchmark in the next section.

5.1.1.2 Minibioreactor Study of the Fermentation of *Staphylococcus carnosus*

As described in the introduction, miniature bioreactors (volumes ranging from 10 to 500 ml) are being used to speed up bioprocess development. In this sense, it was worthwhile to characterize the growth of *Staphylococcus carnosus* in a minibioreactor and compare performance with the microbioreactor cassette. The system chosen was the DASGIP mini bioreactor from Eppendorf®. These bioreactors are autoclavable glass vessels stirred by a powerful overhead drive. Some relevant features of the minibioreactor system are stated in Materials and Methods (2.3.2).

Before performing fermentations with the minibioreactor, characterization of oxygen transfer was needed. Thus, k_La was measured in the minibioreactor at different operational conditions (Table 5.1). k_La measurements were performed using the gassing-out method and the coefficient calculated using the response time of the polarographic oxygen probes (45 s).

Table 5.1. Measurements of the oxygen transfer coefficient (k_La) in the minibioreactor. Mean and standard deviation. n=3 measurements per agitation condition.

Agitation (rpm)	Aeration (vvm)	k_La (h^{-1})	k_La standard deviation (h^{-1})	Tip speed ($m \cdot s^{-1}$)	Reynolds number
200	0.5	10	1.0	0.1	3344
200	1	20	1.5	0.1	3344
200	2	29	0.2	0.1	3344
400	2	58	7.7	0.2	6689
500	2	62	4.6	0.3	8361
600	2	67	16.1	0.3	10033
700	2	109	31.0	0.4	11706
800	2	143	8.2	0.4	13378
1000	2	165	22.7	0.5	16722

k_La data obtained with the minibioreactor was consistent with reported values for reactors of similar volume (Table 1.2 in Introduction).

The maximum aeration rate of the minibioreactor was 2 vvm. When this aeration rate was used at high stirring speeds (>500), the flow regime was fully turbulent (Reynolds numbers ≥ 10000) and the operation of the reactor became unstable due to rising bubbles. Thus, a stirring speed of 500 rpm and 2 vvm were chosen as conditions for a more stable operation. These values were used also for comparison with the microbioreactor (scale-translation).

Once oxygen transfer in the minibioreactor was characterized, three parallel fermentations with *Staphylococcus carnosus* were performed (Fig.5.3)
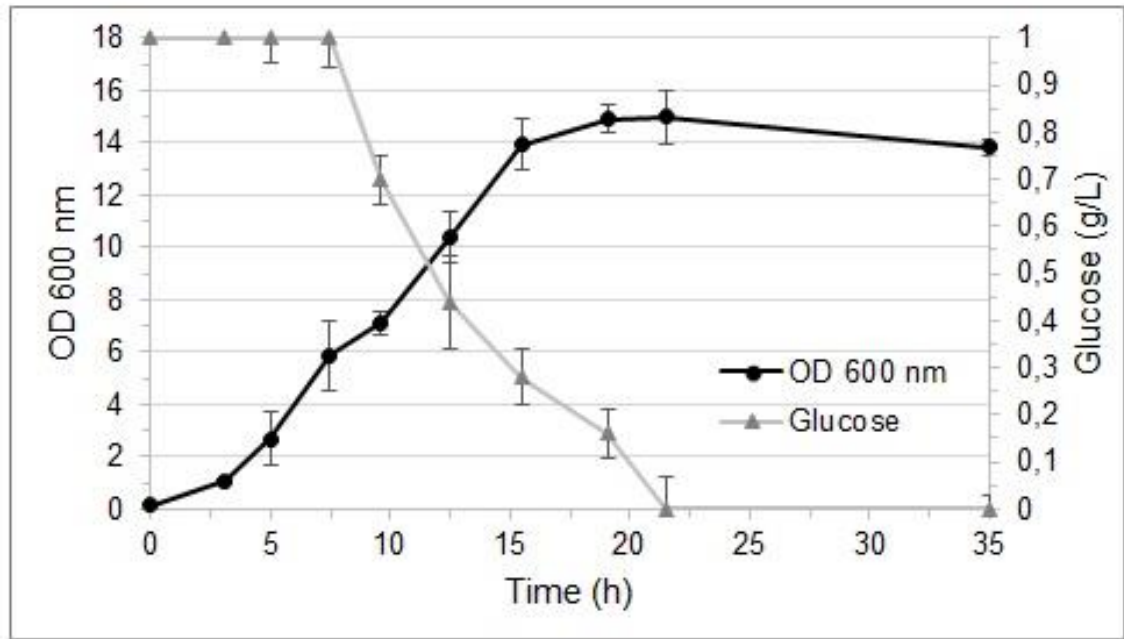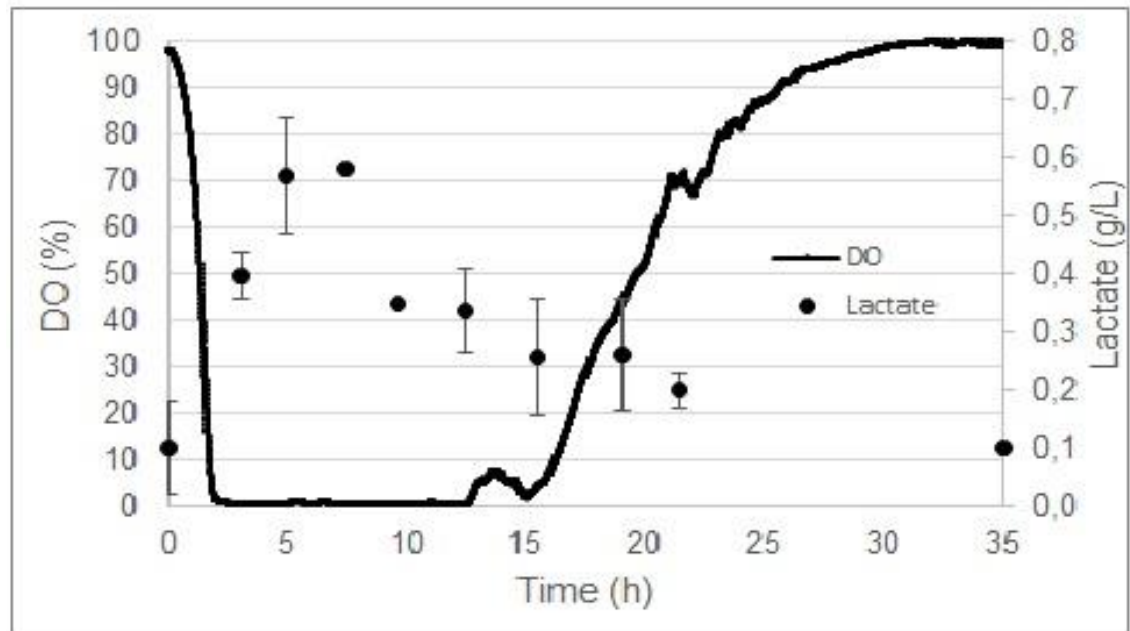
Figure 5.3. Batch fermentation of *Staphylococcus carnosus* TM300 in minibioreactor (200 ml). (A) OD and glucose profiles (mean ± 1 standard deviation) (B) DO % and lactate profiles (mean ± 1 standard deviation). Conditions were 37°C, 500 rpm and 2 vvm. Fermentation started with a 2% inoculum (OD=0.16). n=3 independent repetitions for OD, glucose and lactate. n=1 for DO.

A 2% inoculum (OD=0.16) in the minibioreactor was chosen to mimic initial conditions in shake flasks. When compared to shake flasks, data in the minibioreactor showed higher final OD concentrations (final OD=13.8). One reason for this was the better and more efficient oxygenation in the minibioreactor (gas sparging). This happened despite the shake flasks including baffles for maximized aeration (thus k_La values in shake flasks were probably lower than the 63 h^{-1} obtained in the minibioreactor at 500 rpm and 2 vvm). The specific growth rate in the minibioreactor was 0.49 h^{-1}, which was slightly higher than the value obtained with shake flasks. This further confirmed better growth in the minibioreactor.

Second, the overall duration of the fermentation was longer in the minibioreactor (21.5 h). Thus, more time was required for the total consumption of glucose compared to shake flasks (12.5 h). One explanation for this is that the length of exponential growth phase was increased due to better oxygenation, although this would need to be confirmed by measuring DO in shake flasks. In addition, once glucose started to become limiting (from 15 hours onwards), DO data started to increase due to the reduced cell activity and lower oxygen demand.

Third, DO data showed that a good part of the growth of *Staphylococcus carnosus* occurred under oxygen limitation. This is consistent with *Staphylococcus carnosus* being a facultative anaerobe microorganism which makes ATP *via* aerobic fermentation if oxygen is present but switches to anaerobic respiration if oxygen is absent (Hogg 2005:99-100).

Finally, considering the DO data in the liquid phase it was possible to calculate the oxygen uptake rate (OUR) using Equation 5.1:

$$OUR = k_L a \cdot (C^* - C_L) - \frac{dC_L}{dt}$$

Equation 5.1

Where C^* is the saturation concentration (6.7 mg/L at 37 °C) and C_L the oxygen concentration in the liquid phase.

Equation 5.1 was solved using the Runge-Kutta method for numerical solving of differential equations (Devries and Hasbun 2011). Maximum OUR value achieved (OUR_{MAX}) was 549 mg h^{-1} L^{-1} (Fig. 5.4). This value was calculated considering the mean of the DO data points between 5 and 10 hours. The results agree with the typical evolution of the oxygen uptake rate in the time course of a fermentation for bacterial cultures (Garcia-Ochoa *et al* 2010).
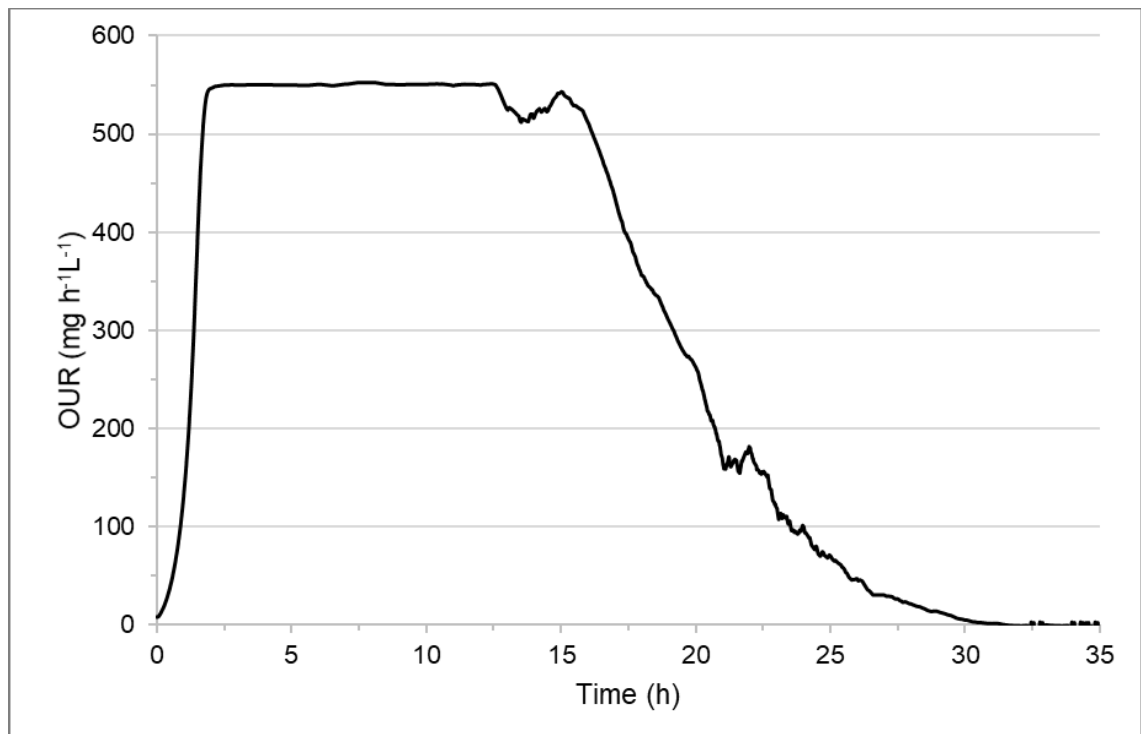
Figure 5.4. Evolution of the oxygen uptake rate (OUR) for the batch fermentation of *Staphylococcus carnosus* TM300 in the minibioreactor. Oxygen uptake rate was calculated from the averaged DO data using the Runge-Kutta method. A $k_L a$ value of 63 h^{-1} was considered in the calculation. Maximum OUR value achieved (OUR_{MAX}) was 549 mg h^{-1} L^{-1}.

5.1.1.3 Microbioreactor Set-up

Once the growth kinetics of *Staphylococcus carnosus* was studied in conventional systems the next step was fermentations in the microbioreactor. The microbioreactor experimental set-up (Fig. 5.5) included optical and fluidic components in addition to the appropriate instrumentation.

Among the fluidics components, two syringes reservoirs were connected to the two reactor inlets. One inlet was used to pump inoculum and media to the reactor (an inoculum waste line allowed complete removal of the inoculum before pumping medium) and the other one was used to deliver a water flow to compensate for evaporation.

Pumping water at the evaporation rate was the preferred option to address evaporation of the reactor contents. Passive replenishment of previously evaporated water by connecting an elevated water reservoir was discarded since it implied the introduction of a fluid input of undefined characteristics. In this sense, pumping extra water was preferred since even though the flow represented an extra input (for chemostat operation) it was at least a known value.

The set up for continuous operation required also to control inflow and outflow. As mentioned in chapter 3 (3.1.1), it takes very little force of pressure (such as the one introduced by the flow) to deform the aeration membrane and change the volume of the reactor. The reactor design addressed this by means of a grid structure in the top plate designed to avoid the bulging of the membrane upwards. Additionally, a back-pressure regulator was used to control the upstream pressure, maintaining the reactor volume filled with liquid.
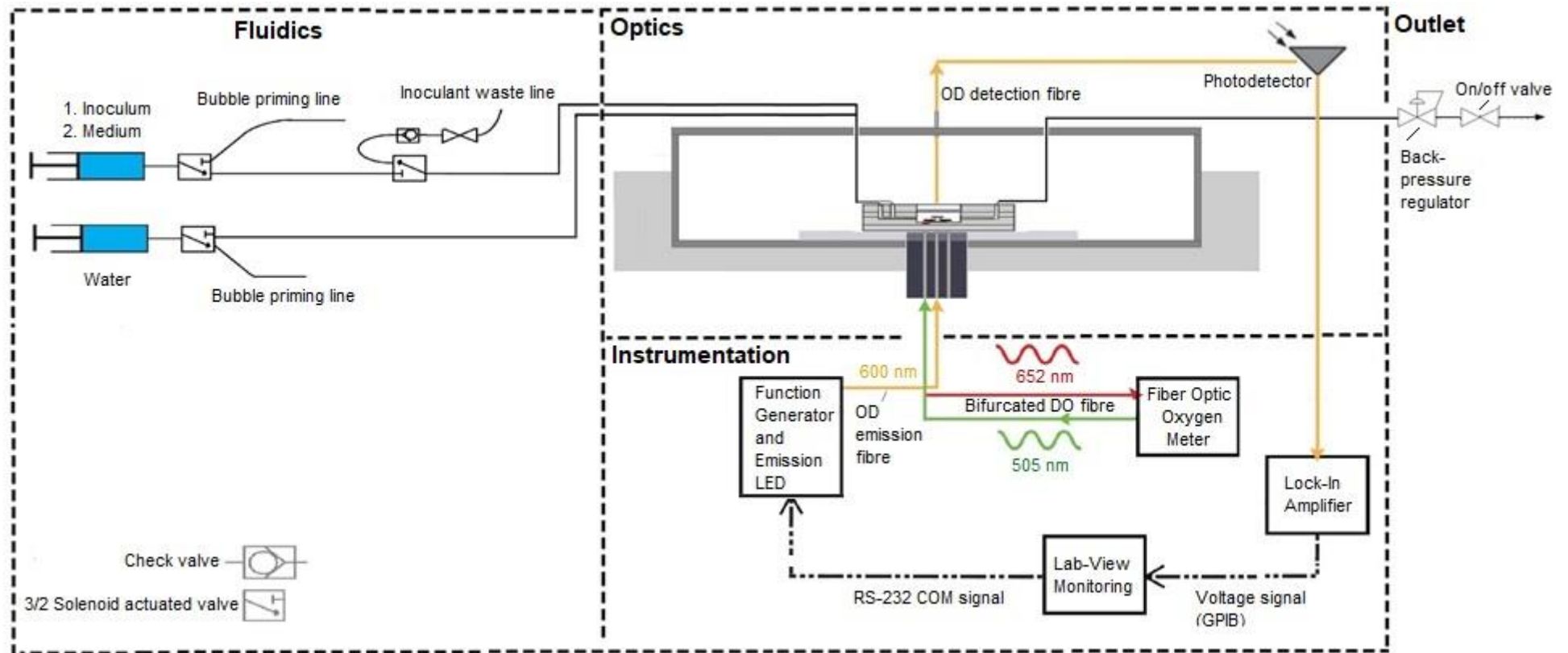
Figure 5.5. Microbioreactor set up for batch and continuous fermentations. Two optical fibers were connected to the bottom of the microbioreactor for the measurement of OD and DO. From the top, a photodetector collected the OD signal transmitted through the microbioreactor chamber and send it to a lock-in amplifier. The lock-in amplifier was connected to a computer using a GPIB cable. A back-pressure regulator (BPR) was incorporated at the outlet line before the on/off exit valve to control the upstream flow and provide positive pressure to the reactor chamber.

Once the reactor set up was established, the optical instrumentation for OD measurements required calibration. Inert polystyrene particles were used for this since cells were potentially capable of multiplexing during experiments. 1 µm diameter particles were used to imitate the size of *Staphylococcus carnosus.*

Six solutions of different concentrations of polystyrene particles were measured in both the microbioreactor and in a conventional spectrophotometer. The photodetector connected to the OD detection fiber sent a voltage signal to the lock-in amplifier for analysis, so the raw data obtained with the microbioreactor was in voltage (V).

Once voltage measurements were performed at different particle concentrations, OD values were calculated using Equation 2.2 (Materials and Methods). In this equation, a conversion factor of 8.33 was used to account for the path length followed by light in the reactor chamber. The path length corresponded only to the distance between the top of the central post (stirrer bar) to the PDMS membrane (Fig 5.6). This distance was 1.2 mm.
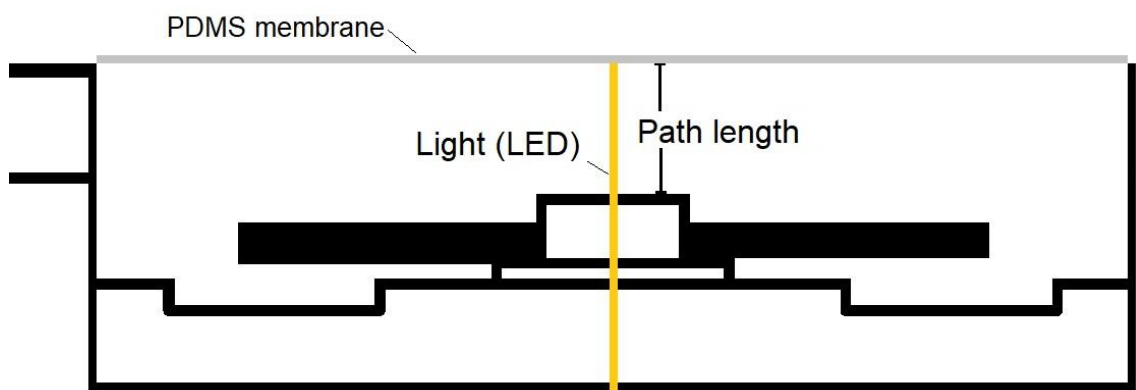
Figure 5.6. Path length for the measurement of optical density in the microbioreactor. The distance considered was 1.2 mm (from top of the central post to the PDMS membrane).

When comparing values of OD obtained with the microbioreactor and the spectrophotometer, reasonable agreement was found for a OD range between 0 and 2. A relationship of y=0.997·X+0.02 with r^2=0.997 was obtained. This confirmed comparability between microbioreactor and spectrophotometer measurements.

5.1.2 Scale Comparison between Microbioreactor and Minibioreactor

Once the OD instrumentation was calibrated, the next step was to evaluate scalability of the microbioreactor results. This was not easy since process variables (*e.g.* aeration rate and stirring speed) change with scale. The problem thus became to reproduce the results achieved in one scale into another scale (which used different variable settings).

A few criteria are reported in the literature for the scale-translation of bioprocesses. These criteria are thought to control the local cellular environment (e.g. DO concentration, pH, shear stress, etc.) to create reproducible conditions among scales. Among them, the most reported and of widespread use are the power number to volume ratio (P/V) and the volumetric oxygen transfer coefficient (k_La).

Although a very reliable methodology (Junker 2004), application of matched P/V ratios between the minibioreactor and the microbioreactor was not possible. As indicated in Table 3.3 (chapter 3), P/V ratios for the microbioreactor were extremely high (values ranging from 642 to 4334 kW/m^3 for rotation speeds from 200 to 1350 rpm) due to the tiny volume of the reactor. These values were much higher to what is normally reported for the DASGIP minibioreactor (2.42 KWatt/m^3 by Li and Sha 2016) which did not allow direct matching of P/V values.

Additionally, this confirmed one of the limitations of the P/V ratio as scale up criterion which is that it decreases when the scale increases (Acevedo *et al* 2002:255).

Another technique that has been commonly applied in scale-up is a matched oxygen transfer rate (OTR) or volumetric oxygen transfer coefficient (k_La). K_La is usually applied to aerobic fermentations where oxygen is a key substrate (Garcia-Ochoa and Gomez 2009). In these fermentations oxygen transfer is usually a rate-limiting step due to the low solubility of oxygen in the liquid medium. Even if not the growth-limiting substrate (as glucose usually is), oxygen still has an important effect on the microorganism's performance. For example, under oxygen limitations, cellular growth is slower and lower OD values are achieved. This suggested oxygen was an important substrate in the fermentation of the facultative anaerobe *Staphylococcus carnosus*.

For these reasons, k_La was chosen as the main criterion for scale-translation of the microbioreactor results. Additionally, geometrical similarity between the microbioreactor and the minibioreactor was considered, as some classic studies in biochemical engineering advise the use geometrical similarity in conjunction with other criteria of kinematic similarity (Aiba *et al* 1973; Wang and Cooney 1979).

A comparison of geometrical features (ratio liquid height to chamber diameter and ratio impeller diameter to chamber diameter) showed that the microbioreactor and the minibioreactor were of similar geometry (Table 5.2). A small difference was found in the ratio impeller diameter to chamber diameter. One attempt to reduce the diameter of the stirrer bar was tried in the microbioreactor, however, this resulted in lower k_La values. Therefore, the

diameter of the impeller was kept at 6 mm and the difference in ratio not considered important.

Table 5.2. Technical comparison between microbioreactor and DASGIP minibioreactor.

Parameter	Microbioreactor	DASGIP minibioreactor
Maximum gas flow (SLPM*)	NA (Diffusion aerated)	0.5
Chamber material	Polycarbonate	Glass
Working volume	157 µL	200 ml
V_{max} height** (mm)	2 (no headspace)	30
Chamber inner diameter (mm)	10	100
Ratio liquid height to chamber diameter	0.2	0.3
Impeller type	Paddle	Rushton turbine
Impeller quantity	1	2
Impeller diameter (mm)	6	40
Ratio impeller diameter to chamber diameter	0.6	0.4
Maximum agitation (rpm)	1350	2500 ***
Maximum tip speed ($m \cdot s^{-1}$)	0.45	3

*SLPM is Standard Litre Per Minute.

** V_{max} height is the height from bottom of the reactor to the top surface of the liquid at the operating volume.

*** Maximum agitation depends on the model of the motor used.

Another difference between the systems was that the minibioreactor used two Rushton turbines whereas the microbioreactor used a single paddle (centrally fixed bar) for mixing. Mixing in the microbioreactor was not necessarily worse because of this since data in chapter 4 (Table 4.2) showed mixing times of ~1.2 s for 850 rpm and 1030 rpm. Mixing time was not measured in the DASGIP minibioreactor although the manufacturer reports 1 s mixing time for a stirring speed of 2453 rpm. Operation at lower speeds of course will result in higher mixing times.

Scalability of results considered the comparison of OD and DO concentration profiles (Fig. 5.7) and the final fermentation values (Table 5.3).

500 rpm and 2 vvm were selected in the DASGIP minibioreactor as stirring and aeration conditions, respectively, which resulted in a value of k_La of 63 h^{-1} (Table 5.1). Although higher k_La values that could have provided optimum growth conditions for scale up were possible, a k_La of 62 h^{-1} was chosen to provide stable operation without extreme turbulence in the DASGIP reactor. Considering this, a stirring speed of 750 rpm and an aeration membrane with a thickness of 54 μm were selected for the microbioreactor resulting in a matched k_La of ~63 h^{-1}.

The difference in final OD values is significant and requires further investigation. This manifested in both OD and time profiles (as reflected by the value of the specific growth rate in Table 5.3). Growth in the microbioreactor was slower compared to the DASGIP reactor.

The difference in DO profiles was not extreme and might be due to design characteristics of both reactors (*i.e.* an sparged reactor versus a diffusion-based microbioreactor). In the DASGIP minibioreactor, air bubbles travelled from the bottom to the top of the reactor and thus oxygen was in direct contact with the media and the cells. This may have caused some difference in the way oxygen was assimilated by the cells. Despite this, DO profiles were similar as reflected in the maximum OUR value (547 mg h^{-1} L^{-1} for the microbioreactor and 550 mg h^{-1} L^{-1} for the DASGIP minibioreactor).
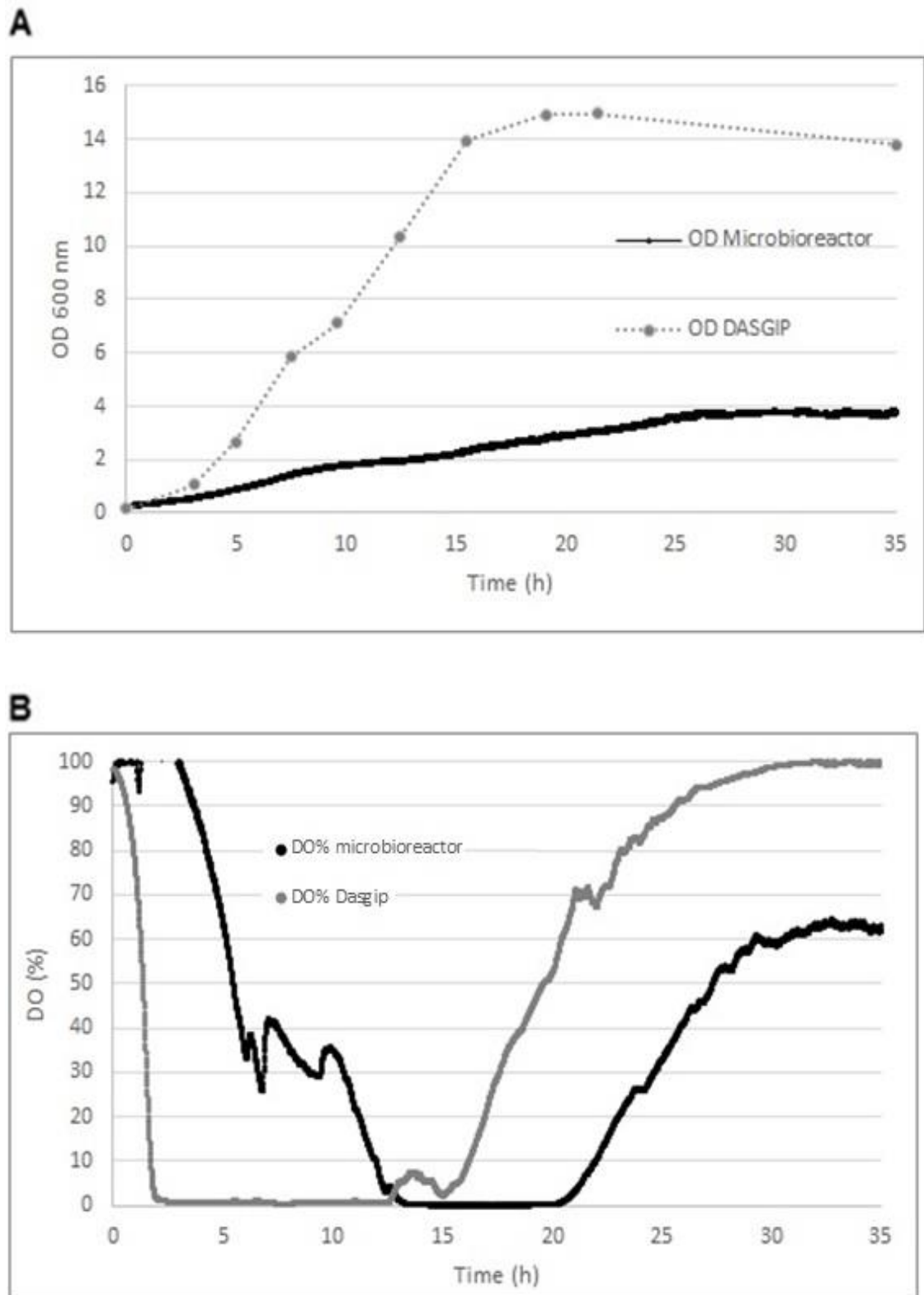
Figure 5.7. Scale comparison between microbioreactor and minibioreactor for the batch fermentation of *Staphylococcus carnosus* TM300. (A) Optical density profiles (mean vales for the DASGIP reactor). (B) Dissolved oxygen (DO%) profiles. A matched k_La of 63 h^{-1} was used. Temperature was 37°C.

Table 5.3. Comparison of operational parameters of the microbioreactor and the minibioreactor for the fermentation of *Staphylococcus carnosus* TM300.

Parameters	Microbioreactor	DASGIP minibioreactor
Stirring speed (rpm)	750	500
Tip speed ($m \cdot s^{-1}$)	0.1	0.25
Reynolds number	647	8361
$k_L a$ (h^{-1})	63	62
OD $_{initial}$	0.2	0.16
OD $_{final}$	3,8	13.8
DO $_{final}$ (%)	62	100
μ_{max}* (h^{-1})	0.25	0.49

*μ_{max} is maximum specific growth rate

The data presented here compares with the literature. Most scale up studies use *Escherichia coli* as microorganism. For example, Zhang *et al* (2006b) compared *E. coli* fermentation data from their microbioreactor (150 µL) with fermentations performed in 500 ml stirred tanks with three Rushton impellers (Sixfors ®, Infors AG, Switzerland) at a matched $k_L a$. Authors reported similar OD profiles values and specific growth rates, although the DO profiles presented a significant mismatch.

A more detailed comparison was performed by Funke *et al* (2010b) who compared a microbioreactor (comprised of a shaken microtiter plate) to a 2 L stirred-tank reactor (working volume 1 L) at a constant $k_L a$. The authors demonstrated very comparable OD, DO and pH profiles and a 2000-fold scale-translation for pH-controlled fermentations of *E. coli.*

5.1.3 Operation of the Microbioreactor in Chemostat Mode

Once batch operation was demonstrated the next step was chemostat operation. The chemostat mode of operation creates steady state conditions (*i.e.* chemical environment is static) which can facilitate the analysis of the growth of the strain and the determination of parameters.

The ideal chemostat reactor is essentially a perfectly mixed, continuous flow, stirred-tank reactor (Shuler and Kargi 2002; Acevedo *et al* 2002:125-126). It is important that the growth chamber is well-stirred, since this implies equal concentration of microorganisms and substrates in the reactor and at the outlet. Perfectly mixed conditions were proven in chapter 4 using a residence time distribution analysis. This determined that a stirring speed of 850 rpm created a mixing behaviour that resembled a continuous flow stirred-tank reactor. Thus, 850 rpm stirring speed was used in all experiments.

The first step to operate at chemostat conditions was to determine the value of the dilution rate (D) to use. The dilution rate is the rate of nutrient exchange and, at steady state conditions where the concentration of metabolites and cells is constant, can be considered equal to the specific growth rate of the microorganism (μ).

First, the Monod Equation (Monod 1949) was used to describe the specific growth rate as Equation 5.3:

$$\mu = \frac{\mu_m \cdot S}{K_s + S}$$

Equation 5.3

Where S is the concentration of the limiting substrate for growth and K_s the value of S when the ratio μ to μ_m is 0.5. S in this case is glucose, and as demonstrated in Figure 5.1 and 5.3, is the growth limiting substrate for the fermentation of *Staphylococcus carnosus.*

Second, the range of operation for the dilution rate was estimated using the concept of critical dilution rate D_{crit}. This is the highest dilution rate that can be used in the reactor before leading to cell washout. At washout conditions the concentration of substrate in the reactor equals the concentration of substrate in the feed, therefore equation 5.3 becomes:

$$D_{crit} = \mu = \frac{\mu_m S_0}{K_S + S_0}$$

From the above expression, it was noticed that $D_{crit} < \mu_m$. Additionally, the value of D_{crit} is very close to μ_m when the value of K_s is much lower than S_0.

The maximum specific growth rate for *Staphylococcus carnosus* in the microbioreactor was 0.4 h^{-1}. This value was reported in the work by Krull 2017.

Assuming a very assimilable substrate implies that $K_s \ll S_0$ and $D_{crit} \approx \mu_m$.

Thus, the maximum flow rate F allowed in the reactor can be calculated as:

$$F = D_{crit} \cdot V = 0.4 \, [h^{-1}] \cdot 157 \, [\mu L] \cdot \left[\frac{1\,h}{60\,min}\right] = 1.05 \, \mu L \cdot min^{-1}$$

Considering the above upper limit, two dilution rates (0.11 h⁻¹ and 0.38 h⁻¹ at 0.3 $\mu L \cdot min^{-1}$ and 1 $\mu L \cdot min^{-1}$, respectively) were chosen for chemostat experiments. The flow rates associated to these dilution rates allowed operation without worrying about the wash-out of cells.

The right time to start the feeding of nutrients after initial batch operation was also in question. If the time was too early a risk of cell washout existed (the cells may not be growing rapidly enough or in insufficient concentration). Thus, 3 hours of batch fermentation were allowed before initiating the feed.

As explained in the review at the beginning of the chapter, a stirring speed of 850 rpm and a membrane thickness of 100 μm were selected for chemostat experiments. This resulted in a k_La value of 62 h⁻¹ in RO water and 53 h⁻¹ in fermentation media. This difference was determined experimentally and considered due to an increment in liquid viscosity when using LB media (LB media contains yeast extract, amino acids and peptides that can affect the liquid phase viscosity.) Viscosity of the fermentation media was measured using a rotational rheometer and was a 15% percent higher compared to the viscosity of RO water at 37 °C. Values for LB fermentation media were 0.79 mPa·s and for RO water 0.7 mPa·s.

Two different steady states were achieved for the stated dilution rates (Fig. 5.8 and Fig. 5.9). The use of glass syringes allowed precise control over the flow rate with no pulsation effects that affected the achievement of a constant concentration value.

For Fig. 5.8 (D = 0.11 h⁻¹) a steady state was achieved after 40 hours of operation (37 hours after the feed was switched on). Both OD and DO profiles evidenced a low cell growth rate with a DO concentration of 83.1% (mean of the last 5 hours

of operation) achieved at the steady state. OD values between 4 and 5 were achieved, which is comparable to batch fermentations, and a low oxygen consumption demonstrated low microbial activity.

5.1.3.1 Effect of Dilution Rate on Chemostat Growth

Figure 5.8. Optical density and dissolved oxygen profiles for the chemostat fermentation of *Staphylococcus carnosus* TM300 at D=0.11 h^{-1}. Experimental conditions were 37°C, 850 rpm and a 100 μm thickness aeration membrane (k_La=53 h^{-1}). n=1 run.

Steady state operation allowed the potential to probe cell metabolism through the determination of growth parameters. For example, OUR was calculated for D=0.11 h^{-1} at the steady state (DO concentration = 83.1%) using Equation 5.1 as:

$$OUR_{D=0.11} = k_L a \cdot (C^* - C_L) - \frac{dC_L}{dt}^{SS}_{D=0.11} = 53 \cdot (6.7 - 0.831 \cdot 6.7) - \frac{dC_L}{dt}^{SS}_{D=0.11} =$$

$$125 \; mg \cdot h^{-1} \cdot l^{-1} = 3.9 \; \text{mmol } O_2 \, h^{-1} \cdot l^{-1}$$

For Fig.5.9 (D=0.38 h^{-1}) steady state was achieved after approximately 10 hours of operation (9 hours after the feed was switched on). This was very rapid and consistent with higher specific growth rates.
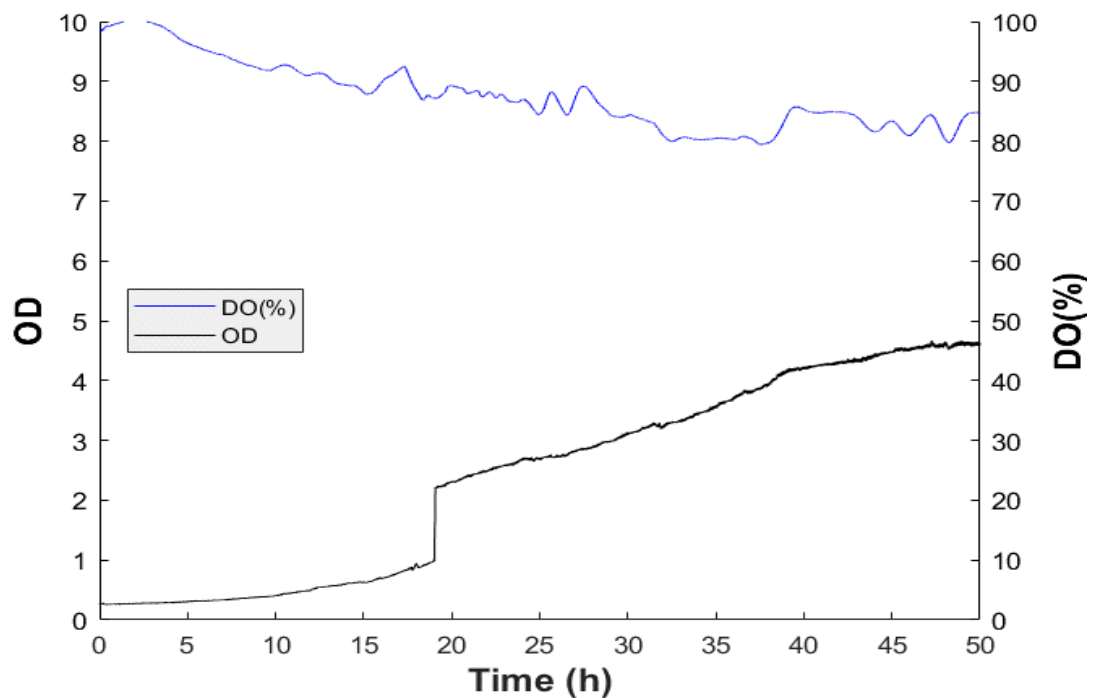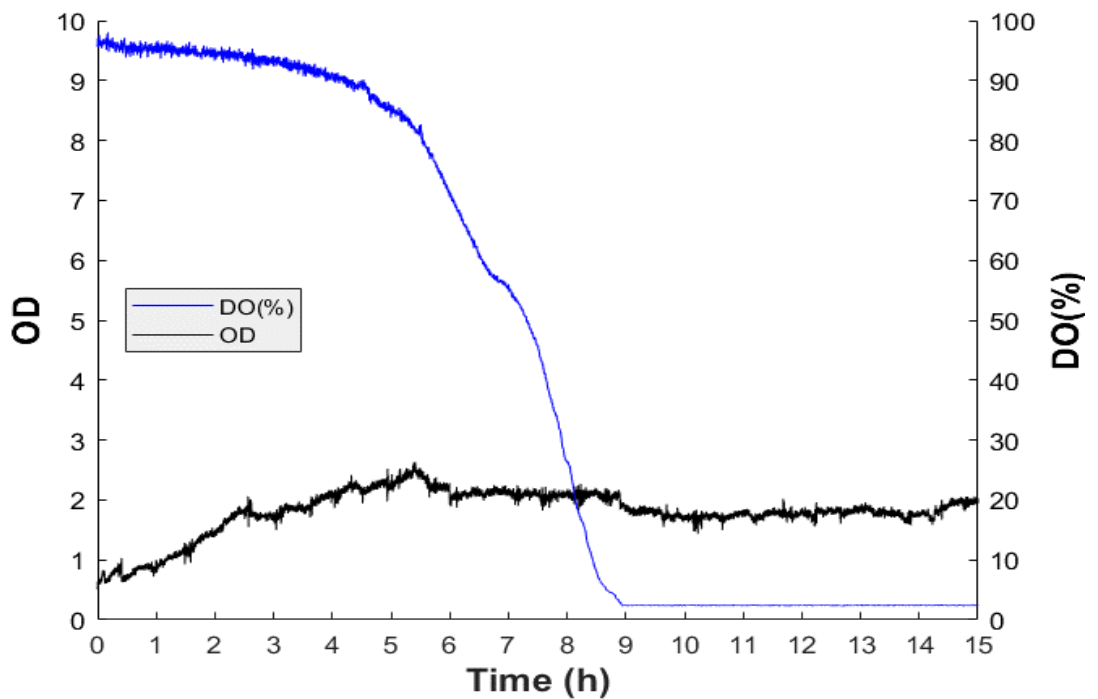

Figure 5.9. Optical density and dissolved oxygen profiles for the chemostat fermentation of *Staphylococcus carnosus* TM300 at D=0.38 h^{-1}. Experimental conditions were 37°C, 850 rpm and a 100 µm thickness aeration membrane (k$_L$a=53 h^{-1}). n=1 run.

OUR for D=0.38 h^{-1} was calculated as:

$$OUR_{D=0.38} = k_L a \cdot (C^* - C_L) - \frac{dC_L}{dt}^{SS}_{D=0.38} = 53 \cdot (6.7 - 0.024 \cdot 6.7) - \frac{dC_L}{dt}^{SS}_{D=0.38} =$$

$$347 \; mg \cdot h^{-1} \cdot l^{-1} = 11 \; \text{mmol} \; O_2 \, h^{-1} \cdot l^{-1}$$

Data showed that the lower the dilution rate the latest the stationary state was reached. Additionally, higher OD values were achieved at the lower dilution rate which was expected since the wash-out of cells was minimized. Opposite to this, the higher the dilution rate the lower the value of OD achieved at the steady state and the earlier the steady state was achieved, as confirmed in other studies Edlich *et al* (2010).

Microbioreactor DO data in chemostat mode confirmed a proportional relationship between OUR and the specific growth rate (dilution rate). This is reported in the literature (Garcia-Ochoa *et al* 2010) for the OUR determination *via* stoichiometric balance of the oxygen assimilated into biomass.

For each steady state, samples from the outlet were taken for visualisation of cell morphology under the microscope. No significant changes were found compared to cells grown in batch cultures either in the microbioreactor or in shake flasks (Fig. 5.10). Additionally, pH levels were not measured, although the pH buffer (K_2HPO_4/KH_2PO_4) was expected to maintain values stable.
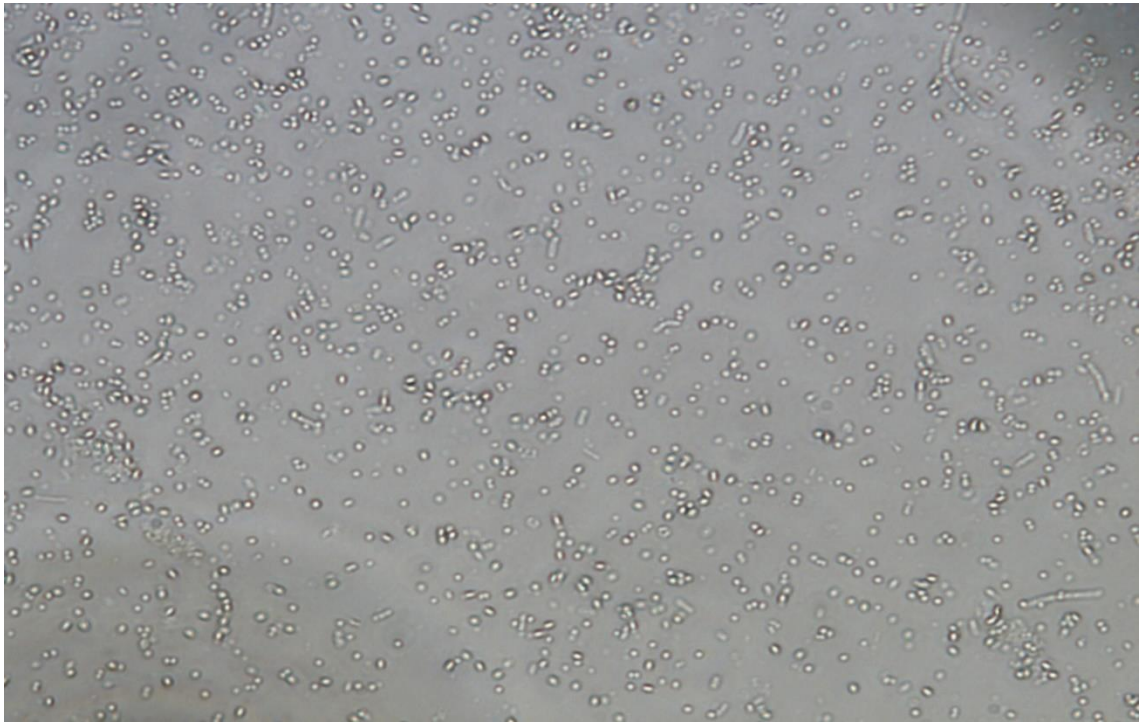
Figure 5.10 Confirmation of morphological properties of *Staphylococcus carnosus* TM300. A sample from the outlet of the microbioreactor was taken for visualisation of cell morphology under the microscope when operating at D=0.38 h^{-1}.

Values of doubling time in the steady state achieved were 6.3 hours for (D=0.11 h^{-1}) and 1.8 hours (D=0.38 h^{-1}). These values are very similar to the ones obtained with *Saccharomyces cerevisiae,* which grows quickly in glucose achieving doubling times between 1 and 4 hours (Acevedo *et al* 2002:97).

During chemostat operation, one important check is the existence of chemotaxis. Chemotaxis is the movement of the microorganism towards the syringe reservoir where a high concentration of glucose exists, provoking contamination. Although this problem was not expected since *Staphylococcus carnosus* is a non-motile microorganism, verification was needed.

Two samples from the syringe reservoir and the feeding tubing were collected in tubes and used to inoculate agar plates (Fig. 5.11). The agar plates were

cultivated at 37°C for 24 hours. No growth was observed in the plates which confirmed no chemotaxis phenomenon.
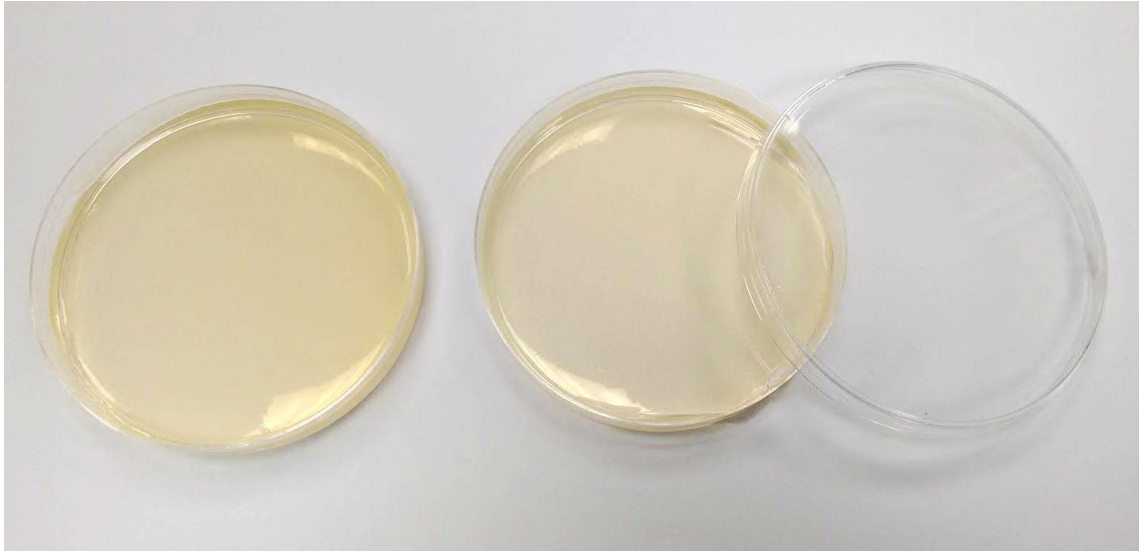
Figure 5.11. Confirmation of chemotaxis during the chemostat fermentation of *Staphylococcus carnosus* TM300. Samples from media reservoir and feeding tubing were used to inoculate agar plates, which after being incubated for 24 hours at 37 °C, exhibited no growth.

One point to consider was the effect of the evaporation compensation rate on chemostat operation. This water compensation flow of 0.15 µL/min was included as a second input. The value was not considered when calculating the dilution rate since the water entering was assumed to be used exclusively in replenishing the evaporated water from the reactor. Thus, the water entering was not supposed to leave by the effluent. Nevertheless, at very low operational flow rates (*i.e.* F=0.3 µL/min for D = 0.11 h^{-1}) the water flow was half the value for the feed flow entering to the reactor. This may have influenced the OD and DO profiles and the time needed to achieve steady state.

.

5.1.3.2 Perturbation of chemostat operation by changing the concentration of glucose in the inlet

Besides the change in dilution rate, it was also possible to obtain a steady state by changing the concentration of glucose at the inlet (Fig. 5.12). The change consisted in doubling the concentration of glucose from 1 g·l^{-1} to 2 g·l^{-1} after 20 hours of operation after achieving steady state. As expected from chemostat operation with glucose as a growth-limiting substrate, data showed that cells grew in direct proportion with respect to the new glucose input (at the steady state: $ODsteady\ state \propto Y_{X/S} \cdot (S_0 - S)$).

Indeed, optical densities changed from 2.21 in the first steady state to 3.74 in the second steady state after the perturbation (values calculated as the mean of the OD points at the steady state). This represented a 68% increase in OD values.

Before achieving steady state at time equals zero, cells grew in aerobic conditions for approximately 25 hours (data not shown but included high variability in both DO and OD profiles). After this, cells started to grow under anaerobic conditions from 20 hours onwards (Fig. 5.13).

Although the production of carbonaceous compounds was not measured, anaerobic conditions very likely resulted in high amounts of lactate due to the homofermentative nature of *Staphylococcus carnosus*.
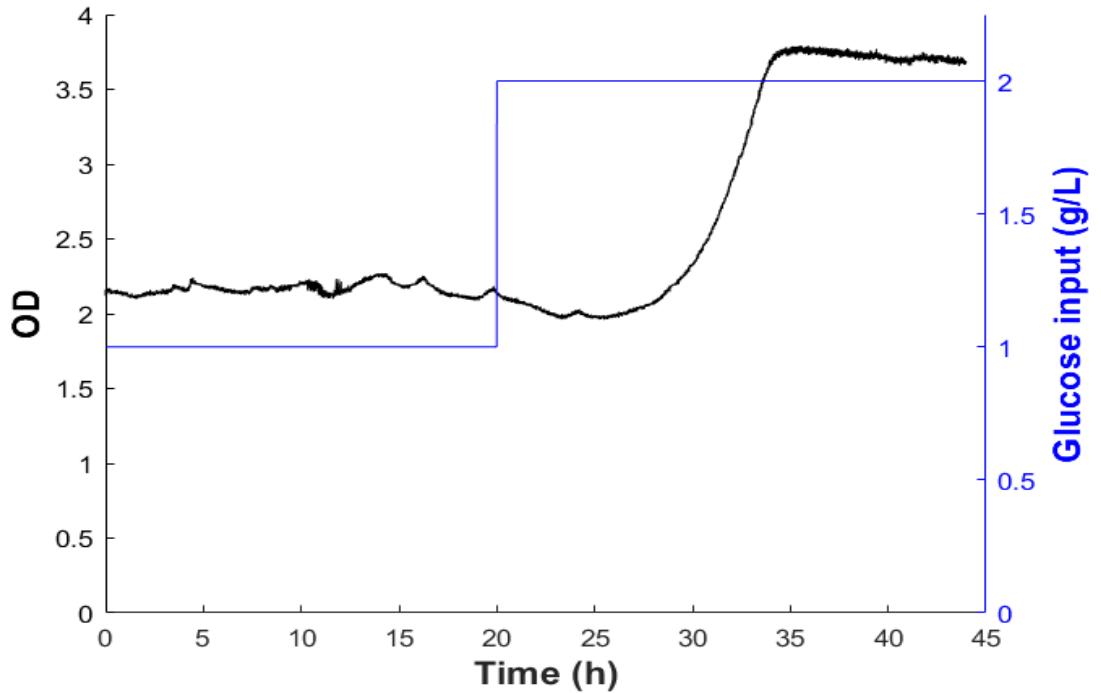
Figure 5.12. Perturbation of the chemostat fermentation of *Staphylococcus carnosus* TM300 by changing the glucose concentration in the feed. A steady state was achieved when glucose concentration was doubled from 1 g·l^{-1} to 2 g·l^{-1}. n=1.
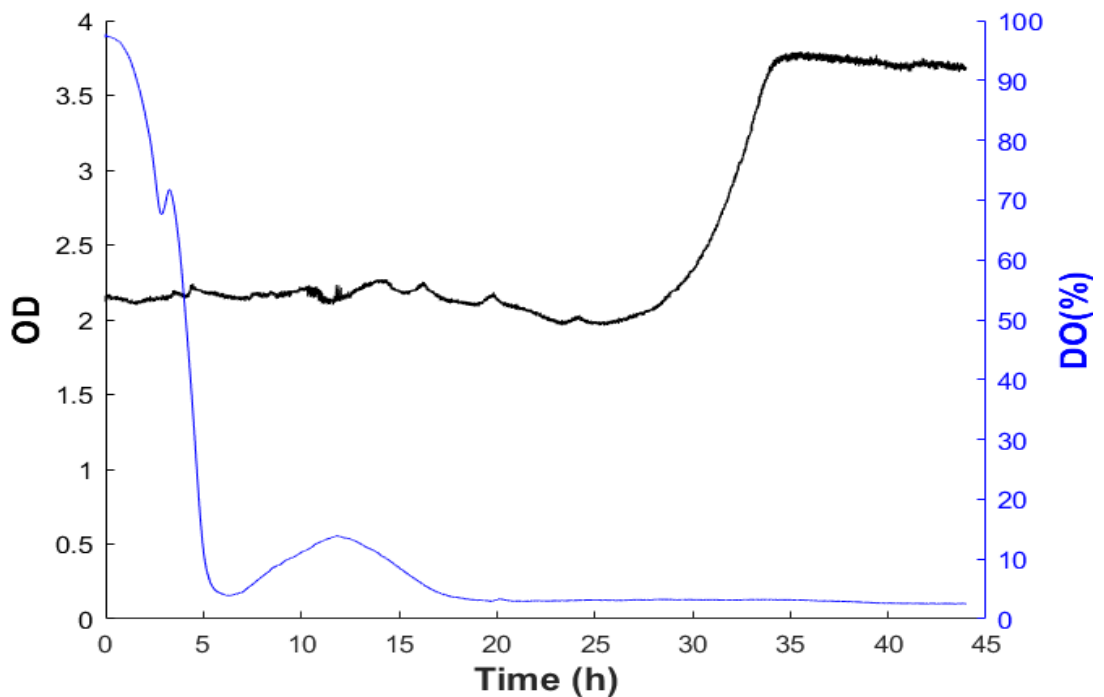
Figure 5.13. OD and DO% dynamics during the Perturbation of the chemostat fermentation of Staphylococcus carnosus TM300 by changing the glucose concentration in the feed. Dilution rate used (0.11 h^{-1}) created anaerobic growth conditions for the second steady state. Experimental conditions were 37°C, 850 rpm and a 100μm thickness aeration membrane (k$_L$a=53 h^{-1}).

Chemostat experiments with feed concentration control demonstrated the ability of the system to create controlled perturbation and change OD values. Dynamic operation (*i.e.* a perturbation of the steady state) can be used to understand how cells responds to environmental changes.

The perturbation experiment could be further developed by introducing a second change in the glucose input (back to 1 g·l^{-1}) and evaluating the response in OD values. A 68% decrease in OD values would be expected. Additionally, it is desired to exert control over DO (%) to ensure cells do not switch from aerobic metabolism to anaerobic metabolism.

Results in this section compare favourably with the literature. Lee *et al* (2011), for example, reported a 1 ml plastic-PDMS device for dynamic continuous culture of *Escherichia coli* for over 500 hours. The authors achieved several steady states by changing the inlet glucose concentration and other process variables. They reported a proportional relationship between OD and time when a perturbation in glucose was performed. The authors controlled dissolved oxygen concentration to a desired set point of 50%.

5.2 Conclusions

In chapter 4 studies were made on the effect of design parameters on microbioreactor performance. Specifically, the effect of stirring speed and membrane thickness in $k_L a$ was determined. Data in chapter 4 also showed the stirring speed conditions in which the reactor operated as a perfectly mixed, continuous flow stirred-tank reactor. The next step was then to use the $k_L a$ and the stirring speed information obtained in the scale-translation of fermentation results and the chemostat operation at perfectly mixed conditions, respectively.

Benchmarking studies using both shake flasks and the minibioreactor showed that *Staphylococcus carnosus* can grow aerobically and anaerobically with a significant part of the fermentation being anaerobic.

Scale-up of the microbioreactor results was attempted for the fermentation of *Staphylococcus carnosus* growing in lysogeny broth. Both bioreactor systems were compared on a geometrical basis and on an oxygen transfer basis. Fermentations at a matched $k_L a$ of 63 h^{-1} demonstrated comparable volumetric oxygen uptake rates in both systems. Although a noticeable limitation was that the highest $k_L a$ value obtained with the DASGIP system was 62 h^{-1}. Values higher than this provided extreme turbulence and demonstrated unsuitable for stable operation. Additionally, the highest $k_L a$ value obtained with the microbioreactor was ~113 h^{-1}, which limited the amount of growth conditions that can be tested with the device for scale-up purposes.

Some questions remained after the scale-up attempt. For example, when k_La is fixed OTR can also be increased by increasing the mol fraction of oxygen in the media (*i.e.* the oxygen saturation concentration). Higher OTRs would allow optimum grow profiles for scale-up. In addition, a higher mol fraction of oxygen in the media would allow better oxygenation of the minibioreactor under stable conditions without increasing stirring speed or gas flow rate.

Once scale-translation was attempted chemostat operation was addressed. The aim was to prove operation in the microbioreactor at steady state for the rigorous analysis of growth conditions. Two important questions were: what variables can be controlled? and what is their effect on growth?

First, chemostat operation with the microbioreactor was studied measuring the influence of dilution rate on OD and DO profiles. Chemostat operation at different dilution rates resulted in well-defined steady states in terms of OD and DO concentrations. Variation of the dilution rate demonstrated the capability of the device of rapidly screening for growth conditions. As expected from chemostat operation, OD and DO profiles demonstrated a dynamic balance between cell growth and medium feed rate at the steady state. This was consistent with chemostat operation reported at larger scales but with ~1000 times smaller volumes. For the dilution rate condition D=0.38 h^{-1}, steady state was achieved quickly after the feed was introduced. This demonstrated robust flow conditions maintained with little variation over time.

Chemostat operation allowed the determination of OUR values at different dilution rates. Determination of growth parameters is useful when a detailed characterization of the properties of the strain is required.

A change in the concentration of glucose at the inlet created a proportional change in OD concentration. This was expected from chemostat theory for the operation of the reactor at steady state with glucose as the only growth-limiting substrate. Nevertheless, this experience needs further investigation of the carbonaceous compounds being produced and repetition under DO controlled conditions to avoid changes from aerobic to anaerobic metabolism.

Overall the microbioreactor platform proved reliability and comparability with other bioreactors. Chemostat operation at different dilution rates demonstrated the ability of the microfluidic device of rapidly screening for growth conditions Control over parameters such as the specific growth rate, and the ability of the system to create controlled perturbations to the reactor microenvironment proved successful.

6   CONCLUDING REMARKS

6.1 Summary of results

This project aimed to build on existing work to develop a microfluidic system for cell culture process development with application in synthetic biology. Synthetic biology aims to engineer cells to create a variety of products with applications in healthcare, food, materials and biofuels. This requires of the rigorous characterization of the growth conditions of the strains which encompasses growing cells in reactor chambers.

Microbioreactors for cell culture studies offer the potential to alleviate issues encountered at larger scales. The aim of this thesis was the development and engineering characterization of an instrumented microbioreactor system capable to operate in chemostat mode to aid scientists in the biological characterization of strains with minimal use of reagents and control over the microenvironment.

Through this investigation, an existing device (microbioreactor cassette) was further developed and characterized. This included the evaluation of two options for mixing and a comparison with a second microbioreactor design (suspension microbioreactor). The microbioreactor cassette design was flexible and able to include two mixing (stirring) methods: a free-rotating stir bar and a centrally fixed stir bar. Mixing with the free-rotating bar was poor as confirmed by low Reynolds numbers and oxygen transfer rates. The centrally fixed bar, on the other hand, provided high oxygen transfer rates.

Analysis of the suspension microbioreactor considered residence time distribution studies and oxygen transfer measurements. Residence time distribution analysis proved that the device was not suitable for fermentation work due to deficient mixing with a high percentage of stagnant zones (over 10%).

Additionally, very low oxygen transfer rates were obtained, which discarded application of the device in bacterial culture where higher rates are needed.

Appearing as the most promising option to use in fermentation, the microbioreactor cassette with the centrally fixed bar as stirring method was fully characterized in terms of oxygen transfer, mixing and residence time distribution. Data on oxygen transfer studies showed that the most influential parameter on k_La was the stirring speed followed by the thickness of the aeration membrane. In terms of mixing, an automated and accurate methodology for the measurement of mixing time was developed and implemented. Mixing times decreased at higher stirring speeds and values lower than 10 seconds were achieved for all stirring conditions, which demonstrated rapid mixing in the device. RTD analysis demonstrated that the reactor can operate at nearly ideally mixed conditions (*i.e.* as a continuous flow stirred-tank reactor) which was confirmed by the low percentage of stagnant volumes (~1%).

Characterization of the microbioreactor cassette provided information that allowed the selection of stirring speed conditions and membrane thickness for scale-translation and chemostat studies.

The microbioreactor was compared to an industry standard minibioreactor based on a matched k_La value of 63 h^{-1}. Scale-translation results showed comparable volumetric oxygen uptake rates. A noticeable limitation was that the highest k_La value obtained with the microbioreactor was ~113 h^{-1} which limited the amount of growth conditions that can be tested with the device for scale-up purposes.

Once batch operation was ensured and linked to larger bioreactors, continuous operation was addressed. The aim was to demonstrate that chemostat operation at steady-state conditions facilitated characterization of growth conditions.

Chemostat operation was then studied from the viewpoint of the influence of two operational variables on performance: dilution rate and glucose input concentration.

Well-defined steady states in terms of OD and DO concentrations were found for the range of dilution rates tested. Microbioreactor operation was consistent with chemostat operation reported at larger scales but with 1000 times smaller volumes. Variation of the dilution rate in this experiment demonstrated the ability of the device of rapidly screening for growth conditions.

A change in glucose input concentration at the steady state resulted in a proportional change in OD and the achievement of a second steady state. A proportional increase was expected from theoretical considerations and demonstrated the ability of the system to control the OD value to a steady point.

Finally, chemostat operation allowed the easy determination of growth parameters such as OUR. This demonstrated the potential application of the microbioreactor in synthetic biology studies where a full characterization of the properties of the strain is required.

6.2 Future work

Future work related to this research can be divided into: (1) extension of the investigations in the microbioreactor cassette system, (2) expansion of those investigations (3) development of cheap and disposable online sensors, (4) implementation and demonstration of different modes of operation and substrate feeding strategies (5) parallelization of microbioreactors (6) software aspects.

Firstly, regarding extending the investigation presented here, chemostat experiments should be repeated to have three good trials per dilution rate condition. This would allow the calculation of standard deviations for the OD and DO profiles and a quantification of the variability observed. Repetition of experiments is linked to parallelization of reactors which will be described later in this section (5). Additionally, repetition of experiments could provide useful information about how to improve the fluidic configuration and the method for reactor priming.

Measuring the evaporation rate more accurately for the specific stirring speed condition used here (850 rpm) should be considered. This can be achieved by measuring the weight increase of anhydrous calcium sulphate pellets placed in a closed chamber with the microbioreactor (Zhang *et al* 2006b). Additionally, other options that involve prevention of evaporation rather than compensation should be explored (*e.g.* humidifying the gas entering to the incubator). This would improve reliability of continuous operation since extra inputs would not be needed.

Testing dilution rates between 0.38 and 0.46 is needed to provide a complete description of the operational range of dilution rates for chemostat operation.

Additionally, the method of wash-out described by Pirt and Callow 1960 should be implemented to determine the value of the critical dilution rate D_{crit}.

Finally, it is suggested to further develop the experiment of change in the concentration of glucose at the reactor inlet. First, this experience need to be repeated under DO controlled conditions to avoid changes from aerobic to anaerobic metabolism. Second, measurement of the carbonaceous compounds being produced is needed. Third, experiments involving several changes in glucose concentration during operation and the evaluation of cell response are suggested.

Expansion of the investigations performed in this thesis consider the study of the effect of dilution rate and glucose input on gene and protein expression during chemostat operation. Quantification of protein expression (for example GFP), however, requires the implementation of *in-situ* measurement of fluorescence in the microbioreactor. For this, a blue LEDs (465 nm), a collimating lens, a band pass filter and a collecting lens should be integrated to the current optical set-up. Fluorescence measurements combined with DO monitoring of the culture could provide interesting information such as whether proteins are being expressed constitutively or under oxygen limitations.

Quantification of product expression would allow a full description of the chemostat fermentation of *Staphylococcus carnosus*. This would facilitate writing the mass balance for carbon utilization and product formation. Using the mass balance with kinetic expressions for growth and production (*e.g.* the empirical model of Luedeking and Piret 1959) would allow the determination of growth and production parameters from experimental data. This would require testing more

dilution rates and measuring the concentration of glucose and product regularly at the effluent.

The development of cheap and disposable online sensors is a whole area of development for microbioreactor technology (Gruber *et al* 2017; Pfeiffer and Nagl 2015). The current reactor system could easily add a pH sensor. pH optodes have already been developed and are a commercial standard for some companies, although they need to ensure measurement over the whole pH range of the fermentation.

Glucose sensing could be addressed by spectroscopic methods, optical sensors or electrochemical probes. Glucose sensing *via* spectroscopic methods is suggested here and could involve Raman spectroscopy. A commercial Raman Analyser could be integrated to the current microbioreactor optical system using an OPC (Object linking and embedding for process control) communication protocol related to LabVIEW.

The implementation and demonstration of different modes of operation (*e.g.* turbidostat) and substrate feeding strategies (*e.g.* fed-batch) also needs consideration. This thesis includes information about batch and continuous operation. Batch operation was the easiest to handle from a fluidic point of view requiring only to manage liquid evaporation. Chemostat operation, however, required also to control in and out-flow to the reactor. Other operational modes would require the development of control loops.

The parallelization of microbioreactors is clearly desirable for all the applications discussed here. The main requirement is to be able to run multiple experiments where different strains or culture conditions can be compared. This would improve reproducibility of experiments and allow the quantification of the

observed variability as discussed in (1). The issue with multiple bioreactors is the development of smart technical solutions to perform multiple measurements (*e.g.* integration of multiple optical fibers), and to provide multiple reactor conditions (*e.g.* mixing or oxygenation) in parallel and in the same experimental platform.

Finally, if large numbers of experiments will be performed and real-time data acquired then software aspects will need to be considered. Handling very large amounts of data will pose problems in terms of computer power (data processing) and storage. At the level of multiple parallel reactors specially dedicated software would certainly be a requirement. A first step, in terms of the research presented here, is to modify the MATLAB script written for OD and DO processing to allow on-line processing and plotting of the data. This modification would allow to keep track of the state of the fermentation and detect if abnormal situations occur.

7   APPENDIX I – ENERGY BALANCE TO INCUBATOR

If we consider a steady-state flow process (*i.e.* all properties of the system are invariant, therefore there is no accumulation or change over time in the energy of the system) an energy balance can be applied to the incubator as:

$$\sum_{INPUT\ STREAMS} (M_i h_i) - \sum_{OUTPUT\ STREAMS} (M_o h_o) + Q + W = 0$$

Where *i* represents the inlet conditions and *o* the outlet conditions, $+ Q$ the energy that enters to the system as heat, $+ W$ the energy that enters to the system as work (for the motor at 1350 rpm is 0.686 Watts or 2470 J/h), M the mass flow that enters to the system, and h the specific enthalpy.

If we consider the inlet flow conditions as:

Temperature = 37.5 °C, Density at 37.5 °C (g/ml) = 0.9932 (Frostburg state university 1997) Enthalpy at 37.5 °C (J/g) = 311 (Doran, 1995:410), M_i= 1 ml/s (3575.8 g/h)

And the outlet flow conditions as:

Temperature = 36 °C (measured at the outlet flow), Density at 36 °C (g/ml) = 0.9936 (Frostburg state university 1997), Enthalpy at 36 °C (J/g) = 306.98 (Doran, 1995:410)

M_o= 1 ml/s (3577 g/h)

And we replace these numbers in the provided equation we find:

$$(3575.8 \times 311 - 3577 \times 306.98 + 2470) = -Q = 16476 \text{ J/h} = 16.48 \text{ KJ/h}$$

7 APPENDIX II – PIECES OF CODE

a) Matlab code for counting the movement of the centrally fixed bar

```matlab
all=dir ('C:\Users\nlobo\Desktop\Back up PhD Nelson B\Back up UCL
NICOLAS\Data Nelson Thesis\Chapter 1\2 PRELIMINARY
TESTS\2.1\2.1.1\198'); all=all(3: end);


for i=1:size(all,1)

filename=sprintf('%s','C:\Users\nlobo\Desktop\Back up PhD Nelson B\Back
up UCL NICOLAS\Data Nelson Thesis\Chapter 1\2 PRELIMINARY
TESTS\2.1\2.1.1\198'), all(i).name); %import files

im=imread(filename);

im=single(im);

s(i)=im(227,427); % identify specific pixel point

 end

s=double(s);

figure, plot(s)

 [PKS,LOCS]       =       findpeaks(s*(-1),'MINPEAKHEIGHT',       -
50,'MINPEAKDISTANCE',10); % identify pixel height and distance between
peaks

 hold on,plot(LOCS,s(LOCS),'r*')

for j=1:size(LOCS,2)-1


p(j)=LOCS(j+1)-LOCS(j);

end

pp=mean(p)

rpm= (0.5*60*250)/pp %calculate number of rotations per minute
```

8 REFERENCES

Abate, A.R., Hung, T., Sperling, R.A., Mary, P., Rotem, A., Agresti, J.J., Weiner MA., and DA. Weitz. 2013. DNA sequence analysis with droplet-based microfluidics. *Lab on a Chip*, 13(24): 4864-9.

Acevedo, F., Gentina, J.C., and A. Illanes. 2002. Fundamentos de ingeniería bioquímica. 2nd edition. Valparaíso: Ediciones Universitarias de Valparaíso. Chile. p. 97, pp.125-126, p.223, p.255.

Adams, BL. 2016. The next generation of synthetic biology chassis: moving synthetic biology from the laboratory to the field. *ACS Synthetic Biology*, 5(12): 1328-1330.

Aiba, S., Humphrey, AE., and NF. Millis. 1973. Biochemical engineering. 2nd Edition. New York: Academic Press. Chapter 6, 7 and 8.

Anderlei, T., Zang, W., Papaspyrou, M., and J. Büchs. 2004. Online respiration activity measurement (OTR, CTR, RQ) in shake flasks. *Biochemical Engineering Journal*, 17, 187-194.

Applikon Biotechnology, B.V. 2017. *Applikon Mini bioreactor systems*, viewed 07 September 2017, <http://www.applikon-bio.com/en/news2/itemlist/category/35-mini-bioreactors>.

BacMap Genome Atlas. 2017. *Staphylococcus carnosus subsp. carnosus TM300*, viewed 07 September 2017, <http://bacmap.wishartlab.com/organisms/844>.

Balagaddé, FK., You, L., Hansen, CL., Arnold, FH., and S.R. Quake. 2005. Long-term monitoring of bacteria undergoing programmed population control in a microchemostat. *Science*, 309(5371):137-140.

Becker, H., and C. Gärtner. 2008. Polymer microfabrication technologies for microfluidic systems. *Analytical and Bioanalytical Chemistry*, 390(1): 89-111.

Bennett, MR., and J. Hasty. 2009. Microfluidic devices for measuring gene network dynamics in single cells. *Nature Reviews Genetics*, 10, 628-638.

Berney, M., Weilenmann HU., Ihssen, J., Bassin, C., and T. Egli. 2006. Specific growth rate determines the sensitivity of *Escherichia coli* to thermal, UVA, and solar disinfection. *Applied Environmental Microbiology*, 72(4): 2586-2593.

Berthier, E., Warrick, J., Yu, H. and DJ. Beebe. 2008. Managing evaporation for more robust microscale assays: Part 1. Volume loss in high throughput assays. *Lab on a Chip*, 8(6): 852.

Betts, JI., and Baganz, F. 2006. Miniature bioreactors: current practices and future opportunities. *Microbial cell factories,* 5, 21.

Betts, JI., Doig, SD. and F. Baganz. 2006. Characterisation and application of a miniature 10 mL stirred-tank bioreactor, showing scale-down equivalence with a conventional 7 L reactor. *Biotechnology Progress,* 22(3): 681-688.

Betts, JI., Doig, SD and Baganz F. 2005.The characterisation and application of a novel miniature stirred bioreactor for the scale down of industrially-relevant microbial fermentations. In *Biochemical Engineering XIV: Frontiers and Advances in Biotechnology, Biological and Biomolecular Engineering,* British Columbia, Canada.

Bin, AK. 1984. Mass transfer to the free interface in stirred vessels. *Chemical Engineering Communications,* (31): 155–183.

Bird, RB., Steward, WE., and E.N. Lightfoot .2002. Transport phenomena. New York: John Wiley and Sons, Inc.

Blanch, HW., and Clark DS. 1996. Biochemical engineering. New York: Marcel Dekker, Inc.

Boccazzi, P., Zhang, Z., Kurosawa, K., Szita, N., Bhattacharya, S., Jensen, K.F., and A.J. Sinskey. 2006. Differential gene expression profiles and real-time measurements of growth parameters in *Saccharomyces cerevisiae* grown in microliter-scale bioreactors equipped with internal stirring. *Biotechnology Progress*, 22(3):710-7.

Boccazzi, P., Zanzotto, A., Szita, N., Bhattacharya, S., Jensen, K.F., and A.J. Sinskey. 2005. Gene expression analysis of *Escherichia coli* grown in miniaturized bioreactor platforms for high-throughput analysis of growth and genomic data. *Applied Microbiology and Biotechnology,* 68(4):518- 532.

Bruus, H. 2007. *Theoretical Microfluidics*. Oxford: Oxford University Press. p.1.

Brückner, N. 1997. Gene replacement in *Staphylococcus carnosus* and *Staphylococcus xylosus. FEMS Microbiology Letters,* 151 (1): 1-8.

Cameron, D.E., Bashor, C.J., and J.J. Collins. 2014. A brief history of synthetic biology. *Nature reviews. Microbiology*, 12(5): 381-90.

Cornell science and engineering. 1996. *Calculating the oxygen diffusion coefficient in water*, viewed 07 September 2017, <http://compost.css.cornell.edu/oxygen/oxygen.diff.water.html>.

Davies, M.J., Nesbeth, D.N., and N. Szita. 2013. Development of a microbioreactor "cassette" for the cultivation of microorganisms in batch and chemostat mode. *Chimica Oggi/Chemistry Today,* 31(3):46-49.

Davies, J., and D. Davies. 2010. Origins and evolution of antibiotic resistance. *Microbiology and Molecular Biology Reviews*, 74(3):417-433.

Davis, M.E., and R.J. Davis. 2003. Nonideal flow in reactors. In: Fundamentals of chemical reaction engineering. New York: McGraw-Hill Higher Education. p.262.

Dénervaud, N., Becker, J., Delgado-Gonzalo, R., Damay, P., Rajkumar, A.S., Unser, M., Shore, D., Naef, F., and S.J. Maerkl. 2013. A chemostat array enables the spatio-temporal analysis of the yeast proteome. In: *Proceedings of the National Academy of Sciences of the United States of America*, 110 (39): 15842-15847.

Devries, P., and Hasbun, J. 2011. A first course in computational physics. 2nd edition. Jones and Bartlett Publishers p. 215.

Dias, A., Freire, M., Coutinho, J., and I.M. Marrucho. 2004. Solubility of oxygen in liquid perfluorocarbons. *Fluid Phase Equilibria*, 222, 325,330.

Dittrich, P.S., and A. Manz. 2006. Lab-on-a-chip: microfluidics in drug discovery. *Nature reviews. Drug discovery*, 5(3): 210-218.

Doran, PM. 1995. Bioprocess engineering principles. Amsterdam: Elsevier Science and Technology Books. p. 154, p. 198.

Dudukovic, M.P., and R.M. Felder. 1983. Mixing Effects in Chemical Reactors. AIChE Modular Instruction, Series E. Kinetics, New York: American Institute of Chemical Engineers. Volume 4.

Dürauer, A., Hobiger, S., Walther, C., and A. Jungbauer. 2016. Mixing at the microscale: power input in shaken microtiter plates. *Biotechnology Journal*, 11, 1539-1549.

Edlich, A., Magdanz, V., Rasch, D., Demming, S., Aliasghar Zadeh, S., Segura, R., Kähler, C., Radespiel, R., Büttgenbach, S., Franco-Lara, E., and R. Krull. 2010. Microfluidic reactor for continuous cultivation of *Saccharomyces cerevisiae*. *Biotechnology Progress*, 26(5): 1259-1270.

Endy, D. 2005. Foundations for engineering biology. *Nature,* 438: 449-453.

Eppendorf, AG. 2017. *DASGIP ® parallel bioreactor systems*, viewed 07 September 2017, <https://online-shop.eppendorf.com/OC-en/Bioprocess-44559/Bioprocess-Systems-60767/DASGIP-Parallel-Bioreactor-Systems-PF-133597.html>.

Fidalgo, L.M., Whyte, G., Ruotolo, B.T., Beneshch, J.L.P., Stengel, F., Abell, C., Robinson, C.V., and Huck, W.T.S. 2009. Coupling microdroplet microreactors with mass spectrometry: reading the contents of single droplets online. *Angewandte Chemie-International Edition*, 48(20):3665-3668.

Fogler, H.S. 2006. Distributions of residence times for chemical reactors. In: Elements of chemical reaction engineering, Fourth Edition. New Jersey: Prentice Hall. p. 868, pp.871-872, p.876, pp.887-888.

Fredlake, CP., Hert, D.G., Kan, C.W, Chiesi, T.N, Root, B.E., Forster, R.E., and A.E. Barron. 2008. Ultrafast DNA sequencing on a microchip by a hybrid separation mechanism that gives 600 bases in 6.5 minutes. In: *Proceedings of the National Academy of Sciences of the United States of America*, 105:476-481.

Frostburg state university, Department of Chemistry.1997. *Density of water at 37.5 °C and 36 °C*, viewed 07 September 2017, <http://antoine.frostburg.edu/chem/senese/javascript/water-density.html>.

Funke, M., Buchenauer, A., Schnakenberg, U., Mokwa, W., Diederichs, S., Mertens, A., Müller, C., Kensy, F., and J. Büchs. 2010a. Microfluidic biolector-microfluidic bioprocess control in microtiter plates. *Biotechnology and Bioengineering*, 107(3):497-505.

Funke, M., Buchenauer, A., Mokwa, W., Kluge, S., Hein, L., Müller, C., Kensy, F., and J. Büchs. 2010b. Bioprocess control in microscale: scalable fermentations in disposable and user-friendly microfluidic systems. *Microbial Cell Factories* 9, 86-98.

Gateway engineering education coalition. 2017. *Growth Kinetics (Doubling time of yeast)*, viewed 07 September 2017, <http://www.gatewaycoalition.org/files/hidden/react/ch4/4_1f.htm>.

Garcia-Ochoa, F., Gomez, E., Santos, V.E. and J.C. Merchuk. 2010. Oxygen uptake rate in microbial processes: an overview. *Biochemical Engineering Journal*, 49(3): 289-307.

Garcia-Ochoa, F. and E. Gomez. 2009. Bioreactor scale-up and oxygen transfer rate in microbial processes: an overview. *Biotechnology Advances* 27(2): 153-176.

Gernaey, K.V., Baganz, F., Franco-Lara, E., Kensy, F., Krühne, U., Luebberstedt, M., Marx, U., Palmqvist, E., Schmid, A., Schubert, F. and C.F. Mandenius. 2012. Monitoring and control of microbioreactors: an expert opinion on development needs. *Biotechnology Journal,* 7(10): 1308-1314.

Godin, M., Brian, AK., and T.P. Burg. 2007. Measuring the mass, density and size of particles and cells using a suspended microchannel resonator. *Applied Physics Letters*, 91: 123121.

Götz, F. 1990. *Staphylococcus carnosus*: a new host organism for gene cloning and protein production. *Society for Applied Bacteriology symposium series* 19, 49S-53S.

Gruber, P., Marques, M.P.C., Szita, N., and T. Mayr. 2017. Integration and application of optical chemical sensors in microbioreactors. *Lab on a Chip,* 17(16): 2693-2712.

Han, N., Purcell, O., Farzadfard, F., Lee, K.S., Lu, T.K., and R.J. Ram. Microfluidics for control in synthetic biology. 2014. *Proceedings of the 18th International Conference on Miniaturized Systems for Chemistry and Life Sciences (MicroTAS 2014)*, 312-314.

Hardt, S., and Schönfeld, F. 2007. *Microfluidic technologies for miniaturized analysis systems*. New York: Springer US. pp. 20-23.

Hegab, H.M., ElMekawy, A and T. Stakenborg. 2013. Review of microfluidic microbioreactor technology for high-throughput submerged microbiological cultivation. *Biomicrofluidics*, 7(2): 21502.

Hermann, R., Lehmann, M. and J. Buchs. 2003. Characterization of gas-liquid mass transfer phenomena in microtiter plates. *Biotechnology and Bioengineering*, 81(2):178-186.

Hitec Zang, GmbH. 2001. *RAMOS (Respiration activity monitoring system)*, viewed 07 September 2017, <http://www.hitec-zang.de/en/fermentation-technology.html>

Hogg, S. 2005. Essential Microbiology. 1st edition. New Jersey: Wiley. pp. 99-100.

Hunter, J.D. 2007. Matplotlib: A 2D Graphics Environment. *Computing in Science and Engineering.* 9: 90-95

Infors, AG. 2017. *Multifors Bioreactor Systems,* viewed 07 September 2017, <http://www.infors-ht.com/index.php/en/products/bioreactors/bench-top-bioreactors/multifors-2>.

International Association for the Properties of Water and Steam. 2017. *Release on the IAPWS formulation 2008 for the viscosity of ordinary water substance*, viewed 07 September 2017, <www.iapws.org>.

Irimia, D., Mindrinos, M., Russom, A., Xiao W., Wilhelmy, J., Wang, S., Heath, JD., Kurn, N., Tompkins, RG., Davis, RW., and Toner, M. 2009. Genome-wide transcriptome analysis of 150 cell samples. *Integrative Biology,* 1, 99-107.

Islam, R., Tisi, D., Levy, M., and G.Lye. 2008. Scale-up of *Escherichia coli* growth and recombinant protein expression conditions from microwell to laboratory and pilot scale based on matched $k_L a$. *Biotechnology and Bioengineering*, 99(5): 1128-1139.

Ju, L.K., Lee, J.F. and W.B. Armiger. 1991. Enhancing oxygen-transfer in bioreactors by perfluorocarbon emulsions. *Biotechnology Progress*, 7(4): 323-329.

Junker, B.H. 2004. Scale-up methodologies for *Escherichia coli* and yeast fermentation processes. *Journal of bioscience and bioengineering*, 97(6): 347-364.

Kamen, A., Garnier, A., Andre, G., Archambault, J., and C. Chavarie. 1995. Determination of mass transfer parameters in surface aerated bioreactors with bubble entrainment. *Chemical Engineering Journal*, 59:187-193.

Karimi, A., Golbabaei, F., Mehrnia, MR., Neghab, M., Mohammad, K., Nikpey, A., and M.R. Pourmand . 2013. Oxygen mass transfer in a stirred tank bioreactor using different impeller configurations for environmental purposes. *Iranian journal of environmental health science & engineering*, 10(1):6.

Karnik, R. 2015. Mircrofluidic Mixing. In: *Encyclopedia of Microfluidics and Nanofluidics*. New York: Springer. p. 1177.

Kewei, X., Guangsu, H., Jing, Z., Xiaoan, W., Guang, L., and H. Jingyun. 2012. Accelerated thermal ageing studies of polydimethylsiloxane (PDMS) rubber. *Journal of Polymer Research*,19 (5): 98690.

Kheradmandnia, S., Hashemi-Najafabadi, S., Shojaosadati, S.A., Mousavi, S.M., and K. Malek Khosravi. 2015. Development of parallel miniature bubble column bioreactors for fermentation process. *Journal of Chemical Technology and Biotechnology*, 90(6):1051-1061.

Kim, M., Lim, J.W., Kim, H.J., Lee, S.K., Lee, S.J., and T. Kim. 2015. Chemostat-like microfluidic platform for highly sensitive detection of heavy metal ions using microbial biosensors. *Biosensors and Bioelectronics,* 65, 257-264.

Kim, S., Li, H., Oh, I., Kee, C.D., and M. Kim. 2012. Effect of viscosity inducing factors on oxygen transfer in production culture of bacterial cellulose. *Korean Journal of Chemical Engineering* 29(6): 792-797.

Kirk, T.V., Marques, M.P., Radhakrishnan, A.N.P., and N. Szita. 2016. Quantification of the oxygen uptake rate in a dissolved oxygen controlled

oscillating jet-driven microbioreactor. *Journal of Chemical Technology and Biotechnology* 91(3): 823-831.

Kirk, T.V., and N. Szita. 2013. Oxygen transfer characteristics of miniaturized bioreactor systems. *Biotechnology and Bioengineering*,110(4): 1005-1019.

Kirk, TV. 2013. Microfluidic microbioreactor for eukaryote culture with dissolved oxygen control. Doctoral thesis, UCL (University College London).

Klein, T., Schneider, K., and Heinzle, E. 2013. A system of miniaturized stirred bioreactors for parallel continuous cultivation of yeast with online measurement of dissolved oxygen and off-gas. *Biotechnology and Bioengineering*, 110(2):535-542.

Krull, J. 2017. Cultivation of *Staphylococcus carnosus* at micro-scale – influence of different reactor performances. Masterarbeit, Technische Universität Braunschweig.

Krull, R., Lladó-Maldonado, S., Lorenz, T., Demming, S., and Büttgenbach, S. 2016. Microbioreactors. In: Dietzel, A, editor. Microsystems for pharmatechnology: manipulation of fluids, particles, droplets, and cells. Cham: Springer International Publishing. pp. 99-152.

Krull, R., and G. Peterat. 2016. Analysis of reaction kinetics during chemostat cultivation of *Saccharomyces cerevisiae* using a multiphase microreactor. *Biochemical Engineering Journal,* 105, 220-229.

Lan, F., Demaree, B., Ahmed, N., and AR. Abate. 2017. Single-cell genome sequencing at ultra-high-throughput with microfluidic droplet barcoding. *Nature Biotechnology*, 35 (7): 640-646.

Lan, F., Haliburton J.R., Yuan, A., and A.R. Abate. 2016. Droplet barcoding for massively parallel single-molecule deep sequencing. *Nature Communications*, 7, 11784.

Lee, K.S., Boccazzi, P., Sinskey, A.J., and R.J. Ram. 2011. Microfluidic chemostat and turbidostat with flow rate, oxygen, and temperature control for dynamic continuous culture. *Lab on a chip*, 11(10):1730-1739.

Lee, H.L., Bocazzi, P., Ram, R.J. and A.J. Sinskey. 2006. Microbioreactor arrays with integrated mixers and fluid injectors for high-throughput experimentation with pH and dissolved oxygen control. *Lab on a Chip*, 6(9): 1229-1235.

Levenspiel, O., 1999. The Convection Model for Laminar Flow. In: Chemical Reaction Engineering. 3rd edition. New York: Wiley. p. 344.

Li, Band., and M. Sha. 2016. Scale-up of *Escherichia coli* fermentation from small scale to pilot scale using Eppendorf fermentation systems. Eppendorf Application Note 306, p.5.

Lin, L., and J.M. Lin. 2015. Development of cell metabolite analysis on microfluidic platform. *Journal of Pharmaceutical Analysis*, 5 (6):337-347.

Lineweaver, H., and D. Burk. 1934. The Determination of Enzyme Dissociation Constants. *Journal of the American Chemical Society*, 56 (3): 658-666.

Lo, R. 2013. Application of Microfluidics in Chemical Engineering. *Chemical Engineering & Process Techniques*, 1: 1001, pp.1-3.

Long, Q., Liu, X., Yang, Y., Li, L., Harvey, L., McNeil., and B. Bai. 2014. The development and application of high throughput cultivation technology in bioprocess development, *Journal of Biotechnology*, 192, 323-338.

Long, Z., Olliver, A., Brambilla, E., Sclavi, B., Cosentino, L., and K.D. Dorfman. 2014. Measuring bacterial adaptation dynamics at the single-cell level using a microfluidic chemostat and time-lapse fluorescence microscopy. *Analyst*, 139(20): 5254-5262.

Luedeking, R., and E.L. Piret. 1959. A kinetic study of the lactic acid fermentation. Batch process at controlled pH. *Biotechnology and Bioengineering* 1 (4): 393-412.

Luk, V.N., and A.R. Wheeler. 2009. A digital microfluidic approach to proteomic sample processing. *Analytical Chemistry*, 81 (11):4524-4530.

Maharbiz, M.M., Holtz, W.J., Howe, R.T. and J.D. Keasling. 2004. Microbioreactor arrays with parametric control for high-throughput experimentation. *Biotechnology and Bioengineering*, 85 (4): 376-381.

Matsuzaki, M; Misumi, O; Shin-I, T; Maruyama, S; Takahara, M; Miyagishima, S; Mori, T; Nishida, K; Yagisawa, F; Nishida, K; Yoshida, Y; Nishimura, Y; Nakao, S; Kobayashi, T; Momoyama, Y; Higashiyama, T; Minoda, A; Sano, M; Nomoto, H; Oishi, K, Hayashi, H; Ohta, F, Nishizaka, S, Haga, S, Miura, S; Morishita, T; Kabeya, Y; Terasawa, K; Suzuki, Y; Ishii, Y; Asakawa, S; Takano, H, Ohta, N; Kuroiwa, H; Tanaka, K; Shimizu, N; Sugano, S; Sato, N; Nozaki, H; Ogasawara, N; Kohara Y., and T. Kuroiwa. 2004. Genome sequence of the ultra-small unicellular red alga *Cyanidioschyzon merolae* 10D. *Nature*, 428(6983): 653-657.

Marques, M. P. C., Cabral, J. M. S., and P. Fernandes. 2010. Bioprocess scale-up: quest for the parameters to be used as criterion to move from microreactors to lab-scale. *Journal of Chemical Technology and Biotechnology*, 85(9): 1184-1198.

Maxon Motor, AG. 2017. Maxon EC Motor. Operating Instructions EC32 Flat. Service and Downloads. Document number 919778. [Online] Available at: www.maxonmotor.com. [Accessed 02 August 2017].

Meier, K., Klöckner, W., Bonhage, B., Antonov, E., Regestein, L., and J. Büchs. 2016. Correlation for the maximum oxygen transfer capacity in shake flasks for a wide range of operating conditions and for different culture media. *Biochemical Engineering Journal*, 109, 228-235.

Merkel, T., Bondar, V., Nagai, K., Freeman, B., and I. Pinnau. 2000. Gas sorption, diffusion, and permeation in poly(dimethysiloxane). J*ournal of Polymer Science Part B Polymers Physics, 38* (3): 415-434.

Mo, Y., and K.F. Jensen. 2016. A miniature CSTR cascade for continuous flow of reactions containing solids. *Reaction Chemistry and Engineering,* 1, 501-507.

Mok, J., Mindrinos, M.N., Davis, R., and M. Javanmard. 2014. Digital microfluidic assay for protein detection. *Proceedings of the National Academy of Sciences* of *the United States of America*, 111(6): 2110-2115.

Monod, J. 1949. The growth of bacterial cultures. *Annual Review of Microbiology*, 3, 371.

Nikaido, H., 2009. Multidrug resistance in bacteria. *Annual review of biochemistry*, 78, 119-46.

Nguyen, N.T., and S.T. Wereley. 2006. Fundamentals and applications of microfluidics. 2nd edition. Massachusetts: Artech House Publishers. p.1.

Nguyen, N.T., and Z. Wu. 2005. Micromixers — a review. *Journal of Micromechanics and Microengineering*, 15(0960): R1-R16.

Oliphant, T. E. 2007. Python for Scientific Computing. *Computin in Science and Engineering.* 9 :10-20.

O'Neil, M.J. 2006a.*The Merck index - an Encyclopedia of chemicals, drugs, and biologicals (data for Tryptophan)*, viewed 07 September 2017, <https://pubchem.ncbi.nlm.nih.gov/compound/L-tryptophan>.

O'Neil, M.J. 2006b. *The Merck index - an Encyclopedia of chemicals, drugs, and biologicals (data for Phenol red)*, viewed 07 September 2017, < https://pubchem.ncbi.nlm.nih.gov/compound/phenol_red. [Accessed 19 August 2017].

O'Neil, M.J. 2006c. *The Merck index - an Encyclopedia of chemicals, drugs, and biologicals (data for Allura red dye)*, viewed 07 September 2017, <https://pubchem.ncbi.nlm.nih.gov/compound/6093299>.

Ossila. 2016. *Spin coating: A guide to theory and techniques*, viewed 07 September 2017, <http://www.ossila.com/pages/spin-coating>.

O'Sullivan, B., Al-Bahrani, H., Lawrence, J., Campos, M., Cázares, A., Baganz, F., Wohlgemuth, R., Hailes, H.C., and N. Szita. 2012. Modular microfluidic reactor and inline filtration system for the biocatalytic synthesis of chiral metabolites, *Journal of Molecular Catalysis B: Enzymatic*, 77, 1-8.

Pallipurath Radhakrishnan, A.N. 2016. Elucidation of flocculation growth kinetics using a microfluidic approach. Doctoral thesis, UCL (University College London).

Pasirayi, G., Auger, V., Scott, S.M., Rahman, P.K.S.M., Islam, M., O'Hare, W.T., and Z. Ali. 2011. Microfluidic bioreactors for cell culturing: A Review. *Micro and Nanosystems* 3,137-160.

Peng, J., and C. Biqiang. 2016. Advanced bioprocess development and manufacturing technologies in high-throughput miniature bioreactors. *Strategic Study of Chinese Academy of Engineering,* 18(4): 44-50.

Perez-Pinera, P., Han, N., Cleto, S., Cao, J., Purcell, O., Shah, K. A., Lee, K., Ram, R., and T. K. Lu. 2016. Synthetic biology and microbioreactor platforms for programmable production of biologics at the point-of-care. *Nature Communications 7*, 12211.

Pfeiffer, S., and S. Nagl. 2015. Microfluidic platforms employing integrated fluorescent or luminescent chemical sensors: a review of methods, scope and applications. *Methods and Applications in Fluorescence,* 3, 1-16.

Pilarek, M., Brand, E., Hillig, F., Krause, M., and P. Neubauer. 2013. Enhanced plasmid production in miniaturized high-cell-density cultures of *Escherichia coli* supported with perfluorinated oxygen carrier. *Bioprocess and Biosystems Engineering,* 36(8), 1079-1086.

Pirt, S.J., and Callow, D.S. 1960. Studies of the growth of *Penicillium chrysogenum* in continuous flow culture with reference to penicillin production. *Journal of Applied Bacteriology,* 23 (1): 87.

Platas Barradas, O., Jandt, U., Da Minh Phan, L., Villanueva, M., Rath, A., Reichl, U., Schräder, E., Scholz, S., Noll, T., Sandig, V., Pörtner, R., and A. Ping Zeng. 2011. Criteria for bioreactor comparison and operation standardisation during process development for mammalian cell culture. *BMC proceedings*, 5: (Suppl 8): P47.

PMT. 2014. *Making the world's smallest tools. 5µm and Up*, viewed 07 September 2017, <http://www.pmtnow.com/>.

PreSens, GmbH. 2010. *SFR (Shake flask reader)*, viewed 07 September 2017, <http://www.presens.de/products/brochures/category/systems/brochure/sfr-shake-flask-reader.html#tab-intro>.

PreSens, GmbH. 2016. *Optical oxygen sensors*, viewed 07 September 2017, <https://www.presens.de/products/o2/sensors.html>.

Puskeiler, R., Kaufmann, K., and D. Weuster-Botz. 2005. Development, parallelization, and automation of a gas-inducing milliliter-scale bioreactor for high-throughput bioprocess design (HTBD). *Biotechnology and Bioengineering*, 89:512-523.

Qian, X., Zhang, W., Peng, C., Liu, X., Yu, Q., Ni, K., and X. Wang. 2016. Characterizing the deformation of the polydimethylsiloxane (PDMS) membrane for microfluidic system through image processing. *Micromachines*, *7*(5): 92.

Ramirez-Vargas, R., Vital-Jacome, M., Camacho-Perez, E., Hubbard, L., and F. Thalasso. 2014. Characterization of oxygen transfer in a 24-well microbioreactor system and potential respirometric applications, *Journal of Biotechnology*, 186, 58-65.

Rappoport, Z. 2004. The Chemistry of Phenols. Chichester: John Wiley and Sons. p.921.

Ren, X., Lu, H., Zhou, J.G., Chong, P.L.G., Yuan, W., and M. Noh. 2017. Porous polydimethylsiloxane as a gas–liquid interface for microfluidic applications. *Journal of Microelectromechanical Systems*, 26 (1), 120-126.

Renaud, P. 2015. Technical note on the design of a suspension microbioreactor for culture of very small quantities of non-adherent cells, in situ analysis and easy

recovery. Technical report performed by Prof. Phillippe Renaud (EPFL Switzerland) during his visit at University College London. p.6.

Reynoso-Cereceda, G.I., Garcia-Cabrera, R.I., Valdez-Cruz, N.A., and M.A.T. Roldán. 2016. Shaken flasks by resonant acoustic mixing versus orbital mixing: Mass transfer coefficient kLa characterization and *Escherichia coli* cultures comparison. *Biochemical Engineering Journal*, 105, 379-390.

Ries, C., John, G., John, C., Eibl, R., and D. Eibl. 2010. A shaken disposable bioreactor system for controlled insect cell cultivations at milliliter scale. *Engineering in Life Sciences*, 10(1):75 -79.

Rosenstein, R., and F. Götz. 2010. Genomic differences between the food-grade and pathogenic staphylococcal species. *International Journal of Medical Microbiology*, 300(2): 104-108.

Rosenstein, R., Nerz, C., Biswas, L., Resch, A., Raddatz, G., Schuster, S.C., and F. Götz. 2009. Genome analysis of the meat starter culture bacterium *Staphylococcus carnosus TM300. Applied and Environmental Microbiology*, 75 (3): 811-22.

Rotem, A., Ram, O., Shoresh, N., Sperling, R.A., Schnall-Levin, M., and H. Zhang. 2015. High-throughput single-cell labeling (Hi-SCL) for RNA-Seq using drop-based microfluidics. *PLoS ONE* 10(5): e0116328.

Running, J.A., and K. Bansal. 2016. Oxygen transfer rates in shaken culture vessels from Fernbatch flasks to microtiter plates. *Biotechnology and Bioengineering*, 113, 1729-1735.

Rushton, J.H., Costich, E.W., and H.J. Everett. 1950. Power Characteristics of Mixing Impellers. *Chemical Engineering Progress*, 46, 467-476.

Sartorius Stedim Biotech, SA. 2017. Advanced microscale bioreactors ambr™ 250, viewed 07 September 2017, <https://www.sartorius.com/sartorius/en/EUR/products/bioreactors-fermentors/single-use/ambr-250>.

Schäpper, D., Stocks, S.M., Szita, N., Eliasson Lantz, A., and K.V. Gernaey. 2010. Development of a single-use microbioreactor for cultivation of microorganisms. *Chemical Engineering Journal*, 160(3): 891-898.

Schäpper, D., Alam, M.N.H.Z., Szita, N., Eliasson Lantz, A., and K.V. Gernaey. 2009. Application of microbioreactors in fermentation process development: A review. *Analytical and Bioanalytical Chemistry*, 395(3), 679-695.

Schliefer, K.H, and U. Fischer. 1982. Description of a new species of the genus *Staphylococcus: Staphylococcus carnosus*". *International Journal of Systematic Bacteriology*, 32 (2): 153-156.

Schmideder, A., Steffen, T., Johannes, S., Cremer, H. and D. Weuster-Botz. 2015. A novel milliliter-scale chemostat system for parallel cultivation of microorganisms in stirred-tank bioreactors, *Journal of Biotechnology*, 210, 19-24.

Schwarz, C., Kuznetsova, Y., and S. Brueck. 2003. Imaging interferometric microscopy. *Optics Letters,* 28(16): 1424-1426.

Simple Motors, LLC. 2015. *Power calculations for DC motor*, viewed 07 September 2017, <http://simplemotor.com/calculations>.

Streets, A.M., Zhang, X., Cao, C., Pang, Y., Wu, X., Xiong, L., Yang, L., Fu, Y., Zhao, L., Tang, F., and Y. Huang. 2014. Microfluidic single-cell whole-transcriptome sequencing. *Proceedings of the National Academy of Sciences* of *the United States of America*, 111 (19): 7048-7053.

Suh, Y.K., and S. Kang. 2010. A review on mixing in microfluidics. *Micromachines*, 1(3):82-111.

Suresh, S., Srivastava, V., and I. Mishra. 2009. Techniques for oxygen transfer measurement in bioreactors: a review. *Journal of Chemical Technology and Biotechnology.* 84 (8):1091-1103.

Szita, N., Polizzi, K., Jaccard, N., F. Baganz. 2010. Microfluidic approaches for systems and synthetic biology. *Current Opinion in Biotechnology.* 21(4): 517-523.

Szita, N., Boccazzi, P., Zhang, Z., Boyle, P., Sinskey, A., and K.F. Jensen. 2005. Development of a multiplexed microbioreactor system for high-throughput bioprocessing. *Lab on a chip*, 5(8): 819-826.

Tan, C., Davies, M., McCluskey, D., Munro, I., Nweke, M., Tracey, M.C. and N. Szita. 2015. Electromagnetic stirring in a microbioreactor with non-conventional chamber morphology and implementation of multiplexed mixing. *Journal of Chemical Technology and Biotechnology,* 90(10): 1927-1936.

Tan, R.K., Eberhard, W., and J. Büchs. 2011. Measurement and characterization of mixing time in shake flasks. *Chemical Engineering Science*, 66(3): 440-447.

Tewhey, R., Warner, J.B., Nakano, M., Libby, B., Medkova, M., David, P.H., Kotsopoulus, S.K., Samuels, M.L., Hutchison, J.B., and J.W. Larson. 2009. Microdroplet-based PCR enrichment for large-scale targeted sequencing. *Nature Biotechnology*, 27:1025-1031.

Tian, Y., Zhang, Y.L., Ku, J.F., He, Y., Xu, B.B., Chen, Q.D., Xia, H., and H.B. Sun. 2010. High performance magnetically controllable microturbines. *Lab on a Chip*, 10(21): 2902–2905.

Toriello, N.M., Douglas, E.S., Thaitrong, N., Hsiao, S.C., Francis, M.B., Bertozzi, C.R., and R.A. Mathies. 2008. Integrated microfluidic bioprocessor for single-cell gene expression analysis. In: *Proceedings of the National Academy of Sciences of the United States of America*, 105, 20173-20178.

Tsai, W.S., Autsen, J.L., Ma, J., Hudson, T., and J. Luo. 2012. *BioProcess international technical note on non-invasive optical sensor technology in shake flasks*, viewed 07 September 2017, <http://www.bioprocessintl.com/upstream-processing/expression-platforms/noninvasive-optical-sensor-technology-in-shake-flasks-325612/>.

UniProt. 2002. Database of protein sequences and function information. L-lactate dehydrogenase in *Staphylococcus carnosus* (strain TM300), viewed 07 September 2017, <http:/www.uniprot.org./uniprot/B9DN51>.

Van den Brink, F.T.G., Zhang, T., Ma, L., Bomer, J., Odijk*, M.,*, Olthuis*, W.,* Permentier, H.P., Bischoff, R., and A. Van den Berg. 2016. Electrochemical protein cleavage in a microfluidic cell with integrated boron doped diamond electrodes. *Analytical Chemistry*, 88 (18): 9190-9198.

Van den Brink, F.T.G., Büter, L., Odijk, M., Olthuis, W., Karst, U., and A. Van den Berg. 2015. Mass spectrometric detection of short-lived drug metabolites generated in an electrochemical microfluidic chip*. Analytical Chemistry*, 87 (3): 1527-1535.

Van der Walt, S., Colbert, S.C., Varoquaux, G. 2011. The NumPy Array: A Structure for Efficient Numerical Computation. *Computing in Science and Engineering*. 13: 22-30.

Walther, I., Van der Schoot, BH., Jeanneret, S., Arquint, P., De Rooij, NF., Gass, V., Bechler, B., Lorenzi, G and Cogoli, A. 1994. Development of a miniature

bioreactor for continuous culture in a space laboratory. *Journal of Biotechnology*, 38(1): 21-32.

Wang D.I.C, Cooney, C.L, Demain, A.L, Dunnill P, Humphrey, A.E., and M.D. Lilly. 1979. Fermentation and Enzyme Technology. New York: John Wiley and Sons. Chapters 9, 10 and 11.

Wagner, E., Doskar, J., and F. Götz. 1998. Physical and genetic map of the genome of Staphylococcus carnosus TM300. *Microbiology*, 144, 507-509.

Weast, R.C. 1979. Handbook of chemistry and physics. 60th ed. Boca Raton, Florida: CRC Press Inc. p. C-534.

Wellhausen, R., and K.A. Oye. 2007. Intellectual property and the commons in synthetic biology: strategies to facilitate an emerging technology. *Atlanta Conference on Science, Technology and Innovation Policy*, Atlanta, GA, 1-2.

Werts, M.H.V., Raimbault, V., Rozenn, T.P., Poizat, R., Franc, O., Griscomab, L., and J.R.G. Navarroa. 2012. Quantitative full-colour transmitted light microscopy and dyes for concentration mapping and measurement of diffusion coefficients in microfluidic architectures. *Lab on a Chip*, 12(4): 808.

Wewetzer, S.J., Kunze, S.J., Ladner, T., Luchterhand, B., Roth, S., Rahmen,N ., Kloß, R., Costa e Silva, A ., Regestein, L., and J. Büchs. 2015. Parallel use of shake flask and microtiter plate online measuring devices (RAMOS and BioLector) reduces the number of experiments in laboratory-scale stirred tank bioreactors. *Journal of biological engineering*, 9(1):9.

Whitesides, G.M. 2006. The origins and the future of microfluidics. *Nature* 442(7101):368-73.

WHO. 2014. *WHO's first global report on antibiotic resistance reveals serious, worldwide threat to public health*, viewed 07 September 2017, < http://www.who.int/mediacentre/news/releases/2014/amr-report/en/>.

Xu, P., Clark, C., Ryder, T., Sparks, C., Zhou, J., Wang, M., Russell, R. and C. Scott. 2017. Characterization of TAP Ambr 250 disposable bioreactors, as a reliable scale-down model for biologics process development. *Biotechnology Progress*, 33: 478-489

Yang, M., Nelson, R., and A. Ros. 2016**.** Toward analysis of proteins in single cells: a quantitative approach employing isobaric tags with MALDI mass spectrometry realized with a microfluidic platform. *Analytical Chemistry*, *88* (13), 6672-6679.

Zanzotto, A., Boccazzi, P., Gorret, N., Van Dyk, T.K., Sinskey, A.J., and K.F. Jensen. 2006. In situ measurement of bioluminescence and fluorescence in an integrated microbioreactor. *Biotechnology and Bioengineering*, 93(1):40-47.

Zanzotto, A., Szita, N., Boccazzi, P., Lessard, P., Sinskey, A.J. and K.F. Jensen. 2004. Membrane-aerated microbioreactor for high-throughput bioprocessing. *Biotechnology and Bioengineering*, 87(2):243-254.

Zilionis, R., Nainys, J., Veres, A., Savova, V., Zemmour, D., Klein, A.M., and L. Mazutis. 2017. Single-cell barcoding and sequencing using droplet microfluidics. *Nature protocols*, 12(1):44-73.

Zhang, Z., Boccazzi, P., Choi, H.G., Perozziello, G., Sinskey, A.J., and K.F. Jensen. 2006a. Microchemostat-microbial continuous culture in a polymer-based, instrumented microbioreactor. *Lab on a chip*, 6(7): 906-913.

Zhang, Z., Szita, N., Boccazzi, P., Sinskey, A.J., and K.F. Jensen. 2006b. A well-mixed, polymer-based microbioreactor with integrated optical measurements. *Biotechnology and Bioengineering*, 93(2): 286-296.

Zhong, J.F., Chen, Y., Marcus, J.S, Scherer, A., Quake, S.R., Taylor, C.R., and L.P. Weiner. 2008. A microfluidic processor for gene expression profiling of single human embryonic stem cells. *Lab on a Chip*, 8, 68-74.